On the Theory of Electron Transfer Reactions: Superexchange Coupling and Polar Solvation Dynamics

Thesis by

Chao-Ping Hsu

In Partial Fulfillment of the Requirements

for the Degree of

Doctor of Philosophy

California Institute of Technology

Pasadena, California

1998

(Submitted December 10, 1997)

To my parents,

Chih-Hau, Bin-Kai and Peilin

Acknowledgements

I will miss the days I spent here, for my time at Caltech has been so fruitful and enjoyable. Even though it takes the effort and support of many people to make Caltech what it is, most of whom I do not know and cannot thank personally, I still wish to express my appreciation and gratitude towards the few I can name.

Having Professor Rudy Marcus for my research advisor has been the most fortunate and wonderful part of my graduate study. He has always been available for guidance and consultations. I especially appreciate his great patience and insightful suggestions towards a young graduate student both in scientific research and in real life. Given any chance for my future career as a scientist, I will carry with me his advice on being a theoretical chemist: focusing on problems relevant to experiments.

Professor Aron Kuppermann, Professor Harry Gray and Professor Fred Anson are not only members of my Ph.D. committee, but also mentors who have generously provided their insightful thoughts and encouragement on many occasions.

It would not have been such a great experience for the past five and half years if there were not wonderful group members like Xueyu Song, Yuri Georgievskii, Aseem Mehta, Bryan Hathorn, Shachi Gosavi, Yiqin Gao, Shige Tanaka and Antonio Hidalgo García. They all have been good friends of mine, helping me with all the odds and ends of daily life, including English writing for many occasions. Most importantly, through many discussions (and arguments) and group meetings, they have helped me to learn and understand so much in science. I also owe a lot to Sheryl Tsai, Chia-Ying Wang, Chin-Yi Chan, Jen-Sue Chen, Richard P. Cheng, Chuo-Han Lee, Sing H. Chong, See-May Phoong, Hui-Ming Hung, Shao-Ching Hung and Meina Xu, for their precious friendship.

I wish to thank my parents, my brothers Chih-Hau and Bin-Kai, and my husband Peilin, for their endless love and support, without which I would not have been able to finish this dissertation.

Abstract

A recursion relation is formulated for the Green's function for calculating the effective electron coupling in bridge-assisted electron transfer systems, within the framework of the tight-binding Hamiltonian. The non-perturbative recursion expression relates the Green's function of a chain bridge to that of a bridge which is one unit less. The method is used to calculate the electronic coupling between a gold electrode and each of the molecules, $(\eta^5\text{-}C_5H_5)Fe(\eta^5\text{-}C_5H_4)CO_2(CH_2)_nSH$ and $(\eta^5\text{-}C_5H_5)Fe(\eta^5\text{-}C_5H_4)(CH_2)_nSH$ ($n = 3$ to 50). At larger numbers of bridge units, the effective coupling strength shows an exponential decay as the number of methylene units increases. This sequential formalism shows numerical stability even for a very long chain bridge and, since it uses only small matrices, requires much less computer time for the calculation. Identical bridge units are not a requirement, and so the method can be applied to more complicated systems, such as proteins. Most of the calculated coupling strengths, if converted to rate constants according to a nonadiabatic expression, agree well with the experimental results.

The time-dependent dynamic Stokes shift function, which describes the solvent response to a sudden change in the charge distribution of a solute molecule, is expressed in terms of experimentally measured dielectric dispersion data of the solvent, using a simple dielectric continuum model. The result is applied to photoexcited coumarin 343 in water, and encouraging agreement with the experimental data is obtained. A simple formula is also derived which includes the effect of a pump pulse of finite duration. Such an effect is negligible when the frequency of a pump pulse is close to the maximum in the absorption spectrum, but a deviation from the standard formula can be expected for the pump pulse tuned to a far wing of the absorption band of the chromophore. To calculate further the time-dependent fluorescence spectral lineshapes, a method is described for incorporating the vibronic transitions of a solute molecule. The intramolecular vibrational relaxation is assumed to be much faster than the observation delay time. Calculations are made for coumarin 153 in acetonitrile. The results are again in encouraging agreement with experimental spectra. Results are also given for the dynamic Stokes shift in methanol.

Contents

List of Figures

List of Tables

Introduction

Electron transfer (ET) has been one of the major subjects in physical chemistry, due to its role in many important chemical reactions including biochemical processes and fundamental reactions in electrochemistry. Those reactions have been studied extensively both experimentally and theoretically. In the following chapters two aspects of ET processes are investigated theoretically, in order to provide fundamental connections to experimental data, available currently and in the future, with physically insightful models.

The first aspect studied in this dissertation is the electronic coupling strength between the electron donor and acceptor. This part of study is described in chapters 1 and 2. Many studies involving long range ET suggest that the reaction rate has an exponential dependence on the distance between the electron donor and the acceptor. In chapter 1, a recursion relation is formulated for the Green's function for calculating the effective electron coupling in bridge-assisted electronic transfer systems, within the framework of the tight-binding Hamiltonian. The recursion expression relates the Green's function of a chain bridge to that of the bridge that is one unit less. This sequential formalism shows numerical stability even for a very long chain bridge and, since it uses only small matrices, requires much less computer time for the calculation.

From such a non-perturbative formalism, the physical origin and conditions for the exponential dependence on the distance between the donor and the acceptor become clear. This sequential formula is then applied to calculate the electronic coupling between a gold electrode and each of the molecules, $(\eta^5\text{-}C_5H_5)Fe(\eta^5\text{-}C_5H_4)CO_2(CH_2)_nSH$ and $(\eta^5\text{-}C_5H_5)Fe(\eta^5\text{-}C_5H_4)(CH_2)_nSH$ (n = 3 to 50). Most of the calculated coupling strengths, if converted to rate constants according to a high-temperature nonadiabatic expression, agree well with the experimental rate constants. In chapter 2 there is a detailed discussion of the exponential distance dependence and more comparison with experimental results.

The second aspect studied in this dissertation is the dynamics of the solvent in a charge-redistributed process, which is the central issue of chapters 3, 4 and 5. More specifically, the solvation dynamics arising from the dielectric interaction of a polar solvent with a solute having its charge redistributed is investigated. Such a process involves the rearrangement of the solvent molecules to a new set of equilibrium configuration with respect to the final charge distribution (electronic state) of the solute. In ET systems, such an interaction is frequently the most important source of the activation free energy of the reaction, and the theory has successfully predicted the reaction rates in many cases. The dynamics of such solvation processes often occurs in picosecond or even femtosecond time regions, and has now been observed experimentally using femtosecond laser techniques.

The dynamic Stokes shifts of chromophores in polar solvents have been observed and reported for a number of systems. Such results describe time-dependent solvation correlation function (also termed the "*Stokes shift response function*"), which is the solvent response to a sudden change in the charge distribution of a solute molecule. We have used a reaction field with the dielectric continuum assumption in our calculation. In chapter 3, application is made to water as a solvent for a comparison to experimental results. A quantum correction due to the finite pulse duration is derived and discussed in chapter 4, and conditions for its observation in future experiments are described.

A description of the time-dependent fluorescence spectrum of a chromophore in a polar solvent is given in chapter 5, which incorporates the vibronic transitions of the solute molecule. The evolution of the emission spectral width of a single vibronic transition is shown to be related with the quantum averaged correlation function, while the overall spectral width contains little information for such quantum effects due to the wide range of the vibronic transitions of coumarin 153, the experimentally used solute. Comparison of such calculated time-dependent emission spectra to experimental results is also given.

Chapter 1 A Sequential Formula for Electronic Coupling in Long Range Bridge-Assisted Electron Transfer. Formulation of Theory and Application to Alkanethiol Monolayers

Chao-Ping Hsu and R. A. Marcus

Arthur Amos Noyes Laboratory of Chemical Physics. 127-72

California Institute of Technology, Pasadena, CA 91125

(Reprinted with permission from *J. Chem. Phys.*, **106**(2). pp. 584 - 598.

Abstract

A recursion relation is formulated for the Green's function for calculating the effective electron coupling in bridge-assisted electronic transfer systems, within the framework of the tight-binding Hamiltonian. The recursion expression relates the Green's function of a chain bridge to that of the bridge that is one unit less. It is applicable regardless of the number of orbitals per unit. This method is applied to the system of a ferrocenylcarboxy-terminated alkanethiol on Au(111) surface. At larger numbers of bridge units, the effective coupling strength shows an exponential decay as the number of methylene($-CH_2-$) units increases. This sequential formalism shows numerical stability even for a very long chain bridge and, since it uses only small matrices, requires much less computer time for the calculation. Identical bridge units are not a requirement, and so the method can be applied to more complicated systems.

1.1 Introduction

Electron transfer (ET) over long distances has been studied extensively in recent experimental and theoretical works, both in homogeneous systems [1–5] and across monolayers on electrodes [6–9]. Some of the work addressed the importance of the role played by long range ET reactions in biological processes while others demonstrated the underlying fundamental properties of such reactions. Many of these studies suggest that typically the rate has exponential dependence on the distance between donor D and acceptor A. Theoretical studies [2, 10] on molecular wires with one orbital representing each site of the wires, show exponential dependence of the conductance with the length of wire when the electron is at an energy outside of the wire's energy band, and large conductance is obtained with oscillatory dependence on wire length for the energy of an electron inside the wire's band. A sequential treatment is formulated here for electron transfer through a linear chain bridge that is allowed to have more than one orbital in each site. When the energy of D and A states lies out of the "energy band" of a long chain bridge, the well known exponential dependence of the matrix element on distance is expected.

For the coupling of the electronic and nuclear motion, a Golden rule treatment has given a satisfactory description of the non-adiabatic reaction rate for weak (i.e., long range) coupling. In this case, the rate constant k for electron transfer from an electronic state of the donor to a state of the acceptor is given by:

$$k = \frac{2\pi}{\hbar}|H_{DA}|^2(FC) \tag{1.1}$$

where (FC) is the Franck-Condon factor, and H_{DA} is the effective electronic coupling. Various approaches for treating the electronic coupling matrix element H_{DA} have provided estimates of the decay coefficient [1–5, 11, 12]. Separability of the electronic and nuclear factors is assumed in Eq. (1.1).

The effective coupling element can be defined as the coupling between the eigenstate $|\psi_D\rangle$ and the zeroth-order state $|\phi_A\rangle$, namely, $\langle\psi_D|H|\phi_A\rangle$. Using the partition-

ing technique [13], it can be shown that this definition of effective coupling is the off-diagonal element after mapping the overall Hamiltonian onto an effective 2×2 Hamiltonian matrix of donor and acceptor states only. In an equivalent approach, a transfer operator T can be defined from scattering theory [14]

$$T = V + VGV, \tag{1.2}$$

where G is the Green's function for the Hamiltonian H. The latter is composed of an unperturbed H^0 and a perturbation V, where H^0 is the Hamiltonian for non-interacting donor, bridge and acceptor states, and V is the interaction among them. By making use of the Lippman-Schwinger equation, it can be shown [14] that the matrix element $\langle \phi_D | T | \phi_A \rangle$ is the same as the effective coupling $\langle \psi_D | H | \phi_A \rangle$, and the latter is denoted H_{DA} throughout this article.

McConnell gave an early molecular derivation of the exponential decay factor [12]. He showed that for a single-band problem, where there is only one orbital per bridge site, the tight-binding Hamiltonian is tri-diagonal and the effective coupling matrix element H_{DA} for a bridge with n repeating units is

$$H_{DA} \propto \left(\frac{\beta}{E - \alpha} \right)^n. \tag{1.3}$$

when $|E - \alpha| \gg 2|\beta|$. Here, β is the interaction between neighboring orbitals, α is the energy of an individual orbital in the bridge, and E is the energy of the electron to be transferred, namely, the energy of the donor orbital, which, in turn, equals the energy of the acceptor orbital when the system is at the transition state of the reaction.

Further studies on the single-band case have appeared recently [2, 3]. Their analytic expression for H_{DA} can be written as follows:

$$H_{DA} = \frac{\beta_A \beta_D (-\beta)^{n-1} 2^{n+1} \zeta}{(E - \alpha + \zeta)^{n+1} - (E - \alpha - \zeta)^{n+1}}, \tag{1.4}$$

where

$$\zeta = ((E - \alpha)^2 - 4\beta^2)^{1/2}, \tag{1.5}$$

where n,E,α and β have the same definition as in Eq. (1.3), and $\beta_D(\beta_A)$ is the interaction matrix element between donor(acceptor) and the bridge unit it is attached to. In Eq. (1.4) it has been assumed that the basis formed by orbitals of donor and acceptor and orbitals on every site of bridge is orthonormalized. Otherwise one can always find a new set of basis by the transformation similar to that described in Ref. [15].

There are two cases when the expression in Eq. (1.4) tends to be exponential. One is for far off-resonance, namely,

$$|E - \alpha| \gg 2|\beta|. \tag{1.6}$$

Then, ζ is very close to $|E - \alpha|$ and so one of the two terms in the denominator vanishes under this condition. In this case McConnell's expression (Eq. (1.3)) is obtained. The other case is from the observation that the absolute values of the two terms in the denominator of Eq. (1.4) differ when ζ is a non-zero real number, which requires that

$$|E - \alpha| > 2|\beta|. \tag{1.7}$$

This condition, together with the condition that n be large, is a weaker condition on the energy of the electron or on the coupling strength. The inequality (1.7) also serves, for large n, as the off-resonance condition, since a tight-binding Hamiltonian of an infinite chain with one orbital per site has an energy band which lies between $\alpha - 2\beta$ and $\alpha + 2\beta$. If Eq. (1.7) holds and n is large, the denominator of Eq. (1.4) is dominated by one of the two terms that has larger absolute value for the case that n is large. Consequently, exponential behavior is obtained in the limit of long chain bridges, where the attenuation factor is close to, but not exactly the same as, the $\beta/(E - \alpha)$ in Eq. (1.3).

Beratan and Hopfield [4] used another approach with which they were able to treat more realistic systems, i.e., several-band systems. Their method is readily understood if we note that surface states exist when the energy of the surface atom (donor/acceptor orbitals) lies outside the energy band of the infinite chain(bridge)

[16]. The usual Bloch states have complex eigenvalues with unit moduli for the translation operator that commutes with the Hamiltonian of the infinite chain, while such surface states have real eigenvalues for the translation operator. Since the wavefunctions must be square-integrable, the wave function for a surface state must be decaying rather than growing exponentially as it penetrates the infinitely long bridge. The energy and the corresponding decaying factor were solved by fitting the boundary condition at each end. Thereby, the exponential behavior was built into their solution. As discussed above, for a single band bridge, the exponential dependence is found either for off-resonant, sufficiently long uniform bridge chains or for energies far moved from the bridge band.

In the present paper we consider a more general case, which is not limited to systems with a single orbital in each bridge site or to a large system. For convenience and simplicity, the term "band" will be used in a loose sense and refers to the region where energy levels are concentrated or where the actual band of an infinite chain would be, even though we will be discussing finite systems only. In Section 1.2, a sequential expression for the Green's function is obtained. The Green's function of n bridge units is written in terms of that for $n-1$ units. The derivation does not require that the bridge units be identical, and they are also allowed to have different numbers of orbitals. In Section 1.3, this method is applied to calculating the electron transfer rate between an electro-active group on an adsorbed alkane thiol molecule and the electrode to which it is attached. The effect of additional parallel chains of alkane thiol molecules was also treated and, together with the comparison between our sequential method and the direct summation over the bridge eigenstates, the results are discussed in Section 1.4. Concluding remarks are given in Section 1.5. The Appendix consists of the graphical derivation of the sequential formula and its possible generalization.

1.2 The Sequential Formula for Green's Function

The tight-binding Hamiltonian is considered with only the nearest-neighbor interaction, namely, between neighboring bridge units, between the first unit and the donor orbital, and between the last unit and the acceptor. An expression for the Green's function for the whole space by the method provided below can always be developed, but the expression for the bridge Green's function is much simpler to introduce and for off-resonant systems it provides a satisfactory approximation. Thereby, it is assumed here that the matrix elements of the Green's function needed in Eq. (1.2) are approximately those of the Green's function for the bridge part only. The error from such an approximation should usually be relatively small when compared to other approximations made in the tight-binding calculation.

It is always possible to calculate the Green's function for short bridge chains, given the explicit Hamiltonian matrix elements. Therefore, we have explored solving the problem for general chain lengths, assuming that the Green's function is known for a chain with one less bridge unit and then, for longer bridge chains, obtaining the recursion equations and iterating them until the desired length. This iteration process involves mostly matrix multiplication and inversion. All the matrices involved will be seen to have dimensions determined by the number of molecular orbitals on each related bridge unit. These numbers are finite and are independent of the number of units of the entire bridge, and so the iteration process for longer bridge chains can be executed without solving a large linear problem. For notational simplicity, the derivation is given for systems with uniform bridge units. The generalization to arbitrary different bridge units can be made without difficulty and is discussed in Section 1.4. The derivation given below for the bridge's Green's function is non-perturbative with respect to the magnitude of the intra-bridge interactions.

It is supposed here that there are n bridge units in the problem, and that each bridge unit has m molecular orbitals. Using the basis that diagonalizes the Hamilto-

nian within each bridge unit [15], the Hamiltonian for a chain bridge is

$$H^{(n)} = \left(\begin{array}{ccccc|c} \mathbf{e} & \mathbf{v} & \mathbf{0} & \mathbf{0} & \cdots & \mathbf{0} \\ \mathbf{v}^T & \mathbf{e} & \mathbf{v} & \mathbf{0} & \cdots & \vdots \\ \mathbf{0} & \mathbf{v}^T & \mathbf{e} & \mathbf{v} & \cdots & \vdots \\ \vdots & \vdots & \vdots & \vdots & \ddots & \mathbf{v} \\ \hline \mathbf{0} & \cdots & \cdots & \mathbf{0} & \mathbf{v}^T & \mathbf{e} \end{array}\right), \tag{1.8}$$

where $\mathbf{e}$ is an $m \times m$ diagonal matrix

$$\mathbf{e} = \begin{pmatrix} \varepsilon_1 & 0 & \cdots & 0 \\ 0 & \varepsilon_2 & \cdots & 0 \\ \vdots & \vdots & \ddots & \vdots \\ 0 & 0 & \cdots & \varepsilon_m \end{pmatrix}, \tag{1.9}$$

and $\mathbf{v}^T$ is the transpose of the interaction matrix $\mathbf{v}$ that couples adjacent bridge units. The lines in Eq. (1.8) partition the matrix into four blocks. The upper left one, a large square block, corresponds to the Hamiltonian for $n-1$ bridge units. The elements in the two off-diagonal blocks arise as a perturbation designated below as $\mathcal{H}_1^{(n)}$. The elements in the two diagonal blocks form the zeroth-order Hamiltonian $\mathcal{H}_0^{(n)}$. Thereby, $\mathcal{H}_0^{(n)}$ and $\mathcal{H}_1^{(n)}$ are defined as

$$\mathcal{H}_0^{(n)} = \left(\begin{array}{ccccc|c} \mathbf{e} & \mathbf{v} & \mathbf{0} & \mathbf{0} & \cdots & \mathbf{0} \\ \mathbf{v}^T & \mathbf{e} & \mathbf{v} & \mathbf{0} & \cdots & \vdots \\ \mathbf{0} & \mathbf{v}^T & \mathbf{e} & \mathbf{v} & \cdots & \vdots \\ \vdots & \vdots & \vdots & \vdots & \ddots & \mathbf{0} \\ \hline \mathbf{0} & \cdots & \cdots & \mathbf{0} & \mathbf{0} & \mathbf{e} \end{array}\right) \equiv \left(\begin{array}{c|c} H^{(n-1)} & \mathbf{0} \\ \hline \mathbf{0} & \mathbf{e} \end{array}\right), \tag{1.10}$$

and

$$\mathcal{H}_1^{(n)} = \left(\begin{array}{ccccc|c} \mathbf{0} & \mathbf{0} & \mathbf{0} & \mathbf{0} & \cdots & \mathbf{0} \\ \mathbf{0} & \mathbf{0} & \mathbf{0} & \mathbf{0} & \cdots & \mathbf{0} \\ \mathbf{0} & \mathbf{0} & \mathbf{0} & \mathbf{0} & \cdots & \mathbf{0} \\ \vdots & \vdots & \vdots & \vdots & \ddots & \mathbf{v} \\ \hline \mathbf{0} & \cdots & \cdots & \mathbf{0} & \mathbf{v}^T & \mathbf{0} \end{array}\right). \tag{1.11}$$

so that $H^{(n)} = \mathcal{H}_0^{(n)} + \mathcal{H}_1^{(n)}$. The $\mathcal{H}_0^{(n)}$ is seen in Eq. (1.10) to refer to a fully coupled $(n-1)$-unit bridge plus an uncoupled nth bridge unit attached.

The Green's function corresponding to the $H^{(n)}$ in Eq. (1.8) is then rewritten as

$$\begin{aligned} G^{(n)} &= (E\mathbf{1} - H^{(n)})^{-1} = (E\mathbf{1} - \mathcal{H}_0^{(n)} - \mathcal{H}_1^{(n)})^{-1} \\ &= \mathcal{G}_0^{(n)}(\mathbf{1} - \mathcal{H}_1^{(n)}\mathcal{G}_0^{(n)})^{-1}. \end{aligned} \tag{1.12}$$

where $G^{(n)}$ is the Green's function for the tight-binding n-unit bridge system, and $\mathcal{G}_0^{(n)}$ is the Green's function corresponding to $\mathcal{H}_0^{(n)}$:

$$\mathcal{G}_0^{(n)} = (E\mathbf{1} - \mathcal{H}_0^{(n)})^{-1} = \left(\begin{array}{c|c} G^{(n-1)} & \mathbf{0} \\ \hline \mathbf{0} & \Delta^{-1} \end{array}\right). \tag{1.13}$$

here Δ denotes the diagonal $m \times m$ matrix

$$\Delta = E\mathbf{1} - \mathbf{e}. \tag{1.14}$$

The term $(\mathbf{1} - \mathcal{H}_1^{(n)}\mathcal{G}_0^{(n)})$ can be written as

$$\mathbf{1} - \mathcal{H}_1^{(n)}\mathcal{G}_0^{(n)} = \left(\begin{array}{c|c} \mathbf{1}_{m(n-1)} & -M_2 \\ \hline -M_1 & \mathbf{1}_m \end{array}\right), \tag{1.15}$$

where $\mathbf{1}_{m(n-1)}$ and $\mathbf{1}_m$ denote unit square matrices of dimensions given by subscript. The M_1 and M_2 are given by

$$M_1 = \left(\begin{array}{cccc} \mathbf{v}^T G_{(n-1,1)}^{(n-1)} & \mathbf{v}^T G_{(n-1,2)}^{(n-1)} & \cdots & \mathbf{v}^T G_{(n-1,n-1)}^{(n-1)} \end{array}\right), \tag{1.16}$$

and

$$M_2 = \begin{pmatrix} \mathbf{0} \\ \vdots \\ \mathbf{0} \\ \mathbf{v}\Delta^{-1} \end{pmatrix}, \tag{1.17}$$

in which $\mathbf{v}$, $\mathbf{v}^T$, Δ^{-1} and $G^{(n-1)}_{(i,j)}$ all represent $m \times m$ matrices. Specifically, $G^{(n-1)}_{(n-1,1)}$ is the $(n-1,1)$ block in the Green's function $G^{(n-1)}$ for $n-1$ bridge units. The inverse of the matrix in Eq. (1.15) can be written as

$$(\mathbf{1} - \mathcal{H}_1^{(n)}\mathcal{G}_0^{(n)})^{-1} = \left(\begin{array}{c|c} \mathbf{1}_{m(n-1)} & M_2 \\ \hline M_1 & \mathbf{1}_m \end{array}\right) \left(\begin{array}{c|c} (\mathbf{1} - M_2M_1)^{-1} & \mathbf{0} \\ \hline \mathbf{0} & (\mathbf{1} - M_1M_2)^{-1} \end{array}\right). \tag{1.18}$$

as can be verified by multiplying both sides of Eq. (1.15) to the left or to the right with the matrix in Eq. (1.18). Since there is negligible direct coupling between the donor and acceptor states in the long-range electron transfer, the effective coupling is calculated from the second term in Eq. (1.2). Also because the tight-binding model is used, only one block of the Green's function $G^{(n)}$ is needed in that expression, namely, the block relating transition from the first bridge unit to the nth one. It is denoted by $G^{(n)}_{(1,n)}$ and is a block of dimensions $m \times m$. The Green's function $G^{(n)}$ is obtained by introducing Eqs. (1.13) and (1.18) into Eq. (1.12) and performing the matrix multiplication in terms of blocks. For the desired $(1,n)$ block, we obtain

$$G^{(n)}_{(1,n)} = G^{(n-1)}_{(1,n-1)}\mathbf{v}\Delta^{-1}(\mathbf{1} - \mathbf{v}^T G^{(n-1)}_{(n-1,n-1)}\mathbf{v}\Delta^{-1})^{-1}. \tag{1.19}$$

In order to iterate Eq. (1.19) further for $G^{(n+1)}_{(1,n+1)}$, an expression for $G^{(n)}_{(n,n)}$ is needed. This $m \times m$ block matrix can be obtained similarly from $G^{(n)}$ but selecting the (n,n) block,

$$G^{(n)}_{(n,n)} = \Delta^{-1}(\mathbf{1} - \mathbf{v}^T G^{(n-1)}_{(n-1,n-1)}\mathbf{v}\Delta^{-1})^{-1}. \tag{1.20}$$

Equation (1.20) is a recursion expression for $G^{(n)}_{(n,n)}$. However, it would be desirable to convert the expression to one in which a dimensionless quantity represents the

deviation from the first-order term in the expansion of Eq. (1.12) [17]. With this goal in mind, we define an $m \times m$ block N_n,

$$N_n = \Delta G^{(n)}_{(n,n)}. \tag{1.21}$$

A recursion expression for N_n then follows from Eq. (1.20):

$$N_n = (\mathbf{1} - \mathbf{v}^T \Delta^{-1} N_{n-1} \mathbf{v} \Delta^{-1})^{-1}. \tag{1.22}$$

Equation (1.19) then becomes

$$G^{(n)}_{(1,n)} = G^{(n-1)}_{(1,n-1)} \mathbf{v} \Delta^{-1} N_n. \tag{1.23}$$

The initial condition for the iteration of $\{N_n\}$ is taken as N_2; N_2 can be obtained by inverting the $2m \times 2m$ tight-binding Hamiltonian, together with Eq. (1.21). Since the above derivation does not introduce any explicit assumption that $\mathbf{v}\Delta^{-1}$ is small, i.e., Eqs. (1.22) and (1.23) were not derived perturbatively, Eqs. (1.22) and (1.23) are mathematically exact for finite n.

The factor $\mathbf{v}\Delta^{-1}$ in Eq. (1.23) resembles McConnell's estimate of the scalar decay factor $\beta/(E-\alpha)$(Eq. (1.3)). If the matrix N_n becomes essentially a constant matrix after a number of iterations, then the overall trend for $G^{(n)}_{(1,n)}$ is to become an exponential as n increases. The sequential formula of N_n (Eq. (1.22)) is a nonlinear first order difference equation for matrices.

It is instructive, for understanding the general properties of Eq. (1.22), to examine the solution of this difference equation for $m = 1$, where N_n becomes a scalar. In this case, N_n can now be solved by the transformation:

$$a_n = \frac{1 - 2r^2 N_n}{\sqrt{|1 - 4r^2|}},$$

so Eq. (1.22) yields

$$\frac{a_n - a_{n-1}}{a_n a_{n-1} \pm 1} = \sqrt{|1 - 4r^2|}, \tag{1.24}$$

where r is defined as the scalar $\mathbf{v}\Delta^{-1}$ ($\equiv \beta/(E-\alpha)$) and the negative sign is taken if $|r| < 1/2$ and the positive sign, otherwise. Equation (1.24) can be solved by writing a_n as $\tanh b_n$ (or $\tan b_n$) and making use of the addition formula of the hyperbolic tangent (or tangent) function. The following solution is then obtained:

$$N_n = \frac{1}{2r^2} - \frac{\sqrt{1-4r^2}}{2r^2} \tanh\left(\tanh^{-1}\frac{(1-2r^2)N_2}{\sqrt{1-4r^2}} + (n-2)\sqrt{1-4r^2}\right), \text{ if } |r| < \frac{1}{2}; \tag{1.25}$$

$$N_n = \frac{1}{2r^2} - \frac{\sqrt{4r^2-1}}{2r^2} \tan\left(\tan^{-1}\frac{(1-2r^2)N_2}{\sqrt{4r^2-1}} + (n-2)\sqrt{4r^2-1}\right), \text{ if } |r| > \frac{1}{2}. \tag{1.26}$$

with

$$N_2 = \frac{1}{1-r^2}.$$

In the former case, N_n approaches a constant as n increases, while in the latter case, N_n has an oscillating behavior arising from equally spaced poles on the real n-axis. Basically this result is the solution of a single-band problem. When compared to Eq. (1.4), Eqs. (1.23) and (1.25) give the same exponential factor for the off-resonance case. It should be noted that the bridge Green's function was used here, while in obtaining Eq. (1.4) the full tight-binding Hamiltonian, including donor and acceptor states, is used instead. The general solution of Eq. (1.23) for multi-band Green's function, $\{G^{(n)}_{(1,n)}\}$, was also obtained without iteration, but the solution we obtained involves the inverse of the sum of the $(n-3)$th power of two matrices for $n \geq 3$, making it numerically unstable to calculate when n is large in its present form. The result is given in Ref. [18]. Practically, the sequential formula, Eq. (1.22), is straightforward and stable to use.

By observing the result of numerical iteration, the behavior of N_n can be described for most cases. As in the corresponding single-band case, the matrix N_n tends to a constant matrix if the energy E is outside all the bridge "bands." In this case, all of the eigenvalues of $\mathbf{v}\Delta^{-1}N_n$ lie inside the unit circle of the complex plane and one or two of them dominate the final decay factor as n becomes large, namely the one with the largest modulus. If there is only one dominating eigenvalue, an exponential decay

in the coupling strength with respect to n would be obtained. If the eigenvalues with the largest modulus are a pair of complex conjugate numbers, the decay is modified by a periodic oscillation. For the cases where E lies inside the bridge bands, Eqs. (1.22) and (1.23) are still mathematically applicable with a complicated dependence of N_n and $G^{(n)}_{(1,n)}$ on n, but physically the assumption of approximating the overall Green's function with the Green's function for the bridge part is not a good one. Therefore, it is inappropriate to discuss the on-resonance condition using the sequential formula in its present form.

We have also obtained a graph-based method of deriving Eqs. (1.22) and (1.23) which is potentially useful for complicated bridge systems. It is outlined in the Appendix. In this graph-based method, an infinite series is obtained, but its summation yields the same equation as that obtained in the above derivation. Since the latter did not involve any infinite series, it is seen that analytical continuation of the series can be used to obtain valid results in a region where the original infinite series of the graph-based method diverges. This property, if it still holds in more complicated problems, enlarges the scope of the graph-based method beyond its infinite series approach, permitting its use in other applications.

1.3 Application

The recent development of self-assembled monolayers of alkane thiol molecules on a gold surface has provided a convenient approach for studying electron transfer between an electroactive group and an electrode, where the electroactive group is held at a fixed distance from electrode surface, or, if in solution, is separated from the electrode by a fixed monolayer [6]. Chidsey measured the voltage dependent ET rate of the ferrocenylcarboxy-terminated alkane thiol/gold surface system including the rate under the exchange current condition (corresponding to the case where the ΔG^0 for the electrode process is zero), and a reorganization energy λ was estimated by fitting the data to an equation whose functional form is similar to Eq. (1.27) below [7].

A study involving electrodes coated with self-assembly monolayers of ω-hydroxy thiols of various lengths (the n's of $(-CH_2-)$ are 6 to 11) was performed by Becka and Miller [8]. The electron transfer current of anions in solution was measured and after corrections for diffusion and other effects were made, the authors reported the length dependence factor $\beta = 1.08 \pm 0.20$ per methylene unit [19]. Carter *et al.* [9] studied, for different lengths of thiol molecules ($n = 8, 12, 16$), the system investigated by Chidsey [7]. The length dependence over the above range was obtained and the decay factor was reported as $\beta = 1.44 \pm 0.12$ per methylene unit.

1.3.1 The Nonadiabatic Reaction Rate

A mathematical form for the nonadiabatic rate between an electron donor group and an electrode, in the high temperature limit, is given by [20, 21]

$$k_{\text{rate}} = \frac{2\pi}{\hbar}(4\pi\lambda k_B T)^{-1/2} \int d\varepsilon |V(\varepsilon)|^2 e^{-(\lambda - e\eta + \varepsilon)^2/4\lambda k_B T} \frac{e^{\varepsilon/k_B T}}{1 + e^{\varepsilon/k_B T}}, \tag{1.27}$$

where $|V(\varepsilon)|^2$ is

$$|V(\varepsilon)|^2 = \int d^3\vec{k} |H_{Dk}|^2 \delta(\varepsilon(\vec{k}) - \varepsilon), \tag{1.28}$$

in which H_{Dk} is used to denote the *effective* coupling element between states $\langle D|$ and $|\vec{k}\rangle$, with the definition similar to that of H_{DA} described in Section 1.1, the wavefunctions $|\vec{k}\rangle$ are normalized to a Dirac delta function, $\langle \vec{k}|\vec{k}'\rangle = \delta(\vec{k} - \vec{k}')$. ε is the energy of an electron in metal with respect to the Fermi energy, $\varepsilon(\vec{k})$ is the energy of the electronic state $|\vec{k}\rangle$ of the metal, λ is the reorganization energy (including both inner and outer contribution), and η is the overpotential $(E - E^0)$, namely the difference between the applied potential and the standard potential of the electrode. The above Eq. (1.27) is an integral of the non-adiabatic electron transfer rate expression [22] over all the possible states $|\vec{k}\rangle$ and all possible energies ε in a metal, using the Fermi-Dirac distribution as a weighting factor. In general, a summation over energy bands of the metal electrode is needed in Eq. (1.28). However, since in the present work we only consider the contribution from the s-band of the gold electrode, the

summation over energy bands is omitted for simplicity. "Work terms" [20] are also omitted in Eq. (1.27) for simplicity of notation. One sees that because of the delta function normalization and the above definition of H_{Dk}, the $|V(\varepsilon)|^2$ in Eq. (1.28) has units of energy.

The electron transfer rate under electrochemical exchange current conditions (i.e., forward rate equal to reverse rate) can be obtained by setting $\eta = 0$. By noting $\lambda \gg \varepsilon$ we can drop the quadratic term of ε in the exponent of Eq. (1.27). The integration over ε is performed by approximating [20]

$$\begin{aligned}\int_{-\infty}^{\infty} \frac{1}{e^{\varepsilon/2k_BT} + e^{-\varepsilon/2k_BT}} f(\varepsilon)d\varepsilon &\equiv \int_{-\infty}^{\infty} g(\varepsilon)f(\varepsilon)d\varepsilon \\ &= f(0)\int_{-\infty}^{\infty} g(\varepsilon)d\varepsilon - f'(0)\int_{-\infty}^{\infty} g(\varepsilon)\varepsilon d\varepsilon + \cdots \\ &\approx \pi k_B T f(0), \end{aligned} \tag{1.29}$$

since $g(\varepsilon)$ here is a symmetric, positive definite function with its weight concentrated around the origin. From Eqs. (1.27) and (1.29), the following expression is obtained:

$$k_{\text{rate}}^{(\text{ex})} = \frac{2\pi}{\hbar}(4\pi\lambda k_B T)^{-1/2} e^{-\lambda/4k_BT}|\bar{V}|^2. \tag{1.30}$$

where

$$|\bar{V}|^2 = \pi k_B T \int d^3\vec{k}|H_{Dk}|^2\delta(\varepsilon(\vec{k})) = \pi k_B T \overline{|H_{Dk}|^2}\rho_f. \tag{1.31}$$

with

$$\overline{|H_{Dk}|^2} \equiv \frac{\int d^3\vec{k}|H_{Dk}|^2\delta(\varepsilon(\vec{k}))}{\int d^3\vec{k}\delta(\varepsilon(\vec{k}))}$$

and

$$\rho_f \equiv \int d^3\vec{k}\delta(\varepsilon(\vec{k})).$$

Namely, $\overline{|H_{Dk}|^2}$ is the effective coupling strength averaged over the $\vec{k}$'s on the Fermi surface and has units of (energy)^2(wave vector)$^{-3}$ or (energy)^2(volume)^1 because of the normalization of $|\vec{k}\rangle$ described earlier, while ρ_f is the density of states at the Fermi surface, with units of (energy)$^{-1}$(wave vector)^3. In the present work, the unit length is chosen to be the nearest-neighbor distance of the fcc lattice of Au atoms, and so

(wave vector)^3 equals (number of atoms)$^{-1}$.

To calculate theoretically the effective coupling matrix element H_{Dk} between the ferrocenylcarboxyl group and the gold electrode and compare with the experimental data, two of the schemes, (a) and (b), which are developed from Eq. (1.2), assuming no direct coupling, are listed:

(a) A direct summation over all bridge molecular orbitals can be made by using the following expression:

$$T_{Dk}(\equiv H_{Dk}) = \sum_B \frac{V_{DB}V_{Bk}}{E - E_B}. \tag{1.32}$$

where $\{B\}$ denotes the set of molecular orbitals of the bridge. It can be shown that the matrix element T_{Dk} of the transfer operator equals the effective coupling H_{Dk} [14], as discussed in Section 1.1. The bridge Green's function is used to replace the overall Green's function. Also, the perturbation V is regarded as the interaction of any state of the entire bridge with the donor and with the acceptor. Namely, V_{DB} is the interaction matrix element between the donor state and the orbital B of the entire bridge.

(b) The sequential formula derived in Section 1.2 (Eqs. (1.22) and (1.23)) can be used:

$$H_{Dk} = V_{D,1}G^{(n)}_{(1,n)}V_{n,k} \tag{1.33}$$

where $V_{D,1}$ and $V_{n,k}$ denote interaction between donor state and the molecular orbitals in the first bridge unit and between those in the nth bridge unit and the state $|\vec{k}\rangle$ of the metal electrode, respectively. For a bridge with more than one orbital on each site, $V_{D,1}$ denotes a row vector, $G^{(n)}_{(1,n)}$ a matrix, and $V_{n,k}$ a column vector.

In both cases, the wave functions used for the Au(111) surface are linear combinations of atomic s-orbitals obtained with the tight-binding approximation [23], and to evaluate Eq. (1.31), the coupling strength of 60 wave vectors ($\vec{k}$) random sampled over the Fermi surface were calculated and averaged to obtain $\overline{|H_{Dk}|^2}$. All of the interaction matrix elements were obtained using an extended Hückel program [24].

The coordinates of atoms in the alkane thiol portion of the system are those of Klein and coworkers, who employed a molecular dynamics calculation in conjunction with structural data [25, 26]. The geometry of ferrocenylcarboxyl group is obtained from the crystal structure of similar molecules [27]. In the supplemental material [28] we deposited the full cartesian coordinates for the molecules being used in the present work.

1.3.2 The Energy Difference at Transition State

To calculate the denominator of Eq. (1.32) or the Green's function $G^{(n)}_{(1,n)}$ of Eq. (1.33), it is necessary to know the energy of the various electronic states of the bridge (B) relative to the Fermi level of the metal (M). We consider the free energy *vs.* the reaction coordinate q diagram in Fig. 1.1. which describes the reaction which involves transfer of an electron from D to a specific orbital $|\vec{k}\rangle$ at Fermi energy in the metal [21]:

$$D + B + M \rightarrow D^{+}(\text{solvated}) + B + M(e). \tag{1.34}$$

Curves I and II describe the left side and the right side of (1.34) respectively. Curve III corresponds to the superexchange state denoted by $D^{+} + B^{-}(\text{unsolvated}) + M$, if it is an electron transfer. (For a hole transfer, a curve representing $D + B^{+}(\text{unsolvated}) + M(e)$ should be used instead.) The energetics for I and II for the free energy $G(q)$ as a function of q are described by:

$$G_{\text{I}}(q) = G_D(q) + E_D \tag{1.35}$$

$$G_{\text{II}}(q) = G_{D^{+}}(q, \text{solv}) + \bar{\mu}_m + e\phi_s \tag{1.36}$$

where E_D is the energy of the electronic orbital of donor D with respect to vacuum, $G_D(q)$ is the solvation free energy of D, as a function of q, and $G_{D^{+}}(q, \text{solv})$ is similarly the solvation free energy of D^{+}; $\bar{\mu}_m$ is the electrochemical potential (Fermi level) of an electron in M, and is equal to $\mu^0_m - e\phi_m$. The ϕ's denote electrostatic potentials (the so-called *inner electric potential* or the *Galvani potential* [29, 30]) for the metal

eletrode (ϕ_m) and in solution (ϕ_s).

The bridge B can become a B^+ (or a B^-) in the virtual state which occurs in the superexchange mechanism, but because of the off-resonance condition this supertransient B^+ or B^- can be regarded as unsolvated. There may be some interaction of this virtual electronic state with the electrons in the surrounding medium, but we will neglect such details here. If the potential change $\phi_m - \phi_s$ occurs across the adsorbed monolayer B, then a first approximation would be to treat the energy levels of B as being at a mean electrostatic potential $(\phi_m + \phi_s)/2$. In that case we have, for the electron-transfer scheme,

$$G_{\mathrm{III}}(q, B_i) = G_{D^-}(q, \mathrm{solv}) + E_{Bi} + e\phi_s - \frac{e}{2}(\phi_m + \phi_s), \tag{1.37}$$

where E_{Bi} is the energy of the ith orbital of the bridge in the absence of an electrostatic potential.

The vertical difference between I and III at the transition state is denoted by $\Delta E(q^\dagger)$ in Fig. 1.1. It is seen from Eqs. (1.35) and (1.37) to be

$$\begin{aligned} \Delta E(q^\dagger) &= G_{\mathrm{I}}(q^\dagger) - G_{\mathrm{III}}(q^\dagger) = G_{\mathrm{II}}(q^\dagger) - G_{\mathrm{III}}(q^\dagger) && (1.38)\\ &= \mu_m^0 - E_{Bi} - \frac{e}{2}(\phi_m - \phi_s) && (1.39)\\ &= \mu_m^0 - E_{Bi} - \frac{e}{2}(\phi_m^0 - \phi_s^0 + \eta), && (1.40) \end{aligned}$$

since $G_{\mathrm{I}} = G_{\mathrm{II}}$ in the transition state, $q = q^\dagger$. In Eq. (1.40) the over-potential η has been defined as $\phi_m - \phi_s - \phi_m^0 + \phi_s^0$ while $(\phi_m^0 - \phi_s^0)$ is the standard metal-solution potential difference of the electrode. From Fig. 1.1 and Eq. (1.38), $\Delta E(q^\dagger)$ is seen to be independent of the reorganizational energy λ since the solvational free energies of the intermediate state (III) and the final state (II) are the same (for D^+ ion) and so the reorganizational energy cancels in the $G_{\mathrm{I}}(q^\dagger) - G_{\mathrm{III}}(q^\dagger)$ difference. η equals zero for the exchange current condition.

In Eq. (1.39) both μ_m^0 and E_{Bi} are negative quantities that describe the energy required to move the electron from the neutral materials to vacuum at infinity, while

$-e\phi_m$ and $-e(\phi_m + \phi_s)/2$ adjust that energy for the effect of the electric potential. This process of moving an electron to vacuum at infinity can also be described as occurring in the following two steps: the electron is first moved to just outside the surface of the material in vacuum, and then it is moved from that point to infinity. The energy needed in the first step is the definition of the work function of the material [31], and that for the second step is the electronic charge times the *outer potential* ψ (termed also the *Volta potential*) [29, 32], namely, the electric potential of the material due to its total charge. The inner potential ϕ's and outer potential ψ's differ by a surface term which is due to the dipolar distribution of charge at the surface of the material. If the work function of the metal is denoted Ψ_m (a positive quantity), and the corresponding quantity for the bridge molecule is Ψ_B, the ionization potential, we have the following relations for metal and bridge respectively, equating the two ways of accounting for the energy of the electron in the material relative to its value when at rest in vacuum at infinity:

$$\mu_m^0 - e\phi_m = -\Psi_m - e\psi_m, \tag{1.41}$$

$$E_B(\mathrm{HOMO}) - \frac{e}{2}(\phi_m + \phi_s) = -\Psi_B - \frac{e}{2}(\psi_m + \psi_s), \tag{1.42}$$

and for other molecular states in B, the same energy difference $\Delta\epsilon_i (= E_{Bi} - E_B(\mathrm{HOMO}))$ can be added to both sides of Eq. (1.42).

With Eqs. (1.41) and (1.42), Eq. (1.40) can be written as follows: (For the exchange current condition, the over-potential η has been set to zero.)

$$\begin{aligned} \Delta E(q^\dagger) &= -\Psi_m - e(\psi_m^0 - \psi_s^0) + \Psi_B - \Delta\epsilon_i + \frac{e}{2}(\psi_m^0 - \psi_s^0) \\ &= -eE_{(abs)}^0 + \frac{e}{2}(\psi_m^0 - \psi_s^0) + \Psi_B - \Delta\epsilon_i, \end{aligned} \tag{1.43}$$

where ψ^0 denotes the corresponding outer potential when the potential of the electrode is at the standard potential of the redox species, and $E_{(abs)} = \Psi_m/e + (\psi_m - \psi_s)$ is the absolute electrode potential with its reference state being an electron at rest in vacuum close to the surface of the solution, as discussed by Trasatti in Refs. [30] and

[32]. The absolute potential for some of the commonly used reference electrodes are also listed in Ref. [32]. With this data, the absolute potential for the electrode described by Chidsey [7] is estimated to be 5.13 V, if the standard potential E^0 is taken as 0.08 V above the Ag/(1 mM $AgClO_4$, 1 M $HClO_4$) reference electrode. Together with the work function of Au(111) surface, 5.31 eV [33], we obtain −0.18 V for the potential difference, $\psi_m^0 - \psi_s^0$. With these quantities, Eq. (1.40) becomes

$$\Delta E(q^\dagger) = -5.22 \text{ eV} + \Psi_B - \Delta\epsilon_i \tag{1.44}$$

for the ith molecular orbital of the bridge. $\Delta E(q^\dagger)$ is the quantity that is needed both in the denominator of Eq. (1.32) and the Green's function of Eq. (1.33). The quantity $-\Psi_B + \Delta\epsilon_i$ representing the energy of the ith bridge state is obtained in the following section.

1.3.3 Energy of Bridge States

For use in both the summation and the sequential methods in the present calculation, the energy eigenvalues for a long alkane chain ($(CH_2)_n$, $n = 40$ or more) were obtained from either the extended-Hückel or the tight-binding Hamiltonian, for comparison with the experimental data on the band structure of polyethylene. To obtain a better agreement with those data, adjustments of the Hamiltonians are given below. Such adjustments are then applied to each alkanethiol bridge in the calculation.

In the direct summation calculation, a full extended-Hückel calculation was performed. As noted in Ref. [34], in describing the valence band structure of polyethylene, the extended-Hückel method itself does surprisingly well. By comparing the distribution of calculated energy levels (Fig. 1.2-I) with the experimental valence band structure [34], we concluded that the following adjustments were needed for the position of each bridge level (denoted by E_B in Eq. (1.32)): first, a factor of 0.7 is used to multiply the energies of the levels in the *filled* extended-Hückel band formed from C $2p$ and H $1s$ orbitals (denoted by (a) in Fig. 1.2-I) so that the bandwidth is closer to that given by experiment, and then the two valence bands ((a) and (b) in

Fig. 1.2-I) are shifted to fit the experimental band edges for each band [34]. Prior to any adjustment, the position of the lower edge of band (c) is calculated to be about -0.6 eV relative to vacuum, and the resulting band gap agrees very well with the experimentally measured band gap of polyethylene [35] ($8-9$ eV). No adjustment was therefore made for the energies of the states in the unfilled bands (band (c) in Fig. 1.2 and the higher energy band not shown there). The interaction between donor (acceptor) and bridge orbitals and the composition (coefficients) of molecular orbitals are obtained directly from the extended-Hückel calculation without any adjustment.

For the sequential method, the tight-binding Hamiltonian is obtained from the same extended Hückel program, but all the interactions beyond nearest neighbors are now ignored and the overlap integrals are considered within each bridge unit only. The molecular orbitals of individual bridge units are obtained by solving the secular equation of each unit. Fig. 1.3-I shows the distribution of energy levels from such a tight-binding Hamiltonian. It is necessary to ensure that both the upper edge of the valence band (the HOMO) and the lower edge of the conduction band (the LUMO) of the bridge agree with the experimental values. From the observed band gap ($8-9$ eV) [35] and the ionization potential (8.8 eV) [34] of the bridge, these values are -8.8 eV and -0.8 to 0.2 eV, respectively. The calculated band gap is only 6.2 eV in Fig. 1.3-I, which is smaller than experimental values. To obtain a better agreement with the band gap measurement, some of the six molecular orbital energies of a CH_2 unit was adjusted. The third and fourth states (the CH_2 HOMO and LUMO, respectively) were found to have a large effect on the states close to the band edges; those two energies were shifted by -1 eV and $+1$ eV, respectively, an adjustment which served to give a larger band gap (7.4 eV). All of the six MO energies were then shifted upward by 2.0 eV so that the upper band edge of the highest filled band agrees with the ionization potential of polyethylene. (This shift has no effect on the band gap.) With these corrections the HOMO of the bridge is -8.8 eV and the LUMO is -1.4 eV, which are moderately close to the above experimental values. The MO energies after the above adjustments are now used as the diagonal matrix elements in Eq. (1.9). The interaction matrix elements between nearest neighbors, denoted by

$\mathbf{v}$ in Section 1.2, are obtained from the extended-Hückel calculation using the MO's of each bridge unit as the basis. The distribution of energy levels from the adjusted Hamiltonian is plotted in Fig. 1.3-II.

The trend of coupling strength with length of chain calculated from the sequential method is shown in Fig. 1.4. The results of both the direct summation and sequential methods are given in Fig. 1.5. Various aspects of there results are discussed and compared next.

We have also calculated the effect of additional parallel alkane thiol chains using the structure from Klein [25]. For one of the possible conformations of the ferrocenyl-carboxyl group [28], the effective coupling calculated from direct summation method for different numbers of additional chains is listed in Table 1.1.

1.4 Discussion

In the following discussion, we first consider and compare the results shown in Figs. 1.4 and 1.5 and in Table 1.1. We then discuss the generalization to a more complicated bridge system that has different bridge units or that has a complex geometrical structure instead of being a linear chain. The flexibility of the graph-based method described in the Appendix will be discussed in the end of that section.

Using Eqs. (1.30), (1.31), the sequential formula (Eqs. (1.22) and (1.23)), Eq. (1.33) and the experimental value of λ [7], 0.85 eV, we obtained a coupling strength ($\overline{|H_{Dk}|^2}$) of about 5.6×10^{-12} eV^{2}atom for $n = 16$, which yields a rate constant of about 0.11 sec^{-1}. In obtaining the latter, the density of states of gold electrode was estimated from the tight-binding formalism by a Monte Carlo method. At the Fermi energy of gold, the value 0.05 ± 0.002/eV/atom was obtained. As a comparison, if the density of states of Au at the Fermi level, obtained from low temperature specific heat, 0.3/eV/atom [36] is used, instead, one would obtain a reaction rate that is a factor of six larger. The reaction rates calculated above roughly agree, within one order of magnitude, with the 1.25 sec^{-1} measured from the electrochemical exchange current voltage by Chidsey [7].

The sequential method is numerically easy to calculate with good precision. In Fig. 1.4 the coupling strength calculated by the sequential method is shown for up to 50 bridge units ($-CH_2-$) [37]. It can be seen that for longer bridge chains, there is an excellent exponential decay, while for shorter chains, the decay is modulated with an initial oscillation. Fitting the electronic coupling of the long chains ($n = 30 - 50$) with a term proportional to $\exp(-\beta n)$ yields $\beta = 1.05$ per methylene unit. For even-numbered short chains ($n = 6 - 20$) the value calculated for β is 1.00 per methylene unit.

The direct summation method gives an electronic coupling strength for short chains similar to that for the sequential method. The linear fit for the result of the direct summation yields $\beta = 1.27$ per methylene unit for $n = 6 - 20$. These data decay with n slightly differently from that of sequential method because the Hamiltonian for both cases is not exactly the same. For the present form of the sequential method we need to use a tight-binding approximation which neglects all the interaction beyond nearest neighbor units. For the direct summation calculation, on the other hand, all Hamiltonian matrix elements generated by the extended-Hückel program were included. It should be stressed, however, that since the sequential formula for the bridge Green's function (Eqs. (1.22) and (1.23)) is mathematically exact and numerically stable, the difference in the two sets of data points in Fig. 1.5 arises only from the difference in the two model Hamiltonians. The Hamiltonians have been adjusted independently, as described in Section 1.3.3, to agree better with the experimental band structure measurements.

We also calculated the coupling strength through hole transfer mechanism by doing the direct summation only over the filled states of bridge part. Our result shows that the hole transfer scheme provides the major pathways of the coupling, and it yields more than 89% of the total coupling strength.

For a long chain bridge, direct summation method performs summations (instead of merely multiplications) resulting in a large amount of cancellation to yield a small value. So numerically it requires more care for the number of significant figures of interaction matrix elements as well as the coefficients in describing MO's with

atomic orbitals, and the method can be expected to fail when the effective coupling strength is smaller than the significant digits of the numbers being summed. The direct summation calculation, even after all the bridge states were pre-diagonalized, also still required at least ten times more computer time than that for the sequential method.

Our sequential calculation is based on a tight-binding Hamiltonian. Matrix elements and overlap integrals from the extended-Hückel program are not always the best choice for the tight-binding model. In our calculation we found that the band gap obtained in this tight-binding model is too small (it is about 6.2 eV) compared with that from experiment (8−9 eV [35]). The band structure of the tight-binding model also does not resemble that from full extended-Hückel calculation. Since the energy of the electron being transferred lies between the conduction band and the valence band of polyethylene, the position of the band edges are a most crucial factor in determining the effective coupling across the hydrocarbon chain. In the sequential (nearest-neighbor tight-binding) calculation we adjusted the position of two of the MO energies of CH_2, as described in Section 1.3.3, so that the band gap is larger than the 6.2 eV, namely 7.4 eV, which is fairly close to that of experiments. In applying this method to other systems, the tight-binding Hamiltonian for the bridge part used should fit band structure measurements.

Turning now to the effect studied in Table 1.1, there is seen to be little effect from additional chains. This result indicates that in this system electron transfer occurs mainly through the chain covalently bonded to the redox active group. The closest atom-to-atom distance from the first added alkane thiol molecule to the ferrocenylcarboxyl group is 1.6 Å[28]. Even with such close contact between molecules, the additional thiol chains still do not effectively provide an alternate route for the electron to be transferred to the electrode, according to the results in Table 1.1.

In Fig. 1.6 is a test of the condition discussed at the end of Section 1.2, where the energy of electron is deliberately shifted to a place where the matrices $\{\mathbf{v}\Delta^{-1}N_n\}$ are almost constant with respect to the iteration (Eq. (1.22)), but where two of the important eigenvalues are a pair of conjugate complex numbers. For this alkane

bridge chain the energy needed for this effect to occur is not physically accessible, but it is still possible for other homogeneous chain bridges to have this kind of oscillatory length dependence. Moreover, there is no corresponding trend in a single-band model: in an off-resonance, single-band system, $\{\mathbf{v}\Delta^{-1}N_n\}$ is a scalar series, and therefore the magnitude of $G^{(n)}_{(1,n)}$ (which is also a scalar now) decays monotonically as $\mathbf{v}\Delta^{-1}N_n$ goes to a small constant real or complex number.

As mentioned earlier, in the derivation in Section 1.2 it is not required to have a bridge of identical subunits. For different bridge units with either the same or a different number of orbitals, $\mathbf{v}$ is now a square or rectangular matrix, respectively, describing the interaction between specific neighboring bridge sites, n and $(n-1)$ in Eqs. (1.22) and (1.23), and the diagonal matrix Δ must be then labeled with a subscript n, e.g., Δ_n. Eqs. (1.22) and (1.23) now become

$$N_n = (1 - \mathbf{v}^T_{(n-1,n)}\Delta^{-1}_{n-1}N_{n-1}\mathbf{v}_{(n-1,n)}\Delta^{-1}_n)^{-1}. \tag{1.45}$$

$$G^{(n)}_{(1,n)} = G^{(n-1)}_{(1,n-1)}\mathbf{v}_{(n-1,n)}\Delta^{-1}_n N_n, \tag{1.46}$$

where $\mathbf{v}_{(n-1,n)}$ denotes the interaction matrix between the $(n-1)$th and the nth bridge units. The initial condition $G^{(2)}_{1,2}$ is defined as the corresponding matrix between the first and the second bridge units. In this way, the Green's function can be obtained for an arbitrary tight-binding linear chain bridge, without solving a large linear system. There are already strategies for solving such large set of linear equations, e.g., that of Stuchebrukhov [5], and others [11], and it will be interesting to compare those methods with the present sequential method, both with respect to computation and physical insight.

Formally, in applying the sequential formula, the only limit on the range of energy of transferred electron is that it should not be coincident with the poles of Δ^{-1} and of the final Green's function $G^{(n)}$. However, the Green's function for the bridge is not a good approximation for the overall Green's function when the energy is close to one of the energy levels of the bridge. Also, the physical situation of an on-resonant system is quite different. It may not even involve an electron transfer from a state

localized on the donor to one localized on the acceptor.

A further generalization can be made for more complicated structures of bridges using the graph-based method described in the Appendix.

1.5 Conclusion

The sequential formula (Eqs. (1.22) and (1.23)) developed in the present paper is numerically stable even for the case of a large number of bridge orbitals. Since it involves only the inversion and multiplication of small matrices whose sizes are independent of the chain length, it is also much less computationally time-consuming than the direct summation method.

This new method can be applied to various kinds of bridge molecules and, we believe, by extending the one-orbital per site case to many orbitals per site, as in the present paper, provides added physical insight into various effects. To the best of our knowledge, the present work appears to be the first that rigorously treats a multiple band, tight-binding Hamiltonian and, thereby, the origin of and the condition for the exponential dependence for such cases. As seen in the calculation, by investigating conditions for constancy of N_n in the case of a uniform bridge, it directly reflects the origin of any exponential or other regular dependence (Fig.1.6) for multiband systems. This exponential dependence for an off-resonant bridge was assumed, and reasonably so, in earlier work [4]. For a linear bridge, no further assumption need be made for the calculation of the coupling strength, apart from the tight-binding Hamiltonian and, in the present case, using the Green's function for bridge subspace instead of that of the whole donor-bridge-acceptor system. The method can be applied to a wide class of systems, including non-uniform bridges, and could be extended to non-linear bridge molecules, perturbatively if necessary.

Acknowledgements

It is a pleasure to acknowledge the support of National Science Foundation, the Office of Naval Research, and NEDO (Japan), and the very helpful comments of Mark Ratner and Aseem Mehta.

Appendix A: A Graph-Based Approach

Another approach of deriving the sequential formula, using a graph representation for the terms in the expansion of the Green's function, is given in this Appendix. This method yields the same final answer as that derived in Section 1.2 (Eqs. (1.22) and (1.23)), and it provides a physical picture of the coupling scheme. Thereby, this graph-based method may prove useful in generalizing the calculation for more complex structures of the bridge.

A.1 The Hamiltonian and the Green's Function

Using Eq. (1.8), instead of treating only the interaction between the last two bridge units as a perturbation ($\mathcal{H}_1$), we now regard all the off-diagonal matrix elements as perturbations (H') and so H_0 now contains only diagonal matrix elements. For simplicity of presentation, the case of identical bridge units will be considered. The new zeroth order Hamiltonian is, thereby,

$$H_0 = \begin{pmatrix} \mathbf{e} & \mathbf{0} & \mathbf{0} & \mathbf{0} & \cdots & \mathbf{0} \\ \mathbf{0} & \mathbf{e} & \mathbf{0} & \mathbf{0} & \cdots & \vdots \\ \mathbf{0} & \mathbf{0} & \mathbf{e} & \mathbf{0} & \cdots & \vdots \\ \vdots & \vdots & \vdots & \vdots & \ddots & \mathbf{0} \\ \mathbf{0} & \cdots & \cdots & \mathbf{0} & \mathbf{0} & \mathbf{e} \end{pmatrix}, \tag{1.47}$$

and the perturbation H' is now

$$H' = \begin{pmatrix} \mathbf{0} & \mathbf{v} & \mathbf{0} & \mathbf{0} & \cdots & \mathbf{0} \\ \mathbf{v}^T & \mathbf{0} & \mathbf{v} & \mathbf{0} & \cdots & \vdots \\ \mathbf{0} & \mathbf{v}^T & \mathbf{0} & \mathbf{v} & \cdots & \vdots \\ \vdots & \vdots & \vdots & \vdots & \ddots & \mathbf{v} \\ \mathbf{0} & \cdots & \cdots & \mathbf{0} & \mathbf{v}^T & \mathbf{0} \end{pmatrix}, \tag{1.48}$$

where the block matrices $\mathbf{e}$,$\mathbf{v}$ and $\mathbf{0}$ are the same as defined in Section 1.2. Thus, the Green's function can be expressed as the following expansion:

$$\begin{aligned} G &= (E\mathbf{1} - H_0 - H')^{-1} \\ &= G_0 + G_0 H' G_0 + G_0 H' G_0 H' G_0 + \cdots, \end{aligned} \tag{1.49}$$

where G_0, the Green's function corresponding to H_0, is now the inverse of a diagonal matrix

$$G_0 = (E\mathbf{1} - H_0)^{-1}, \tag{1.50}$$

or,

$$(G_0)_{n_i,m_i;n_j,m_j} = \delta_{n_i,n_j}\delta_{m_i,m_j}\frac{1}{E - \varepsilon_{m_i}}, \tag{1.51}$$

where n_i is the index for the n_ith bridge unit, so the indices n_i and n_j refer to the block matrix at (n_i, n_j) position of G_0. Similarly, m_i is the index for the m_ith molecular orbital; therefore m_i and m_j refer to a matrix element inside the (n_i, n_j) block.

A.2 Graph Representation

One way of calculating G in Eq. (1.49) is to draw a graph whose vertices represent zeroth-order states and where lines exist between two states only if they interact (Fig. 1.7). We then make use of a theorem which states that there is a one-to-one correspondence between each possible path on such a graph and each term in each of the matrix element products in the complete expansion of the Green's function [14].

The connection is as follows: each path begins and ends with a dot, and between two dots the path is connected with a line. The corresponding quantity obtained from the path is a product of the following factors:

$$\text{for every dot it visits:} \qquad 1/(E-\varepsilon_{m_i}); \tag{1.52}$$

$$\text{for every line:} \qquad \mathbf{v}_{m_i,m_j}. \tag{1.53}$$

For each overall matrix element there are an infinite number of paths corresponding to it, but by classifying the paths in a suitable way, it is often possible to obtain the exact expression. One example is the RPE (renormalized perturbative expansion) which selects the "skeleton" (self-avoiding) paths and then adds "decoration" to make an arbitrary path [14, 38].

We consider the part of G that is needed to obtain the effective coupling strength, and denote it now by $G^{(n)}_{(1,n)}(m_1, m_n)$. It consists of all possible paths from any orbital m_1 in the first site to any orbital m_n in the last (nth) site. At the vertical column of points for the $(n-1)$th site (Fig. 1.8) all such paths must cross this column at least once and all of them cross it an odd number of times. One can then cut the paths into pieces at the place where they cross this dividing line. The paths are composed of segments that are either within the first $n-1$ units or wandering between the $(n-1)$th and the nth units. The former type of segments are related to the Green's function for $(n-1)$ bridge units, $G^{(n-1)}$, while the latter type of segment is a computable quantity.

We define the segments as the paths without their beginning dots so that there is no confusion upon connecting segments into a longer piece. The corresponding terms with respect to such segments, i.e., matrix elements apart from the initial $1/(E-\varepsilon)$ factor (Eq. (1.52)), is denoted as F, with proper superscript and notation defined later. F will represent this new set of matrices modified from Green's function G. In order to describe all possible variations of different molecular orbitals in the same unit, our notation is for $m \times m$ matrices, with specific indices for the starting and ending sites only; the matrix elements of these $m \times m$ matrices correspond to orbital-

to-orbital transition. So described, we define $F^{(n)}_{(1,n)}$ by:

$$G^{(n)}_{(1,n)} = \Delta^{-1} F^{(n)}_{(1,n)}. \tag{1.54}$$

where Δ has already been defined in Eq. (1.14). The inverse Δ^{-1} is the matrix corresponding to the dots that each path starts with, and $G^{(n)}_{(1,n)}$ has the same definition as in Section 1.2. We have, thereby,

$$F^{(n)}_{(1,n)} = \sum (\text{all possible segments from unit 1 to } n). \tag{1.55}$$

As discussed above, all of segments corresponding to $F^{(n)}_{(1,n)}$ cross the dividing line (the shaded bar in Fig. 1.8) an odd number of times. So the segments can be classified by the number of crossings, i.e.,

$$\begin{aligned} F^{(n)}_{(1,n)} &= \sum (\text{segments that cross the } n-1 \text{ site once}) \\ &+ \sum (\text{segments that cross three times}) \\ &+ \cdots + \sum (\text{segments that cross } 2j+1 \text{ times}) + \cdots \end{aligned} \tag{1.56}$$

In the following sections, expressions for terms in Eq. (1.56) are derived.

A.3 The First Term in Calculating $F^{(n)}_{(1,n)}$

The first term representing segments crossing site $n-1$ once is given by:

$$\sum (\text{segments that cross once}) = F^{(n-1)}_{(1,n-1)} F^{(2)}_{(n-1,n)}, \tag{1.57}$$

which is a sum over of all possible segments from site 1 to site $(n-1)$ multiplied by the sum over all possible segments that go from site $(n-1)$ to site n. Since a uniform bridge is treated in the present argument, the transition from bridge site $(n-1)$ to site n is the same as that for any other two neighboring sites. In Eq. (1.57) such a transition is denoted by $F^{(2)}_{(n-1,n)}$. This quantity can be obtained by classifying all the

segments as follows:

- The segments that go directly from site $n-1$ to site n, in only 1 step: those segments contain only one line and one dot on site n, so the corresponding terms are the appropriate elements of $\mathbf{v}$ times the appropriate elements of Δ^{-1} according to Eqs. (1.52) and (1.53). Thereby, this contribution to $F^{(2)}_{(n-1,n)}$ is $\mathbf{v}\Delta^{-1}$, which accounts for all 1-step segments from any orbital in site $n-1$ to any orbital in site n.

- The segments that bounce back and forth between site $n-1$ and site n: An example of such a segment is shown in Fig. 1.9. By an argument similar to the one above, we obtain $\mathbf{v}\Delta^{-1}\mathbf{v}^T\Delta^{-1}\mathbf{v}\Delta^{-1}$ for segments that return to site $n-1$ once and end up at site n, and $(\mathbf{v}\Delta^{-1}\mathbf{v}^T\Delta^{-1})^2\mathbf{v}\Delta^{-1}$ for segments that return twice, etc.

In this way $F^{(2)}_{(n-1,n)}$ is obtained by a summation over the above two contributions:

$$\begin{aligned} F^{(2)}_{(n-1,n)} &= \mathbf{v}\Delta^{-1} + \mathbf{v}\Delta^{-1}\mathbf{v}^T\Delta^{-1}\mathbf{v}\Delta^{-1} + \mathbf{v}\Delta^{-1}\mathbf{v}^T\Delta^{-1}\mathbf{v}\Delta^{-1}\mathbf{v}^T\Delta^{-1}\mathbf{v}\Delta^{-1} + \cdots \\ &= (1 - \mathbf{v}\Delta^{-1}\mathbf{v}^T\Delta^{-1})^{-1}\mathbf{v}\Delta^{-1}. \end{aligned} \tag{1.58}$$

This particular matrix also serves as the initial matrix for $F^{(n)}_{(1,n)}$ for a uniform bridge. For non-uniform bridges, the initial condition for $F^{(n)}_{(1,n)}$ needs to be calculated for the first two units, using the same expression as in Eq. (1.58), but with appropriate matrices $\mathbf{v}$ and Δ.

A.4 The Second and Other Terms in Calculating $F^{(n)}_{(1,n)}$

In Section A.2, it is seen that for segments contributing $F^{(n)}_{(1,n)}$, the number of times they cross the $(n-1)$ dividing line (Fig. 1.8) should be an odd number (Eq. (1.56)). All the possible segments that cross the dividing line three times are next considered. These segments must be composed of four segments: The first segment goes from site 1 to site $n-1$, and its corresponding matrix has already been defined as $F^{(n-1)}_{(1,n-1)}$. The second segment starts from the same final orbital at site $n-1$, and it goes to

site n and then returns to site $n-1$ including bouncing between the two sites for any number of times. We denote this part of the contribution by $F^{(2)}_{(n-1,n-1)}$. It differs from $F^{(2)}_{(n-1,n)}$ in that it finally returns to site $n-1$. The third segment starts from the $n-1$ site, visits the space of the first $n-1$ sites, where it involves an arbitrary 'loop' within the first $n-1$ sites, and it then returns to the $n-1$ site. We denote the matrix for such segments by $F^{(n-1)}_{(n-1,n-1)}$. The final segment goes from any orbital in site $n-1$ to any orbital of site n arbitrarily, so it corresponds to a matrix element of $F^{(2)}_{(n-1,n)}$ as shown in Section A.3. Thereby, we have

$$\sum(\text{segments that cross the } n-1 \text{ site 3 times}) = F^{(n-1)}_{(1,n-1)} F^{(2)}_{(n-1,n-1)} F^{(n-1)}_{(n-1,n-1)} F^{(2)}_{(n-1,n)}. \tag{1.59}$$

Generalizing the above expression to any odd number of crossings of the $n-1$ sites gives

$$\sum(\text{segments that cross } 2j+1 \text{ times}) = F^{(n-1)}_{(1,n-1)} \left[F^{(2)}_{(n-1,n-1)} F^{(n-1)}_{(n-1,n-1)}\right]^j F^{(2)}_{(n-1,n)}. \tag{1.60}$$

To evaluate Eq. (1.56), a summation of the terms in Eq. (1.60) for $j = 0$ to ∞ yields

$$\begin{aligned} F^{(n)}_{(1,n)} &= F^{(n-1)}_{(1,n-1)} \left[\mathbf{1} + F^{(2)}_{(n-1,n-1)} F^{(n-1)}_{(n-1,n-1)} + (F^{(2)}_{(n-1,n-1)} F^{(n-1)}_{(n-1,n-1)})^2 + \cdots\right] F^{(2)}_{(n-1,n)} \\ &= F^{(n-1)}_{(1,n-1)} \left[\mathbf{1} - F^{(2)}_{(n-1,n-1)} F^{(n-1)}_{(n-1,n-1)}\right]^{-1} F^{(2)}_{(n-1,n)}, \text{ for } n = 3, 4, 5, \cdots. \end{aligned} \tag{1.61}$$

Also, Eq. (1.61) can be rewritten in terms of $G^{(n)}_{(1,n)}$,

$$G^{(n)}_{(1,n)} = G^{(n-1)}_{(1,n-1)} \left[\mathbf{1} - F^{(2)}_{(n-1,n-1)} F^{(n-1)}_{(n-1,n-1)}\right]^{-1} F^{(2)}_{(n-1,n)} \tag{1.62}$$

by using Eq. (1.54) for both $G^{(n)}_{(1,n)}$ and $G^{(n-1)}_{(1,n-1)}$.

So now $F^{(n)}_{(1,n)}$ is written in terms of $F^{(n-1)}_{(1,n-1)}$, $F^{(2)}_{(n-1,n)}$, $F^{(2)}_{(n-1,n-1)}$, and $F^{(n-1)}_{(n-1,n-1)}$. The first one is the recursive variable, and the second one, $F^{(2)}_{(n-1,n)}$, has been obtained in Section A.3 (Eq. (1.58)). The next section is then devoted to deriving expressions for $F^{(2)}_{(n-1,n-1)}$ and $F^{(n-1)}_{(n-1,n-1)}$.

A.5 The Expressions for $F^{(2)}_{(n-1,n-1)}$ and $F^{(n-1)}_{(n-1,n-1)}$

We next evaluate $F^{(2)}_{(n-1,n-1)}$, which is the matrix for the sum of the terms corresponding to all possible segments bouncing back and forth between two rows of states that start and end at the $(n-1)$th row. In Fig. 1.10 is shown one of such paths. It differs from the $F^{(2)}_{(n-1,n)}$ by having a return from site n to site $n-1$, contributing a matrix $\mathbf{v}^T\Delta^{-1}$. Thereby,

$$F^{(2)}_{(n-1,n-1)} = F^{(2)}_{(n-1,n)}\mathbf{v}^T\Delta^{-1} = (\mathbf{1} - \mathbf{v}\Delta^{-1}\mathbf{v}^T\Delta^{-1})^{-1}\mathbf{v}\Delta^{-1}\mathbf{v}^T\Delta^{-1}. \tag{1.63}$$

From the above definition and discussion, $F^{(n-1)}_{(n-1,n-1)}$ is related to the $(n-1,n-1)$ block of G matrix in the following way:

$$G^{(n-1)}_{(n-1,n-1)} = \Delta^{-1}(\mathbf{1} + F^{(n-1)}_{(n-1,n-1)}). \tag{1.64}$$

in which a $m \times m$ unit matrix $\mathbf{1}$ is needed because the diagonal matrix elements of $G^{(n)}_{(n,n)}$ include "null paths"(i.e., paths which do nothing) arising from the first term (G_0) in the expansion of Eq. (1.49), and Δ^{-1} represents the missing beginning dots for segments in calculating $F^{(n)}$ (Eq. (1.52)).

By a strategy similar to that which led to $F^{(n)}_{(1,n)}$, one can derive

$$F^{(n)}_{(n,n)} = \mathbf{v}^T\Delta^{-1}(1 + F^{(n-1)}_{(n-1,n-1)})\left[\mathbf{1} - F^{(2)}_{(n-1,n-1)}F^{(n-1)}_{(n-1,n-1)}\right]^{-1}F^{(2)}_{(n-1,n)}. \tag{1.65}$$

in which all the possible segments for $F^{(n)}_{(n,n)}$ are divided into several parts depending on the number of times they cross the dividing site $n-1$. Those segments are classified as follows:

- The first segment is defined as a single step going from site n directly back to site $n-1$. This segment is introduced to force $F^{(n)}_{(n,n)}$ to contain no null segment, and it corresponds to $\mathbf{v}^T\Delta^{-1}$.

- The second segment is either a null one $(\mathbf{1})$ or any loop that begins and stops at $(n-1)$th site $(F^{(n-1)}_{(n-1,n-1)})$.

- On the other hand, the final segment is composed of any number of steps that go from the dividing line (site $n-1$) to a final stop on site n. This part exactly corresponds to the definition of $F^{(2)}_{(n-1,n)}$.

- There can be any number of segments between the second one and the final one. Those segments form loops in either spaces for the last two sites ($F^{(2)}_{(n-1,n-1)}$), or the first $(n-1)$ sites ($F^{(n-1)}_{(n-1,n-1)}$). This set of segments includes the null path so the first term should be $\mathbf{1}$. Two consecutive loops at the same side would contribute to the single $F^{(n-1)}_{(n-1,n-1)}$ or $F^{(2)}_{(n-1,n-1)}$ matrix because of its definition. If the final loop is in the last two sites ($F^{(2)}_{(n-1,n-1)}$), it can also be regarded as a part of the segments corresponding to $F^{(2)}_{(n-1,n)}$, which is the final segment as described above. To avoid over-counting, it is then required to have the last loop at the side of the first $(n-1)$ site ($F^{(n-1)}_{(n-1,n-1)}$). So the contribution of this part of segment is:

$$\begin{aligned} & \mathbf{1} + F^{(2)}_{(n-1,n-1)}F^{(n-1)}_{(n-1,n-1)} + F^{(2)}_{(n-1,n-1)}F^{(n-1)}_{(n-1,n-1)}F^{(2)}_{(n-1,n-1)}F^{(n-1)}_{(n-1,n-1)} + \cdots \\ = \; & \left[\mathbf{1} - F^{(2)}_{(n-1,n-1)}F^{(n-1)}_{(n-1,n-1)}\right]^{-1}. \end{aligned} \tag{1.66}$$

By multiplying the above four factors together, Eq. (1.65) for $F^{(n)}_{(n,n)}$ was obtained.

A.6 The Sequential Formula

Eq. (1.62) is the sequential formula derived in this appendix. To show the equivalence between Eq. (1.19) in the text and this Eq. (1.62), the following identity can be derived:

$$\begin{aligned} & \left[\mathbf{1} - F^{(2)}_{(n-1,n-1)}F^{(n-1)}_{(n-1,n-1)}\right]^{-1} F^{(2)}_{(n-1,n)} \\ = \; & \left[\mathbf{1} - \mathbf{v}\Delta^{-1}(\mathbf{1} + \mathbf{v}^T\Delta^{-1}\mathbf{v}\Delta^{-1} + \cdots)\mathbf{v}^T\Delta^{-1}F^{(n-1)}_{(n-1,n-1)}\right]^{-1} \times \\ & \mathbf{v}\Delta^{-1}(\mathbf{1} + \mathbf{v}^T\Delta^{-1}\mathbf{v}\Delta^{-1} + \mathbf{v}^T\Delta^{-1}\mathbf{v}\Delta^{-1}\mathbf{v}^T\Delta^{-1}\mathbf{v}\Delta^{-1} + \cdots) \\ = \; & \mathbf{v}\Delta^{-1}\left[\mathbf{1} - (\mathbf{1} - \mathbf{v}^T\Delta^{-1}\mathbf{v}\Delta^{-1})^{-1}\mathbf{v}^T\Delta^{-1}F^{(n-1)}_{(n-1,n-1)}\mathbf{v}\Delta^{-1}\right]^{-1}(\mathbf{1} - \mathbf{v}^T\Delta^{-1}\mathbf{v}\Delta^{-1})^{-1} \\ = \; & \mathbf{v}\Delta^{-1}\left[\mathbf{1} - \mathbf{v}^T\Delta^{-1}(\mathbf{1} + F^{(n-1)}_{(n-1,n-1)})\mathbf{v}\Delta^{-1}\right]^{-1}, \end{aligned} \tag{1.67}$$

in which Eqs. (1.58) and (1.63) were used. Therefore, with Eq. (1.64)

$$\left[\mathbf{1} - F^{(2)}_{(n-1,n-1)}F^{(n-1)}_{(n-1,n-1)}\right]^{-1} F^{(2)}_{(n-1,n)} = \mathbf{v}\Delta^{-1}(\mathbf{1} - \mathbf{v}^T G^{(n-1)}_{(n-1,n-1)}\mathbf{v}\Delta^{-1})^{-1}. \qquad (1.68)$$

So Eq. (1.62) becomes Eq. (1.19) with the above identity (Eq. (1.68)) introduced.

Also, if the expression Eq. (1.67) is introduced into Eq. (1.65), the following identity is obtained:

$$\begin{aligned} \mathbf{1} + F^{(n)}_{(n,n)} &= \mathbf{1} + \mathbf{v}^T\Delta^{-1}(\mathbf{1} + F^{(n-1)}_{(n-1,n-1)})\mathbf{v}\Delta^{-1}(\mathbf{1} - \mathbf{v}^T\Delta^{-1}(\mathbf{1} + F^{(n-1)}_{(n-1,n-1)})\mathbf{v}\Delta^{-1})^{-1} \\ &= \left[\mathbf{1} - \mathbf{v}^T\Delta^{-1}(\mathbf{1} + F^{(n-1)}_{(n-1,n-1)})\mathbf{v}\Delta^{-1}\right]^{-1}. \qquad (1.69) \end{aligned}$$

Together with Eq. (1.64), the above expression is equivalent to Eq. (1.20). Comparison of Eqs. (1.21) and (1.64) shows that

$$N_n = \mathbf{1} + F^{(n)}_{(n,n)}. \qquad (1.70)$$

With this identity (Eq. (1.70)), Eq. (1.69) is seen to be the same as Eq. (1.22).

A.7 Discussion

This approach, beginning with an infinite series expansion (Eq. (1.49)), gives the same recursion relation as derived in Section 1.2 by a non-perturbative method. Mathematically, the infinite series expansion in Eq. (1.49) converges inside its radius of convergence, namely when the modulus of every eigenvalue of the matrix G_0H' (or $H'G_0$) is less than unity. A similar restriction appears in Eqs. (1.61) and (1.63), which requires both $F^{(2)}_{(n-1,n-1)}F^{(n-1)}_{(n-1,n-1)}$ and $\mathbf{v}\Delta^{-1}\mathbf{v}^T\Delta^{-1}$ to have all of their eigenvalues within the unit circle in the complex plane. However, the resulting expressions are not limited by such conditions since they can also be derived from the non-perturbative method. This aspect demonstrates a desired property of the graph-based method, namely, that analytic continuation can be applied, in the present case, so as to obtain useful expressions in the range of energies where the infinite series diverges.

This graph-based method can be further generalized for a complex, nonlinear structure of bridge. First, we note that each column of dots in Fig. 1.7 can be "condensed" into a larger vertex, and the graph can be simplified to a row of large vertices with nearest neighbor vertices connected by a "multiple line." In this way, any one path drawn on this new graph represents all the possible paths on the old graph passing the same bridge sites in the same order with any choices of molecular orbitals. It corresponds, thereby, to a matrix, and each additional step on this new graph involves multiplication of matrices. Now a complicated bridge is represented by a simpler graph: a dot is used for each bridge site (which has several molecular orbitals), and lines exist between sites that interact with each other. The way to obtain the corresponding terms of Green's function from paths is to multiply all the matrices of lines and dots in the order given by the paths, as was done for the scalar terms for paths on the original graphs described in Section A.2. This method should provide a different way of calculating an electronic coupling between donor and acceptor in protein or other complicated systems.

With both properties discussed above, this graphical method is potentially useful for a variety of applications.

References and Notes

[1] (a) For example, for ET in biological processes there is a review article by B. E. Bowler, A. L. Raphael and H. B. Gray, *Prog. Inorg. Chem.* **38**, 259 (1990) and references cited therein. C. C. Moser, J. M. Keske, K. Warncke, R. S. Farid and P. L. Dutton, *Nature* **355**, 796 (1992): I. Bertini, H. B. Gray, S. J. Lippard and J. Valentine, *Bioinorganic Chemistry* University Science Books, Mill Valley, CA (1994); (b) for organic bridges, see, for example, G. L. Closs and J. R. Miller, *Science* **240**, 440 (1988); (c) for theoretical works on the electronic coupling of long range ET, see, for example, S. Larsson and M. Braga, *Int. J. Quantum Biol. Symp.* **S20**, 65 (1993) and references cited therein: J. Logan and M. D. Newton, *J. Phys. Chem.* **92**, 3049 (1988); M. D. Newton, *Chem. Rev.* **91**, 767 (1991) and references cited therein; J. R. Reimers and N. S. Hush, *Chem. Phys.* **146**, 89 (1990); J. N. Onuchic, P. C. P. de Andrade and D. N. Beratan, *J. Chem. Phys.* **95**, 1131 (1991); P. Siddarth and R. A. Marcus, *J. Phys. Chem.* **97**, 13078 (1993), and references cited therein; (d) P. Siddarth and R. A. Marcus, *ibid* **96**, 3213 (1992); *ibid* **97**, 2400 (1993).

[2] V. Mujica, M. Kemp and M. A. Ratner, *J. Chem. Phys.* **101**, 6849 (1994).

[3] J. W. Evenson and M. Karplus, *J. Chem. Phys.* **96**, 5272 (1992).

[4] D. N. Beratan and J. J. Hopfield, *J. Am. Chem. Sec.* **106** 1584 (1984); D. N. Beratan, J. N. Onuchic and J. J. Hopfield, *J. Chem. Phys.* **86**, 4488 (1987).

[5] For example, see A. A. Stuchebrukhov, *Chem. Phys. Lett.* **225**, 55 (1994); A. A. Stuchebrukhov and R. A. Marcus, *J. Phys. Chem.* **99**, 7581 (1995).

[6] Experimental investigations of electron transfer across self-assembled monolayers on electrode surfaces include those of J. N. Richardson, S.R. Peck, L. S. Curtin, L. M. Tender, R. H. Terrill, M. T. Carter, R. W. Murray, G. K. Rowe and S.

E. Creager, *J. Phys. Chem* **99**, 766 (1995); R. J. Forster and L. R. Faulkner, *J. Am. Chem. Soc.* **116**, 5444 (1994); *ibid* **116**, 9411 (1994); J. F. Smalley, S. W. Feldberg, C. E. D. Chidsey, M. R. Linford, M. D. Newton and Y. P. Liu, *J. Phys. Chem* **99**, 13141 (1995); M. S. Ravenscroft and H. O. Finklea, *J. Phys. Chem* **98**, 3843 (1994); Z. Q. Feng, S. Imabayashi, T. Kakiuchi and K. Niki, *J. Elec. Chem.* **394**, 149 (1995).

[7] C. E. D. Chidsey, *Science* **251**, 919 (1991); *ibid.* **252**, 631 (1991).

[8] A. M. Becka and C. J. Miller, *J. Phys. Chem.* **96**, 2657 (1992).

[9] M. T. Carter, G. K. Rowe, J. N. Richardson, L. M. Tender, R. H. Terrill and R. W. Murray, *J. Am. Chem. Soc* **117**, 2896 (1995).

[10] V. Mujica, M. Kemp and M. A. Ratner, *J. Chem. Phys.* **101**, 6856 (1994); M. Kemp, V. Mujica and M. A. Ratner, *J. Chem. Phys.* **101**, 5172 (1994); M. Kemp, A. Roitberg, V. Mujica, T. Wanta and M. A. Ratner, *J. Phys. Chem.* **100**, 8349 (1996).

[11] (a) For studies involving large scale Green's function calculations, see, for example, S. S. Skourtis, J. J. Regan and J. N. Onuchic, *J. Phys. Chem.* **98**, 3379 (1994); S. S. Skourtis and J. N. Onuchic, *Chem. Phys. Lett.* **209**, 171 (1993); **211**, 282 (1993); A. A. S. da Gama, *J. Theoret. Biol.* **142**, 251 (1990); M. A. Ratner, *J. Phys. Chem.* **94**, 4877 (1990); J. Malinsky and Y. Magarshak, *J. Phys. Chem* **92**, 2849 (1992); J. W. Evenson and M. Karplus, *Science* **262**, 1247 (1993). (b) for other methods for long range ET, see A. Kuki and P. G. Wolynes, *Science* **236** 1647 (1987); L. S. Conrad, K. V. Mikklesen, M. K. Nielsen and J. Ulstrup, *Inorg. Chem.* **29**, 2808 (1990); S. F. Sneddon and C. L. Brooks, *J. Am. Chem. Soc.* **114**, 8220 (1992); J. M. Gruschus and A. Kuki, *J. Phys. Chem.* **97**, 5581 (1993); A. Okada, T. Kakitani and J. Inoue, *J. Phys. Chem.* **99**, 2946 (1995), among others.

[12] H. M. McConnell, *J. Chem. Phys.* **35**, 508 (1961); the single band problem is also solved and discussed in detail by K. F. Herzfeld, *J. Chem. Phys.* **10**, 508 (1942).

[13] S. Larsson, *J. Am. Chem. Soc.* **103**, 4034 (1981); Cf P. O. Löwdin, *J. Mol. Spectrosc.* **10**,12 (1963); *J. Math. Phys.* **3**,969 (1962).

[14] E. N. Economou, *Green's Functions in Quantum Physics*, 2nd ed. (Springer-Verlag, Berlin, 1990).

[15] The overlap integrals S_{ij} of the atomic orbitals in tight-binding model were treated in the following way: (1) The overlap integrals were only nonzero within each CH_2 bridge unit. (2) Within each CH_2, the molecular orbitals are obtained by solving the linear equation $\mathbf{hp} = \mathbf{e}S\mathbf{p}$ for $\mathbf{e}$ and $\mathbf{p}$, where $\mathbf{h}$ is the Hamiltonian, S is the overlap integral, $\mathbf{e}$ is a diagonal matrix with the eigenvalues as its diagonal matrix elements and $\mathbf{p}$ is composed of column eigenvectors ($\mathbf{p} = (\vec{v}_1, \cdots, \vec{v}_m)$). Solving the above equation is equivalent to solving the usual eigenvalue and eigenvector problem $\mathbf{h}'\mathbf{p}' = \mathbf{e}\mathbf{p}'$, where $\mathbf{h}' = S^{-1/2}\mathbf{h}S^{-1/2}$ and $\mathbf{p}' = S^{1/2}\mathbf{p}S^{1/2} = S^{1/2}(\vec{v}_1, \cdots, \vec{v}_m)S^{1/2}$, and $\mathbf{p}'$ forms an orthonormal basis set with which Eq. (1.8) is written.

[16] S. G. Davison and M. Stęślicka, *Basic Theory of Surface States*, (Clarendon Press, Oxford, 1992).

[17] The first non-zero contribution of $G^{(n)}_{(1,n)}$ in the perturbative expansion of Eq. (1.12) is the first-order term $\mathcal{G}^{(n)}_0\mathcal{H}^{(n)}_1\mathcal{G}^{(n)}_0$. With Eqs. (1.13) and (1.18) the first-order contribution to $G^{(n)}_{(1,n)}$ can be obtained as $G^{(n-1)}_{(1,n-1)}\mathbf{v}\Delta^{-1}$. So $G^{(n)}_{(1,n)} \approx G^{(2)}_{(1,2)}(\mathbf{v}\Delta^{-1})^{n-2}$. This expression is similar to Eq. (1.3), which is McConnell's estimation.

[18] If we denote $G^{(n)}_{(1,n)} = G^{(2)}_{(1,2)}\mathbf{x}_n$ with $\mathbf{x}_n \equiv \prod_{i=3}^{n}\mathbf{v}\Delta^{-1}N_i$, then $\mathbf{x}_n$ has solution $\mathbf{x}_n = [\alpha_1^{n-3}\mathbf{m}_1 - \alpha_2^{n-3}\mathbf{m}_2]^{-1}$, for $n \geq 3$ with

$$\alpha_1 = \Delta\mathbf{v}^{-1}/2 + \delta, \quad \alpha_2 = \Delta\mathbf{v}^{-1}/2 - \delta,$$

$$\mathbf{m}_1 = \alpha_1\delta^{-1}\alpha_1/2 - \delta^{-1}\alpha_1\mathbf{v}^T\Delta^{-1}N_2/2,$$

$$\mathbf{m}_2 = \alpha_2\delta^{-1}\alpha_2/2 - \delta^{-1}\alpha_2\mathbf{v}^T\Delta^{-1}N_2/2$$

and δ is a matrix that satisfies $\delta^2 = -\mathbf{v}^T\mathbf{v}^{-1} + (\Delta\mathbf{v}^{-1})^2/4$. It is seen that upon matrix inversion to obtain $\mathbf{x}_n$, the eigenvalue that is the smallest in modulus of $[\alpha_1^{n-3}\mathbf{m}_1 - \alpha_2^{n-3}\mathbf{m}_2]$ is the most important, while in numerical calculation of $\alpha_{1,2}^{n-3}$ for large n, the smaller eigenvalues of $\alpha_{1,2}$ are usually not preserved. In the present form, a specially designed algorithm would be needed in any numerical calculation using above expressions.

[19] The factor β is conventionally defined as either of the following: $k_{ET} \propto e^{-\beta d}$, or $|\bar{V}|^2 \propto e^{-\beta d}$ (Eq. (1.30)). They are slightly different because the reorganizational energy λ is dependent of distance. Here, the latter definition was used, with d being taken as the number of methylene units.

[20] For integrating over the electronic energy levels in the metal the weighting function in Eq. (6) of R.A. Marcus, *J. Chem. Phys.* **43**, 679 (1965) is used, noting that only the second two factors there vary much with the ϵ in Eq. (6) there.

[21] R. A. Marcus, *J. Chem. Soc. Faraday Trans.* **92**, 3905 (1996).

[22] R. A. Marcus and N. Sutin, *Biochim. Biophys. Acta.* **811**, 265 (1985).

[23] For treating the electronic matrix elements, a method similar to that in H. Ou-Yang, B. Källebring and R.A. Marcus, *J. Chem. Phys.* **98**, 7565 (1993) is used.

[24] R. Hoffmann, *J. Chem. Phys.* **39**,1397 (1963).

[25] J. Hautman and M. L. Klein, *J. Chem. Phys.* **91**, 4994 (1989).

[26] N. Camillone III, C. E. D. Chidsey, G.-Y. Liu and G. Scoles, *J. Chem. Phys.* **98**, 3503 (1993).

[27] International Union of Crystallography, *Structure Reports* **20**, 550 (1956); **35B**, 550 (1970).

[28] A list of the coordinate used for the calculation of those molecules was deposited with the Physics Auxiliary Publication Service (PAPS) of the AIP. A figure showing the geometry of the principal chain and a neighboring chain is also given there.

[29] R. Parsons, *Pure Appl. Chem* **37**, 501 (1974).

[30] S. Trasatti, *Electrochimica Acta* **35**, 269 (1990).

[31] N. W. Ashcroft and N. D. Mermin, *Solid State Physics* (W.B. Saunders Co., 1976), p. 354.

[32] S. Trasatti, *Pure Appl. Chem* **58**, 955 (1986).

[33] *CRC Handbook of Chemistry and Physics*, D.R.Lide, ed., 73rd ed. (CRC Press, 1992-93).

[34] K. Seki, N. Ueno, U. O. Karlsson, R. Engelhardt and E. E. Koch, *Chem. Phys.* **105**, 247 (1986); Ch. Zubrägel, F. Schneider, M. Neumann, G. Hähner, Ch. Wöll and M. Grunze, *Chem. Phys. Lett.* **219**, 127 (1994).

[35] K. J. Less and E. G. Wilson, *J. Phys C: Solid State Phys.* **6**, 3110 (1973); M. Fujihira and H. Inokuchi, *Chem. Phys. Lett* **17**, 554 (1972).

[36] A. P. Cracknell and K. C. Wong, *The Fermi Surface, Its Concept, Determination and Use in the Physics of Metals* (Clarendon Press, Oxford, 1973).

[37] The calculation of effective coupling $\overline{\mid H_{Dk} \mid^2}$ does not depend on λ (Eqs. (1.43) and (1.44)), so the calculation for various of chain lengths is a straightforward generalization without considering the dependence of λ on the chain length n. For calculating the reaction rate with Eq. (1.30), proper values of λ are needed for different chain lengths, which has been discussed in the following reference: Y.P. Liu and M.D. Newton, *J. Phys. Chem.* **98**, 7162 (1994).

[38] C. Goldman, *Phys. Rev. A* **43**, 4500 (1991).

Table 1.1: The effective coupling strengths for $n = 12$, with additional thiol molecules.

no. of additional thiol chains	effective coupling $\overline{\lvert H_{Dk}\rvert^2} \times 10^9$, eV^2atom
0	2.15
1	1.88
2	1.95
3	1.94

Figure 1.1: Free energy *vs.* reaction coordinate for the reactant (curve I) and product (curve II) states of the bridge-mediated electron transfer reaction at an electrode. Curve III is the superexchange off-resonant state for an electron transfer scheme. D is the donor molecule, a ferrocenylcarboxyl group in the present case. $\Delta E(q^\dagger)$ is the energy difference of curves I and III at the transition state.

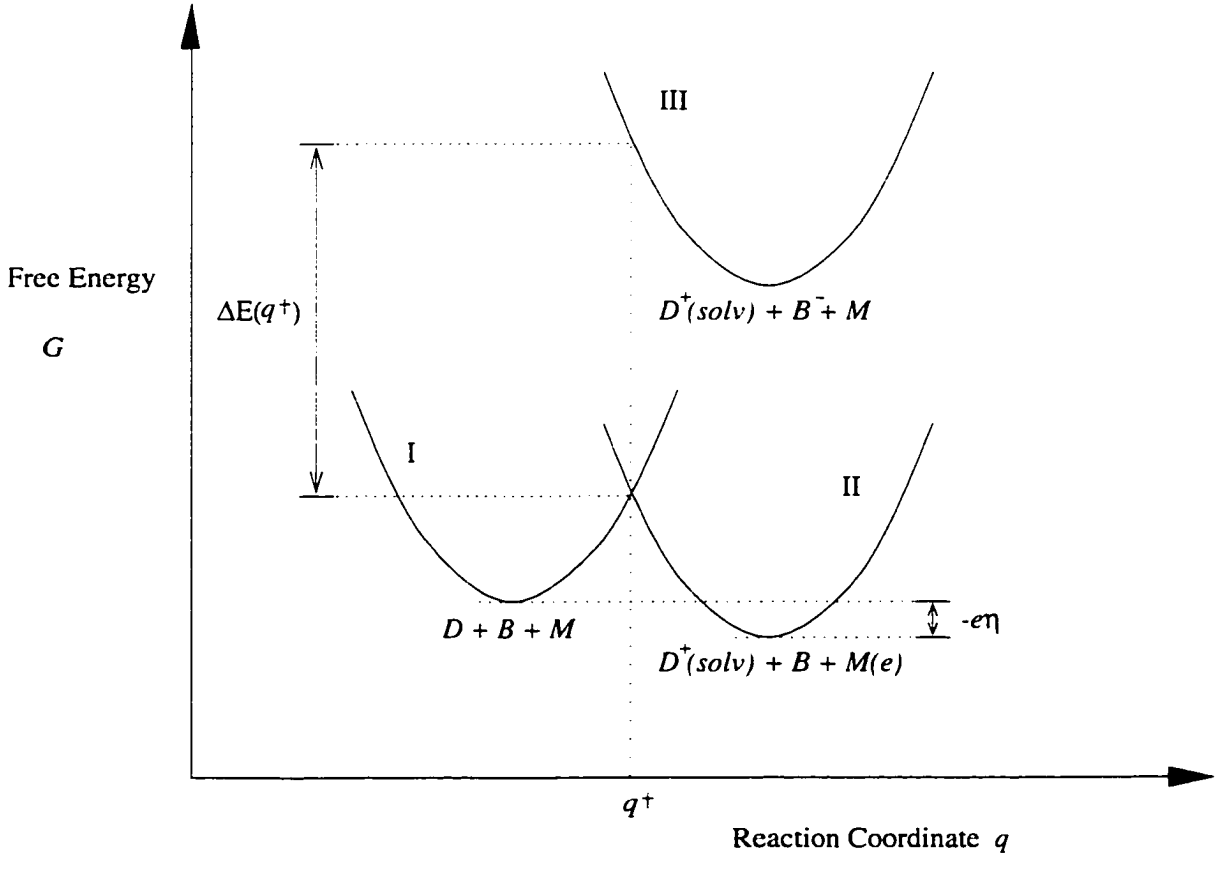

Figure 1.2: The statistics of the energy levels of $C_{40}H_{80}$, from the extended Hückel calculation. Part I shows the statistics of the energy levels before any adjustment. Part II shows these energy levels after the adjustment described in text. The thick bar indicates the position of the energy of the electron being transferred at the transition state (−5.22 eV). Bands (a) and (b) are valence bands. There is a band located between 26 eV and 72 eV that is not shown in this figure. It and band (c) are conduction bands. In the counting the energy axis was divided into cells of 0.66 eV.

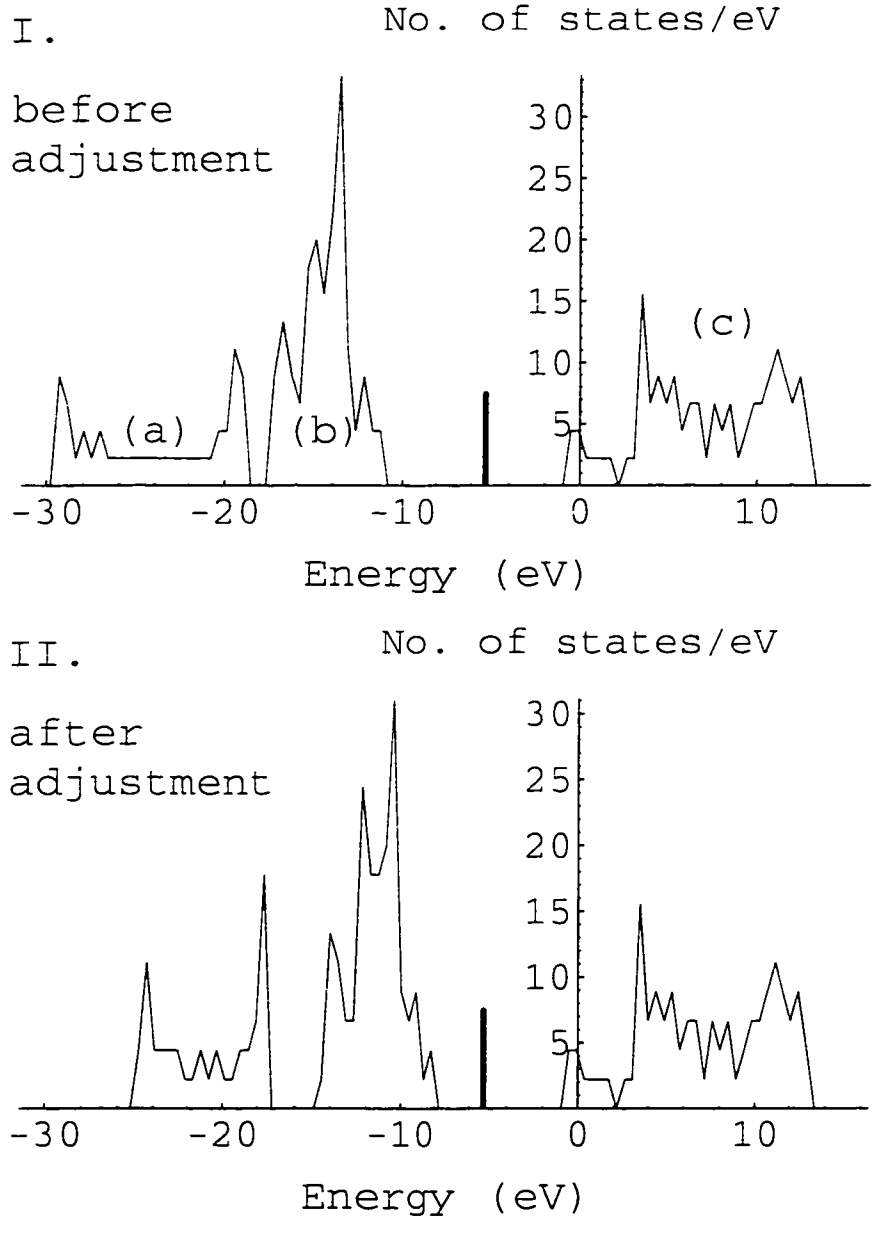

Figure 1.3: Similar to Fig. 1.2. Part I shows the statistics of the energy levels of $C_{40}H_{80}$ from the tight-binding Hamiltonian, while part II shows the statistics of the energy levels after the adjustment described in text. From 30 eV to 35 eV, there is another unfilled band which is not shown. The cell size is now 0.45 eV.

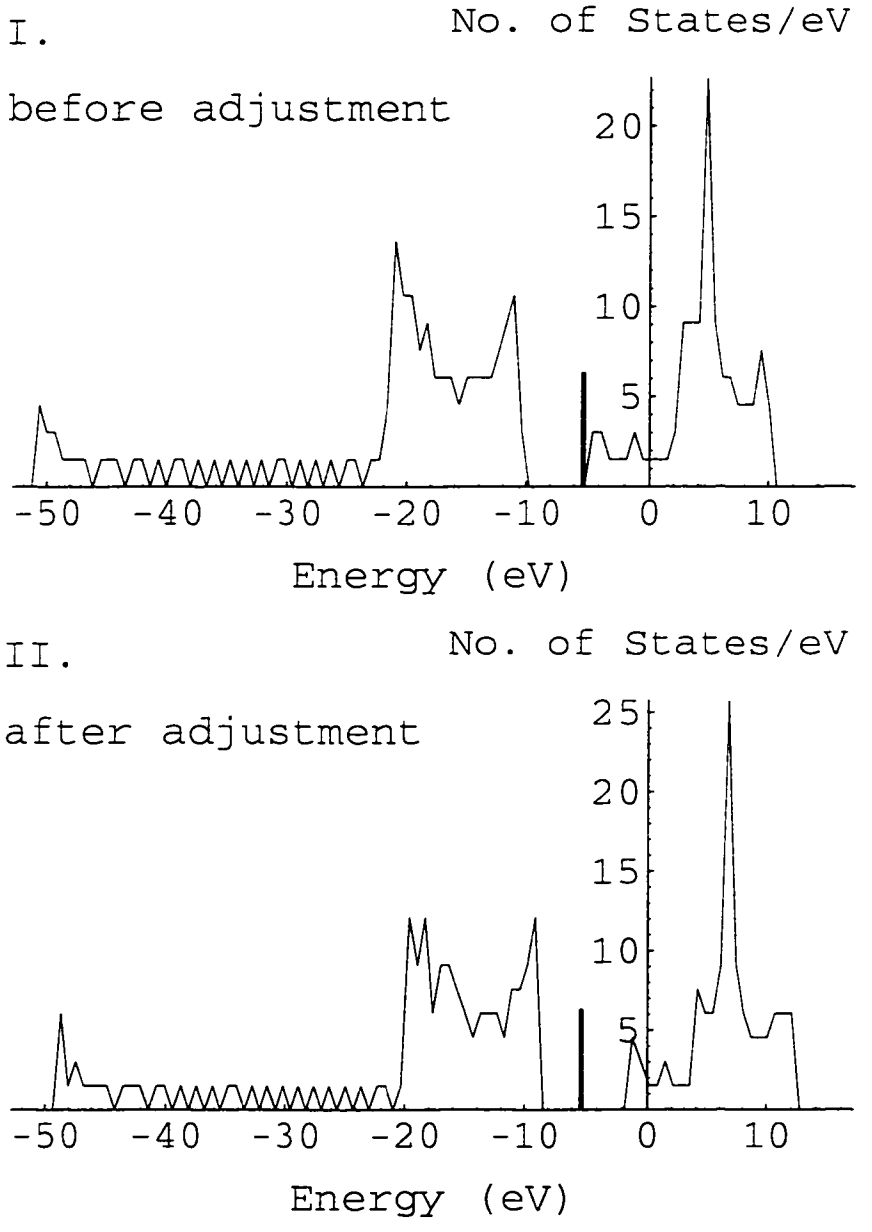

Figure 1.4: Semi-log plot for $\overline{|H_{Dk}|^2}$ as a function of number of methylene units in the bridge. Results are obtained from the sequential formula.

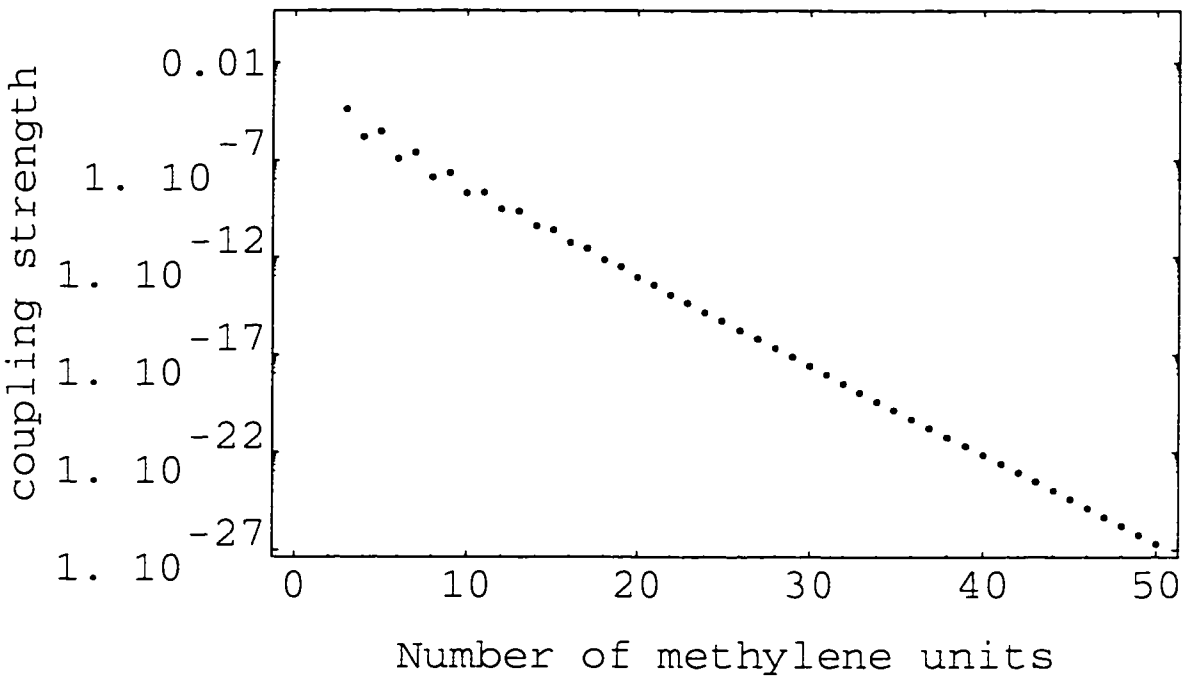

Figure 1.5: A plot for $\log_e \overline{|H_{Dk}|^2}$ vs. different bridge lengths. "o" denotes that for direct summation, "•" from the sequential formula. The difference between the two sets of data is mainly due to their Hamiltonians. See text for the discussions.

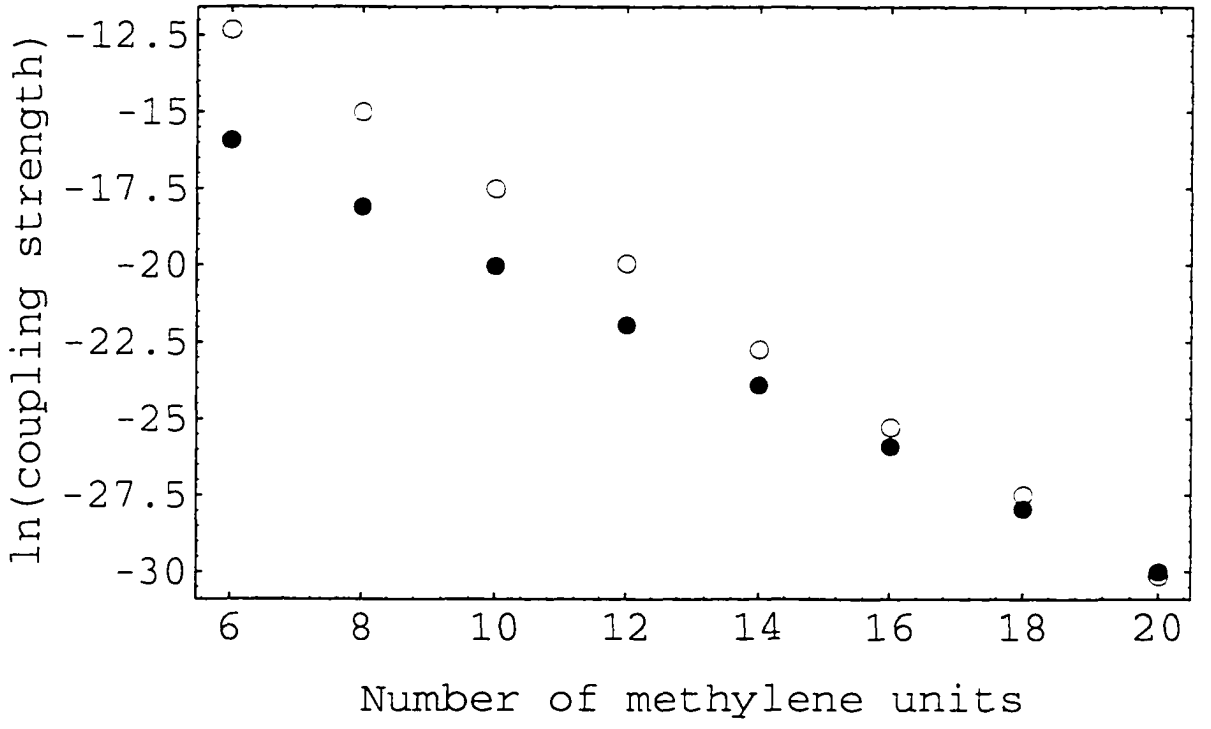

Figure 1.6: Semi-log plot for the same calculation as in Fig. 1.4. except the energy of the electron is shifted to another region for the purpose of demonstrating the effect of oscillation caused by the pair of conjugate complex eigenvalues of the matrix $\mathbf{v}\Delta^{-1}N_n$.

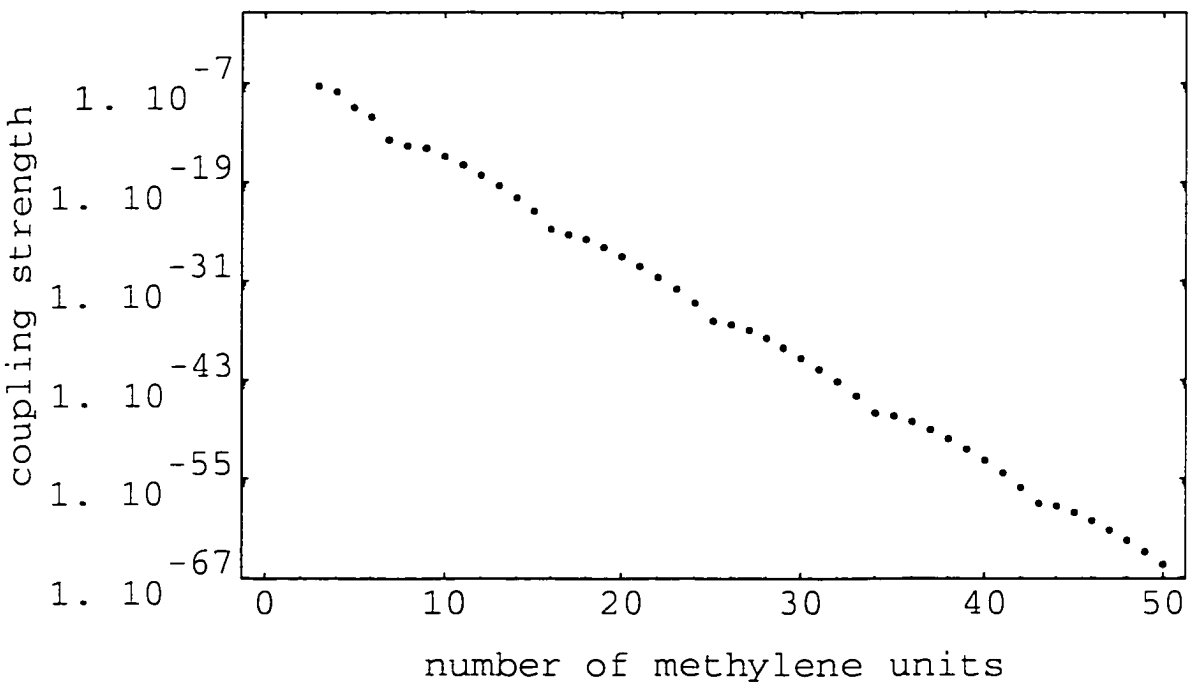

Figure 1.7: Graph representation for the multiple-band tight-binding Hamiltonian. Each vertical column represents a bridge unit. The dots in each column correspond to molecular orbitals in each bridge unit. Lines connecting two dots represent the coupling between the two orbitals, represented by the pair of dots. The lines only connect dots in nearest-neighbor columns. To evaluate the Green's function, all possible pathways from one dot to the other are included, as described in the text.

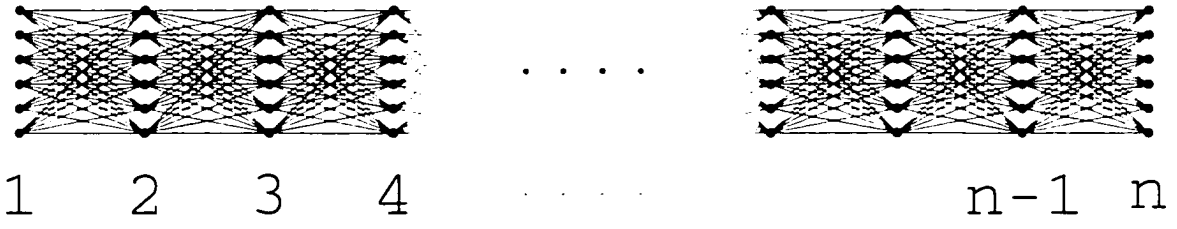

Figure 1.8: A possible path that crosses the dividing column (shaded bar at site $n-1$) three times. ('Visiting' but then returning does not count as 'crossing'.)

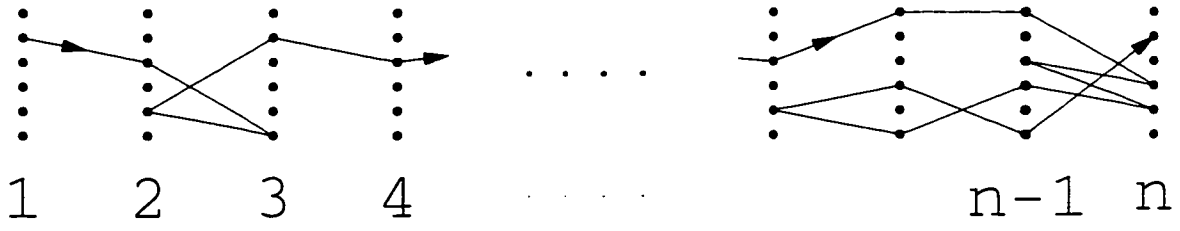

Figure 1.9: A possible path for calculating $F^{(2)}_{(n-1,n)}$.

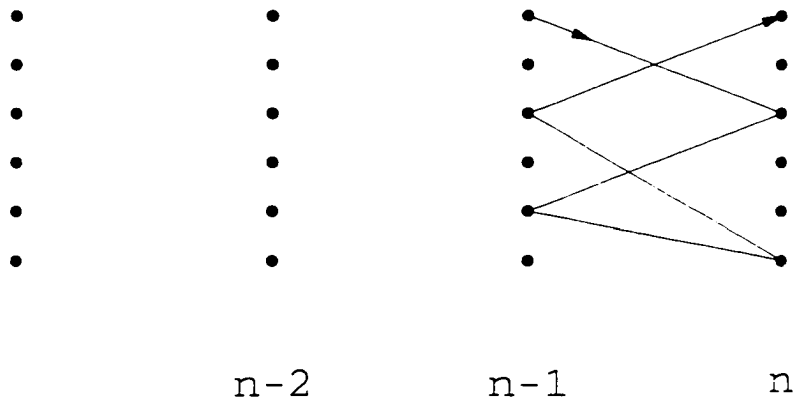

Figure 1.10: A possible path for calculating $F^{(2)}_{(n-1,n-1)}$.

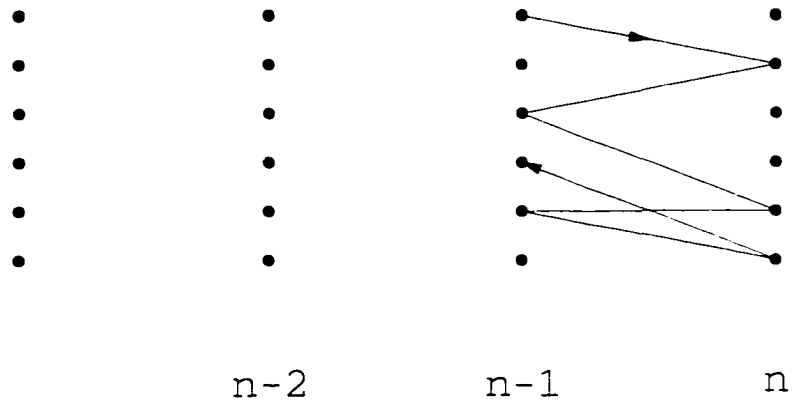

Supplemental Material:

The Geometry of Ferrocenylcarboxy-Terminated Alkanethiol Molecules Attached on Au(111) Surface

In this supplement we present the geometries of molecules calculated in the above paper. For all the extended Hückel calculations, the surface gold atoms are placed on the $z = 0$ plane and the origin is placed at one of the triple hollow sites and the S atom is placed above it. The y-axis is chosen to be the direction of the tilting of the alkane chains. It is also parallel to one of the lines connecting nearest neighbors of gold atoms on this (111) plane. The ferrocenylcarboxyl groups are all of the same orientation and geometry except being shifted for different lengths of alkane thiols. All of the bond lengths and bond angles are obtained from Ref. [25-27] of present work. The only undetermined parameters are the dihedral angles of C15–C16–O(1)–C(101a) and C16–O(1)–C(101a)–C(101), using $n = 16$ as an example. These were chosen to be π and $4\pi/5$ (measured from C16–O(1) bond to C(101a)–C(101) bond counterclockwise, viewed from the direction of O(1) to C(101a)), respectively. The angles were selected among the possible combinations that do not cause an overlap of neighboring alkanethiol chains and that have a reasonable closest atom-to-atom distance (1.6 Å).

In Table 1.S1 the geometry is given for a ferrocenylcarboxyl alkanethiol with $n = 16$, while in Table 1.S2 it is extended to $n = 20$. Table 1.S3 - 1.S5 gives the geometries of molecules for obtaining the coupling strengths listed in Table 1.1 in the main text. The molecules listed in Table 1.S3 and Table 1.S4 are also plotted in Fig. A.7. All the above Tables are for the direct summation calculation. For the sequential formula, the geometry used is the same except that a translational symmetry of CH_2 units is now assumed. In the coordinates in from Ref. [25] for Tables 1.S1 - 1.S5, a thermal fluctuation of the alkanethiol chain was allowed. In Table 1.S6 the coordinate of a ferrocenylcarboxyl alkanethiol molecule with $n = 16$ is given as an example; the coordinate system has been rotated to make easier the

manipulation of the sequential formula developed in this article.

Table 1.S1: The list of Cartesian coordinate (in Å) of atoms in a ferrocenylcarboxyl alkanethiol (cp-Fe-cp-$CO_2C_{16}H_{32}S$) molecule attached on Au(111) surface.

	x	y	z
S-0	0.018571755	-0.04664499	2.407167673
C-1	-0.39778560	1.48973453	3.306130886
C-2	0.286785692	1.587551951	4.670936584
C-3	-0.37827926	2.773877144	5.371808052
C-4	0.262169033	2.985922575	6.745038986
C-5	-0.40408793	4.213794708	7.369003296
C-6	0.195327535	4.450256824	8.756694794
C-7	-0.39179584	5.715893745	9.384667397
C-8	0.221053079	5.96000992	10.76514816
C-9	-0.42140319	7.189139843	11.41118812
C-10	0.200888842	7.411930561	12.79104995
C-11	-0.31154300	8.718402863	13.40025901
C-12	0.382984847	8.948454857	14.74383258
C-13	-0.23381964	10.16055774	15.44473075
C-14	0.37956515	10.33493804	16.83550453
C-15	-0.21606539	11.57585239	17.50352859
C-16	0.321302329	11.68040657	18.93223571
H-1a	-1.42649769	1.540677071	3.450201035
H-2a	1.306356192	1.757302761	4.555782318
H-3a	-1.39342498	2.581081867	5.489743233
H-4a	1.283828871	3.149250031	6.640488148
H-5a	-1.42766606	4.050450802	7.453894615
H-6a	1.226217866	4.557302952	8.670635223
H-7a	-1.42125868	5.60448885	9.481595993
H-8a	1.244048119	6.118290424	10.66502094
H-9a	-1.44500613	7.034953117	11.51150322
H-10a	1.235515475	7.460046768	12.69706821
H-11a	-1.33970975	8.655475616	13.54561996
H-12a	1.396063209	9.120645959	14.58372974
H-13a	-1.25995063	10.01869487	15.53708839
H-14a	1.409625769	10.44884109	16.74831962
H-15a	-1.25272822	11.49573326	17.52613449
H-16b	1.360864639	11.70174980	18.91091728
H-1b	-0.08879834	2.295088768	2.725156307
H-2b	0.140161812	0.713752687	5.215524673
H-3b	-0.25275963	3.630683763	4.795701981
H-4b	0.10412693	2.151144981	7.344846249
H-5b	-0.23444438	5.046031475	6.768834114

H-6b	-0.01889646	3.63485384	9.365650177
H-7b	-0.18750333	6.529761791	8.770271301
H-8b	0.056262076	5.128283024	11.36738491
H-9b	-0.25344795	8.024157524	10.81441688
H-10b	-0.05401825	6.619444847	13.41438388
H-11b	-0.10024076	9.50894928	12.75849533
H-12b	0.264829516	8.106244087	15.34243106
H-13b	-0.05136734	11.01410388	14.87924766
H-14b	0.17126888	9.496114731	17.41393852
H-15b	0.054426014	12.42441558	16.96652221
H-16a	0.002677655	10.85810089	19.48349952
Fe-000	-0.9044609	15.7255707	22.1995931
C-101	-0.5341181	13.7289537	21.8301841
C-102	-0.1202961	14.0781157	23.1645141
C-103	-1.2722555	14.5736977	23.8723191
C-104	-2.3980275	14.5308227	22.9754361
C-105	-1.9418336	14.0087427	21.7133271
C-201	-1.2748038	17.7221877	22.5690021
C-202	-1.6886258	17.3730257	21.2346721
C-203	-0.5366664	16.8774437	20.5268671
C-204	0.5891057	16.9203187	21.4237501
C-205	0.1329117	17.4423997	22.6858591
H-102	0.9008527	13.9826257	23.5731131
H-103	-1.2893339	14.9248617	24.9188411
H-104	-3.4297314	14.8433447	23.2136241
H-105	-2.5623832	13.8507277	20.8140131
H-201	-1.9229869	18.1323677	23.3629971
H-202	-2.7097746	17.4685167	20.8260731
H-203	-0.5195879	16.5262807	19.4803451
H-204	1.6208096	16.6077977	21.1855621
H-205	0.7534613	17.6004137	23.5851731
C-101a	0.3289518	13.1827907	20.7729631
O-101b	1.5154164	12.9804717	20.9723841
O-1	-0.1711625	12.8878357	19.5431311

Table 1.S2: The list of Cartesian coordinate (in Å) of atoms in a ferrocenylcarboxyl alkanethiol (cp-Fe-cp-$CO_2C_{20}H_{40}S$) molecule attached on Au(111) surface. From Table 1.S1, the additional four methylene units (the 17th till the 20th) are extended according to the bond lengths and the averaged bond angles in the previous 16 methylene units.

	x	y	z
S-0	0.018571755	-0.04664499	2.407167673
C-1	-0.3977856	1.48973453	3.306130886
C-2	0.286785692	1.587551951	4.670936584
C-3	-0.37827926	2.773877144	5.371808052
C-4	0.262169033	2.985922575	6.745038986
C-5	-0.40408793	4.213794708	7.369003296
C-6	0.195327535	4.450256824	8.756694794
C-7	-0.39179584	5.715893745	9.384667397
C-8	0.221053079	5.96000992	10.76514816
C-9	-0.42140319	7.189139843	11.41118812
C-10	0.200888842	7.411930561	12.79104995
C-11	-0.311543	8.718402863	13.40025901
C-12	0.382984847	8.948454857	14.74383258
C-13	-0.23381964	10.16055774	15.44473075
C-14	0.37956515	10.33493804	16.83550453
C-15	-0.21606539	11.57585239	17.50352859
C-16	0.321302329	11.68040657	18.93223571
H-1a	-1.42649769	1.540677071	3.450201035
H-2a	1.306356192	1.757302761	4.555782318
H-3a	-1.39342498	2.581081867	5.489743233
H-4a	1.283828871	3.149250031	6.640488148
H-5a	-1.42766606	4.050450802	7.453894615
H-6a	1.226217866	4.557302952	8.670635223
H-7a	-1.42125868	5.60448885	9.481595993
H-8a	1.244048119	6.118290424	10.66502094
H-9a	-1.44500613	7.034953117	11.51150322
H-10a	1.235515475	7.460046768	12.69706821
H-11a	-1.33970975	8.655475616	13.54561996
H-12a	1.396063209	9.120645959	14.58372974
H-13a	-1.25995063	10.01869487	15.53708839
H-14a	1.409625769	10.44884109	16.74831962
H-15a	-1.25272822	11.49573326	17.52613449
H-16a	1.360864639	11.70174980	18.91091728
H-1b	-0.08879834	2.295088768	2.725156307
H-2b	0.140161812	0.713752687	5.215524673
H-3b	-0.25275963	3.630683763	4.795701981
H-4b	0.10412693	2.151144981	7.344846249
H-5b	-0.23444438	5.046031475	6.768834114
H-6b	-0.01889646	3.63485384	9.365650177
H-7b	-0.18750333	6.529761791	8.770271301
H-8b	0.056262076	5.128283024	11.36738491
H-9b	-0.25344795	8.024157524	10.81441688
H-10b	-0.05401825	6.619444847	13.41438388

H-11b	-0.10024076	9.50894928	12.75849533
H-12b	0.264829516	8.106244087	15.34243106
H-13b	-0.05136734	11.01410388	14.87924766
H-14b	0.17126888	9.496114731	17.41393852
H-15b	0.054426014	12.42441558	16.96652221
H-16b	0.002677655	10.85810089	19.48349952
C-17	-0.291605671	12.92008357	19.58678971
H-17a	-1.32112567	12.81280357	19.68764971
H-17b	-0.08610067	13.75129257	18.99648971
C-18	0.33477233	13.11059457	20.96963271
H-18a	1.363391329	13.23007857	20.87338271
H-18b	0.136372329	12.27726457	21.55937171
C-19	-0.278135671	14.35027157	21.62418671
H-19a	-1.307655671	14.24299157	21.72504671
H-19b	-0.072630671	15.18148057	21.03388671
C-20	0.348242329	14.54078257	23.00702971
H-20a	1.376861329	14.66026657	22.91077971
H-20b	0.149842329	13.70745257	23.59676871
Fe-000	-0.8775209	18.5859467	26.2743871
C-101	-0.5071781	16.5893297	25.9049781
C-102	-0.0933561	16.9384917	27.2393081
C-103	-1.2453155	17.4340737	27.9471131
C-104	-2.3710875	17.3911987	27.0502301
C-105	-1.9148936	16.8691187	25.7881211
C-201	-1.2478638	20.5825637	26.6437961
C-202	-1.6616858	20.2334017	25.3094661
C-203	-0.5097264	19.7378197	24.6016611
C-204	0.6160457	19.7806947	25.4985441
C-205	0.1598517	20.3027757	26.7606531
H-102	0.9277927	16.8430017	27.6479071
H-103	-1.2623939	17.7852377	28.9936351
H-104	-3.4027914	17.7037207	27.2884181
H-105	-2.5354432	16.7111037	24.8888071
H-201	-1.8960469	20.9927437	27.4377911
H-202	-2.6828346	20.3288927	24.9008671
H-203	-0.4926479	19.3866567	23.5551391
H-204	1.6477496	19.4681737	25.2603561
H-205	0.7804013	20.4607897	27.6599671
C-101a	0.3558918	16.0431667	24.8477571
O-101b	1.5423564	15.8408477	25.0471781
O-1	-0.1442225	15.7482117	23.6179251

Table 1.S3: The list of Cartesian coordinate (in Å) of atoms in a ferrocenylcarboxyl

dodecanethiol (cp-Fe-cp-$CO_2C_{12}H_{24}S$) molecule attached on Au(111) surface.

	x	y	z
S-0	0.018571755	-0.04664499	2.407167673
C-1	-0.39778560	1.48973453	3.306130886
C-2	0.286785692	1.587551951	4.670936584
C-3	-0.37827926	2.773877144	5.371808052
C-4	0.262169033	2.985922575	6.745038986
C-5	-0.40408793	4.213794708	7.369003296
C-6	0.195327535	4.450256824	8.756694794
C-7	-0.39179584	5.715893745	9.384667397
C-8	0.221053079	5.96000992	10.76514816
C-9	-0.42140319	7.189139843	11.41118812
C-10	0.200888842	7.411930561	12.79104995
C-11	-0.31154300	8.718402863	13.40025901
C-12	0.382984847	8.948454857	14.74383258
H-1a	-1.42649769	1.540677071	3.450201035
H-2a	1.306356192	1.757302761	4.555782318
H-3a	-1.39342498	2.581081867	5.489743233
H-4a	1.283828871	3.149250031	6.640488148
H-5a	-1.42766606	4.050450802	7.453894615
H-6a	1.226217866	4.557302952	8.670635223
H-7a	-1.42125868	5.60448885	9.481595993
H-8a	1.244048119	6.118290424	10.66502094
H-9a	-1.44500613	7.034953117	11.51150322
H-10a	1.235515475	7.460046768	12.69706821
H-11a	-1.33970975	8.655475616	13.54561996
H-12a	1.396063209	9.120645959	14.58372974
H-1b	-0.08879834	2.295088768	2.725156307
H-2b	0.140161812	0.713752687	5.215524673
H-3b	-0.25275963	3.630683763	4.795701981
H-4b	0.10412693	2.151144981	7.344846249
H-5b	-0.23444438	5.046031475	6.768834114
H-6b	-0.01889646	3.63485384	9.365650177
H-7b	-0.18750333	6.529761791	8.770271301
H-8b	0.056262076	5.128283024	11.36738491
H-9b	-0.25344795	8.024157524	10.81441688
H-10b	-0.05401825	6.619444847	13.41438388
H-11b	-0.10024076	9.50894928	12.75849533
H-12b	0.264829516	8.106244087	15.34243106
Fe-000	-0.84277843	12.993619	18.01119
C-101	-0.47243558	10.997002	17.641781
C-102	-0.058613558	11.346164	18.976111
C-103	-1.210573	11.841746	19.683916
C-104	-2.336345	11.798871	18.787033

C-105	-1.8801511	11.276791	17.524924
C-201	-1.2131213	14.990236	18.380599
C-202	-1.6269433	14.641074	17.046269
C-203	-0.4749839	14.145492	16.338464
C-204	0.65078819	14.188367	17.235347
C-205	0.1945942	14.710448	18.497456
H-102	0.96253526	11.250674	19.38471
H-103	-1.2276514	12.19291	20.730438
H-104	-3.3680489	12.111393	19.025221
H-105	-2.5007007	11.118776	16.62561
H-201	-1.8613044	15.400416	19.174594
H-202	-2.6480921	14.736565	16.63767
H-203	-0.45790543	13.794329	15.291942
H-204	1.6824921	13.875846	16.997159
H-205	0.8151438	14.868462	19.39677
C-101a	0.39063436	10.450839	16.58456
O-101b	1.5770989	10.24852	16.783981
O-1	-0.10947999	10.155884	15.354728

Table 1.S4: The list of Cartesian coordinate (in Å) for the first additional alkanethiol molecule ($C_{12}H_{25}S$) attached on the same Au(111) surface, in calculating the effect of through-space coupling (Table 1.1). The long alkane chain of the previous molecule and this alkanethiol form a unit cell in the self-assembly monolayer. The second additional alkanethiol molecule is obtained by shifting -4.997 Å in x direction.

	x	y	z
S-0p	2.4607259	4.351068497	2.410563469
C-1p	2.960823059	5.817650795	3.365255594
C-2p	2.276040554	5.940475941	4.727931976
C-3p	2.761996508	7.225361347	5.401591301
C-4p	2.134157181	7.369000435	6.78942585
C-5p	2.698536634	8.646517754	7.414185524
C-6p	2.114726305	8.841558456	8.814908981
C-7p	2.770359755	10.06203556	9.464123726
C-8p	2.192089081	10.25467300	10.86747455
C-9p	2.791644335	11.51194763	11.50047874
C-10p	2.238713264	11.76659870	12.90415954
C-11p	2.894887924	12.99681377	13.53416347
C-12p	2.278116703	13.22606468	14.91544437

H-1ap	2.731105089	6.664498329	2.80697298
H-2ap	2.520923138	5.1203866	5.318766594
H-3ap	2.492229939	8.042136192	4.817035675
H-4ap	2.378984451	6.546983242	7.377597809
H-5ap	2.447476387	9.461681366	6.819140434
H-6ap	2.303102732	7.996843815	9.391598701
H-7ap	2.578369517	10.90729618	8.889429092
H-8ap	2.423626423	9.427600861	11.45394039
H-9ap	2.568670273	12.33002281	10.89828773
H-10ap	2.428602695	10.93621063	13.50081539
H-11ap	2.72787261	13.82918071	12.93343734
H-12ap	2.448734999	12.39570999	15.51793956
H-1bp	3.988357306	5.772140503	3.519209862
H-2bp	1.244699597	5.979937077	4.599953651
H-3bp	3.797258377	7.192948918	5.495304108
H-4bp	1.099917889	7.440235615	6.706513405
H-5bp	3.733715057	8.570596695	7.479311943
H-6bp	1.088045835	8.992713928	8.746504784
H-7bp	3.797544956	9.912489891	9.528364182
H-8bp	1.159033775	10.35725212	10.80523395
H-9bp	3.823520164	11.39759973	11.56175136
H-10bp	1.212215304	11.92197036	12.84282970
H-11bp	3.91829818	12.83780765	13.62949562
H-12bp	1.25411582	13.38127899	14.82094287
H-12cp	2.796496868	14.05796813	15.26303577

Table 1.S5: The list of Cartesian coordinate (in Å) for the third additional alkanethiol molecule ($C_{12}H_{25}S$) attached on the same Au(111) surface.

	x	y	z
S-0r	5.015571755	-0.04664499	2.407167673
C-1r	4.5992144	1.48973453	3.306130886
C-2r	5.283785692	1.587551951	4.670936584
C-3r	4.61872074	2.773877144	5.371808052
C-4r	5.259169033	2.985922575	6.745038986
C-5r	4.59291207	4.213794708	7.369003296
C-6r	5.192327535	4.450256824	8.756694794
C-7r	4.60520416	5.715893745	9.384667397
C-8r	5.218053079	5.96000992	10.76514816
C-9r	4.57559681	7.189139843	11.41118812
C-10r	5.197888842	7.411930561	12.79104995
C-11r	4.685457	8.718402863	13.40025901

C-12r	5.379984847	8.948454857	14.74383258
H-1ar	3.57050231	1.540677071	3.450201035
H-2ar	6.303356192	1.757302761	4.555782318
H-3ar	3.60357502	2.581081867	5.489743233
H-4ar	6.280828871	3.149250031	6.640488148
H-5ar	3.56933394	4.050450802	7.453894615
H-6ar	6.223217866	4.557302952	8.670635223
H-7ar	3.57574132	5.60448885	9.481595993
H-8ar	6.241048119	6.118290424	10.66502094
H-9ar	3.55199387	7.034953117	11.51150322
H-10ar	6.232515475	7.460046768	12.69706821
H-11ar	3.65729025	8.655475616	13.54561996
H-12ar	6.393063209	9.120645959	14.58372974
H-1br	4.90820166	2.295088768	2.725156307
H-2br	5.137161812	0.713752687	5.215524673
H-3br	4.74424037	3.630683763	4.795701981
H-4br	5.10112693	2.151144981	7.344846249
H-5br	4.76255562	5.046031475	6.768834114
H-6br	4.97810354	3.63485384	9.365650177
H-7br	4.80949667	6.529761791	8.770271301
H-8br	5.053262076	5.128283024	11.36738491
H-9br	4.74355205	8.024157524	10.81441688
H-10br	4.94298175	6.619444847	13.41438388
H-11br	4.89675924	9.50894928	12.75849533
H-12br	5.261829516	8.106244087	15.34243106
H-12cr	4.958294536	9.772737128	15.2174738

Table 1.S6: The list of Cartesian coordinate (in Å) of atoms in a ferrocenylcarboxyl alkane thiol (cp-Fe-cp-$CO_2C_{16}H_{32}S$) molecule attached on Au(111) surface. For a calculation using sequential formula, only interaction matrices between neighboring units are needed. In the present work, the electron donor is the group of surface Au atoms while the acceptor is the ferrocenylcarboxyl group. The first bridge unit is defined as S-CH_2 while all other bridge units are CH_2.

	x	y	z
S-0	0.000000	-1.515278	-1.022684
C-1	0.000000	0.000000	0.000000
C-2	0.000000	1.283165	-0.833298
C-3	0.000000	2.566332	0.000000
C-4	0.000000	3.849498	-0.833298

C-5	0.000000	5.132664	0.000000
C-6	-0.000001	6.415830	-0.833297
C-7	-0.000001	7.698996	0.000001
C-8	0.000000	8.982162	-0.833297
C-9	-0.000001	10.265328	0.000001
C-10	-0.000001	11.548494	-0.833297
C-11	0.000000	12.831660	0.000000
C-12	-0.000001	14.114825	-0.833297
C-13	0.000000	15.397991	0.000001
C-14	0.000000	16.681158	-0.833297
C-15	0.000000	17.964324	0.000000
C-16	-0.000001	19.247489	-0.833297
H-A1	0.819531	0.000001	0.640288
H-A2	0.819531	1.283166	-1.473585
H-A3	0.819531	2.566332	0.640288
H-A4	0.819530	3.849498	-1.473585
H-A5	0.819531	5.132664	0.640288
H-A6	0.819531	6.415830	-1.473585
H-A7	0.819531	7.698996	0.640288
H-A8	0.819531	8.982162	-1.473585
H-A9	0.819531	10.265327	0.640288
H-A10	0.819531	11.548494	-1.473586
H-A11	0.819531	12.831660	0.640288
H-A12	0.819531	14.114826	-1.473585
H-A13	0.819531	15.397991	0.640288
H-A14	0.819531	16.681157	-1.473585
H-A15	0.819531	17.964324	0.640288
H-A16	0.819531	19.247489	-1.473586
H-B1	-0.819532	0.000000	0.640288
H-B2	-0.819531	1.283166	-1.473586
H-B3	-0.819531	2.566332	0.640288
H-B4	-0.819531	3.849498	-1.473586
H-B5	-0.819531	5.132664	0.640288
H-B6	-0.819532	6.415829	-1.473585
H-B7	-0.819531	7.698996	0.640288
H-B8	-0.819531	8.982162	-1.473586
H-B9	-0.819531	10.265327	0.640288
H-B10	-0.819531	11.548493	-1.473585
H-B11	-0.819532	12.831660	0.640289
H-B12	-0.819531	14.114826	-1.473586
H-B13	-0.819532	15.397992	0.640288
H-B14	-0.819532	16.681158	-1.473585
H-B15	-0.819532	17.964323	0.640289
H-B16	-0.819532	19.247489	-1.473585

Fe-000	-0.032405	24.114396	1.369804
C-101	0.674372	22.735601	0.006175
C-102	0.746075	24.065605	-0.541135
C-103	1.583297	24.857555	0.322274
C-104	2.029025	24.017003	1.403198
C-105	1.467279	22.705563	1.207838
C-201	-0.739181	25.493192	2.733433
C-202	-0.810884	24.163189	3.280742
C-203	-1.648107	23.371238	2.417334
C-204	-2.093835	24.211790	1.336409
C-205	-1.532089	25.523231	1.531769
H-102	0.246830	24.416505	-1.461156
H-103	1.838615	25.922217	0.180417
H-104	2.686066	24.324100	2.235548
H-105	1.618034	21.830697	1.864115
H-201	-0.175312	26.340987	3.160180
H-202	-0.311639	23.812288	4.200764
H-203	-1.903426	22.306577	2.559191
H-204	-2.750876	23.904693	0.504061
H-205	-1.682844	26.398096	0.875492
C-101a	-0.076432	21.606744	-0.562049
O-101b	-0.721055	21.734638	-1.589914
O-1	-0.073351	20.388382	0.042253
Au-020d	1.992320	-5.993091	-1.930926
Au-120d	-1.549773	-5.904283	-5.454471
Au-110c	3.909555	-4.386722	3.268755
Au-010d	0.367462	-4.297913	-0.254790
Au-110d	-3.174631	-4.209105	-3.778334
Au-100b	2.284697	-2.691544	4.944891
Au-000a	-1.257396	-2.602735	1.421347
Au-100a	-4.799488	-2.513927	-2.102198
Au-110b	0.659840	-0.996365	6.621028
Au-010a	-2.882253	-0.907557	3.097483
Au-110a	-6.424346	-0.818749	-0.426061
Au-120b	-0.965018	0.698813	8.297165
Au-020a	-4.507111	0.787621	4.773620
Au-120a	-8.049203	0.876430	1.250076
Au-030a	-6.131968	2.482799	6.449757
Au-121c	4.575795	-6.885085	-1.007222
Au-021d	1.033702	-6.796276	-4.530767
Au-111c	2.950937	-5.189907	0.668914
Au-011d	-0.591156	-5.101098	-2.854630
Au-101b	1.326080	-3.494728	2.345051
Au-001a	-2.216013	-3.405920	-1.178494

Au-101a	-5.758106	-3.317112	-4.702038
Au-111b	-0.298778	-1.799550	4.021187
Au-011a	-3.840871	-1.710742	0.497643
Au-111a	-7.382964	-1.621934	-3.025902
Au-121b	-1.923635	-0.104372	5.697324
Au-021a	-5.465728	-0.015564	2.173780
Au-121a	-9.007821	0.073245	-1.349765
Au-131b	-3.548493	1.590806	7.373461
Au-031a	-7.090586	1.679614	3.849916

Figure 1.S1: A three-dimensional plot for the ferrocenylcarboxyl dodecanethiol (cp-Fe-cp-$CO_2C_{12}H_{24}S$) molecule and the first additional dodecanethiol as described in Tables 1.S3 and 1.S4. The hydrogen atoms of the ferrocene part are omitted.

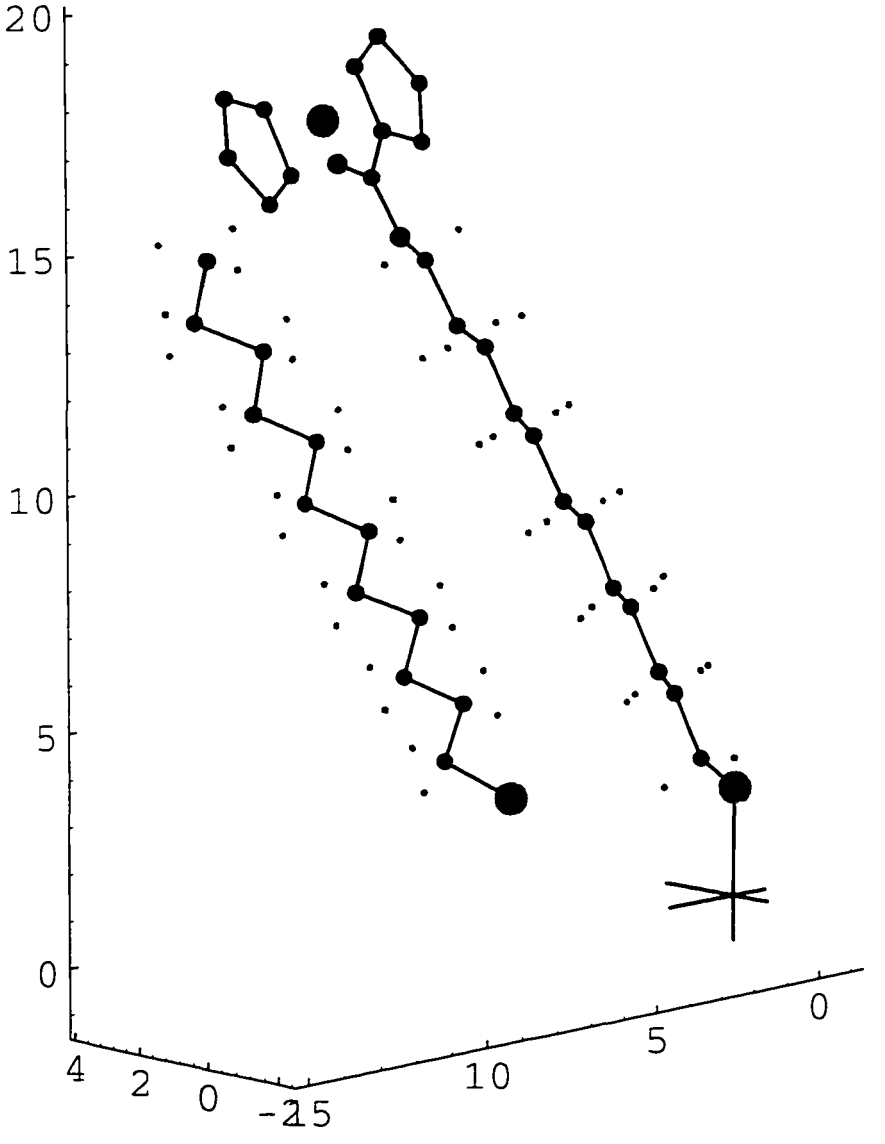

Chapter 2 Application of the Sequential Formula: the Electronic Coupling and the Distance Dependence in the Electron Transfer of Ferrocene-Terminated Alkanethiol Monolayers

Chao-Ping Hsu

Arthur Amos Noyes Laboratory of Chemical Physics, 127-72

California Institute of Technology, Pasadena, CA 91125

(Reprinted with permission from *J. Electroanaly. Chem.*, **438**, pp.27 - 35.

Abstract

A sequential formula developed by Hsu and Marcus [J. Chem. Phys. **106**, 584 (1997)] is applied to calculate the electronic coupling between a gold electrode and each of the molecules, $(\eta^5\text{-}C_5H_5)Fe(\eta^5\text{-}C_5H_4)CO_2(CH_2)_nSH$ and $(\eta^5\text{-}C_5H_5)Fe(\eta^5\text{-}C_5H_4)(CH_2)_nSH$ (n = 3 to 50). Most of the calculated coupling strengths, if converted to rate constants according to a high-temperature nonadiabatic expression, agree well with the experimental rate constants. The exponential coefficients are obtained by a linear fit of the logarithm of the coupling strengths to the chain length. The calculated exponential coefficient is 1.05 per methylene unit for both molecules and for large n. For shorter chains the exponential coefficient is slightly larger with an irregularity caused by an oscillation of coupling strengths between even and odd number of units. The physical origin of such oscillation among short chains is discussed.

2.1 Introduction

The recent development of self-assembled monolayers of alkanethiol molecules on a gold surface [1] has provided a convenient approach for studying electron transfer reactions (ET) between an electroactive group and an electrode, where the electroactive group is held at a fixed distance from the electrode surface, or, if in solution, is separated from the electrode by a fixed monolayer [2]. Chidsey [3] measured the voltage dependent ET rate of the $(\eta^5\text{-}C_5H_5)Fe(\eta^5\text{-}C_5H_4)CO_2(CH_2)_{16}SH$/gold surface system and a reorganization energy λ was estimated from the dependence of reaction rates on the overpotential η. Both the direct-linked $(\eta^5\text{-}C_5H_5)Fe(\eta^5\text{-}C_5H_4)(CH_2)_8SH$ and the ester-linked $(\eta^5\text{-}C_5H_5)Fe(\eta^5\text{-}C_5H_4)CO_2(CH_2)_8SH$ in the monolayers were studied at low temperatures by Richardson *et al.* [4] The λ's were extracted from the Arrhenius (activation) plots.

The distance dependence of ET reactions were also studied with the self-assembled monolayers. The exponential factor β is conventionally defined as either of the following:

$$k_{ET} \propto e^{-\beta d}. \tag{2.1}$$

or

$$(\text{the pre-exponential factor}) \propto e^{-\beta d}. \tag{2.2}$$

The two definitions are slightly different because the reorganization energy λ is dependent on distance (cf. Eq. (2.9) below). d can be taken as the number of bridge units for a linear bridge composed of homogeneous units, or the distance between the donor and acceptor groups.

A study involving electrodes coated with self-assembled monolayers of ω-hydroxy thiols of various lengths (the number of CH_2 units are 6 to 11) was performed by Becka and Miller [5], and an exponential factor $\beta = 1.08 \pm 0.20$ per methylene unit was reported for a series of redox couples. Carter *et al.* [6] studied different lengths of the ester-linked alkanethiol molecules ($CpFeCpCO_2(CH_2)_nSH$ with $n = 8, 12, 16$, $Cp = C_5H_5$ or C_5H_4) at low temperatures. The distance dependence over the above

range was obtained and the decay factor for the pre-exponential factors was reported as $\beta = 1.44 \pm 0.12$ per methylene unit. The ester-linked system was also studied by Smalley and coworkers [7], for $n = 5$ to 9. The exponential factor was reported as $\beta = 1.21 \pm 0.05/CH_2$ for the reaction rate.

Various theoretical approaches for treating the electronic coupling matrix element H_{DA}, between a donor and an acceptor, have provided estimates of the decay coefficient [8–14]. McConnell gave a molecular derivation of the exponential decay factor [8], providing an estimation from perturbation theory. Studies [9, 10] on molecular wires with one orbital representing each site of the wires show exponential dependence of the conductance on the length of wire when the electron is at an energy outside of the wire's energy band. If the energy of an electron is placed inside the wire's band, large conductances are obtained with oscillatory dependence on wire length. Beratan and Hopfield [11] used another approach with which they were able to treat multiple-band systems (i.e., more than one orbital on each bridge site) by assuming the tunneling wavefunction of the electron is exponentially decaying as it penetrates an off-resonant bridge. *Ab initio* calculations on organic bridges [12] have provided detailed understanding on the schemes of coupling. Calculations using extended Hückel basis [15] have been shown to be a simple and useful approach in obtaining the coupling strengths of electron transfer reactions in proteins and scanning tunneling microscopy[14, 16, 17].

A sequential formula has been formulated for multiple-band, linear chain bridges using a non-perturbative method [18]. In that work, a recursion expression for the Green's function for calculating the effective electronic coupling in bridge-assisted electronic transfer systems, within the framework of the tight-binding Hamiltonian, was formulated. The sequential formula relates the Green's function of a chain bridge to that of the bridge that is one unit less. There is also a detailed description on obtaining the correct position of energy levels of donor (acceptor) from electrochemical data. The use of experimental band structure measurements was also described, for obtaining a better description of energy levels of the chain bridge.

In Section 2.2 the non-adiabatic reaction rate expression is described and an in-

troduction to the sequential formula is given. In Section 2.3 the applications of the sequential formula to molecules **I** (ferrocenylcarboxyl alkanethiol) and **II** (ferrocenyl alkanethiol), as shown in Fig. 2.1, are presented. Discussions regarding the comparison of the calculated coupling strength to experimental data are presented in Section 2.4.1. The calculated coupling strengths have slightly irregular length dependence for short chains, and the physical origin of such behavior is discussed in Section 2.4.2. In Section 2.5 conclusions are presented.

2.2 Theory

For long-range electron transfer, there is little direct electronic coupling between the donor and acceptor groups due to spatial separation. It is therefore important to include the bridge-mediated coupling strength. The overall coupling strength is therefore called *effective coupling*. Derived from scattering theory, the effective coupling can be written as [19]

$$H^{\text{eff}} = V + VGV, \tag{2.3}$$

where G is the Green's function for the Hamiltonian H,

$$G = (E\mathbf{1} - H)^{-1},$$

with E being the energy of the electron being transferred. The Hamiltonian H is composed of an unperturbed H^0 and a perturbation V, where H^0 is the Hamiltonian for non-interacting donor, bridge and acceptor states, and V is the interaction among them. In Eq. (2.3), the effective coupling between donor and acceptor (denoted by H^{eff}_{DA}) is seen to be composed of two terms: the first term (V) describes the direct coupling of the donor and acceptor states while the second term is through the coupling with the bridge. In the following calculations, the Green's function G is approximated by the Green's function for the bridge part which corresponds to the bridge's Hamiltonian. It is a good approximation in the off-resonance condition, namely, when the energy of the electron being transferred is placed outside of the

energy band formed by the infinitely extended bridge [18].

In Section 2.2.1, the ET rate constant between an electrode and a donor group is obtained. The Green's function for the bridge part can be solved using the sequential formula, and the method is sketched in Section 2.2.2.

2.2.1 The Reaction Rate

For the cases of weak coupling between the electron donor and acceptor, the Golden rule provides a satisfactory treatment for the electron transfer reaction rate [20]:

$$k = \frac{2\pi}{\hbar}|H_{DA}^{\text{eff}}|^2(FC), \tag{2.4}$$

where (FC) is the Franck-Condon factor, and H_{DA}^{eff} is the electronic coupling. In the high temperature limit, (FC) is given by [20, 21]:

$$(FC) = (4\pi\lambda k_B T)^{-1/2} \exp\left(-\frac{(\Delta G^0 + \lambda)^2}{4\lambda k_B T}\right) \tag{2.5}$$

where λ is the reorganization energy (including both inner and outer contributions). For ET reactions between an electron donor group and an electrode, the nonadiabatic reaction rate is then obtained by integrating over all possible states in the electrode with the Fermi-Dirac distribution:

$$k = \frac{2\pi}{\hbar}(4\pi\lambda k_B T)^{-1/2} \int d\varepsilon |V(\varepsilon)|^2 e^{-(\lambda - e\eta + \varepsilon)^2/4\lambda k_B T} \frac{e^{\varepsilon/k_B T}}{1 + e^{\varepsilon/k_B T}}, \tag{2.6}$$

where $|V(\varepsilon)|^2$ is

$$|V(\varepsilon)|^2 = \int d^3\vec{k} |H_{Dk}^{\text{eff}}|^2 \delta(\varepsilon(\vec{k}) - \varepsilon), \tag{2.7}$$

in which H_{Dk}^{eff} is used to denote the coupling element between states $\langle D|$ and $|\vec{k}\rangle$. The wavefunctions $|\vec{k}\rangle$ of the metal electrode are normalized to a Dirac delta function, $\langle\vec{k}|\vec{k}'\rangle = \delta(\vec{k} - \vec{k}')$, and ε is the energy of an electron in the metal with respect to the Fermi energy. $\varepsilon(\vec{k})$ is the energy of the electronic state $|\vec{k}\rangle$ of the metal, and η is the overpotential $(E - E^0)$. In general, a summation over energy bands of the metal

electrode is needed in Eq. (2.7). However, since only the contribution from the s-band of the gold electrode is considered in the present work. the summation over energy bands is omitted for simplicity.

The electron transfer rate under electrochemical exchange current conditions (denoted by $k^{(0)}$) can be obtained by setting $\eta = 0$. By noting $\lambda \gg \varepsilon$ we can drop the quadratic term of ε in the exponent of Eq. (2.6). The integration over ε is performed by approximating [21]

$$\int_{-\infty}^{\infty} \frac{1}{e^{\varepsilon/2k_BT} + e^{-\varepsilon/2k_BT}} f(\varepsilon) d\varepsilon \approx \pi k_B T f(0). \tag{2.8}$$

From Eqs. (2.6) and (2.8), the following expression is obtained:

$$k^{(0)} = \frac{2\pi}{\hbar}(4\pi\lambda k_B T)^{-1/2} e^{-\lambda/4k_BT} |\bar{V}|^2. \tag{2.9}$$

where

$$|\bar{V}|^2 = \pi k_B T \int d^3\vec{k} |H_{Dk}^{\text{eff}}|^2 \delta(\varepsilon(\vec{k})) = \pi k_B T \overline{|H_{Dk}|^2} \rho_f. \tag{2.10}$$

with

$$\overline{|H_{Dk}|^2} \equiv \frac{\int d^3\vec{k} |H_{Dk}^{\text{eff}}|^2 \delta(\varepsilon(\vec{k}))}{\int d^3\vec{k} \delta(\varepsilon(\vec{k}))} \tag{2.11}$$

and

$$\rho_f \equiv \int d^3\vec{k} \delta(\varepsilon(\vec{k})); \tag{2.12}$$

i.e., $\overline{|H_{Dk}|^2}$ is the effective coupling strength averaged over the $\vec{k}$'s on the Fermi surface [22].

In the following section, the sequential formula is introduced and the expression for calculating H_{Dk}^{eff} is derived.

2.2.2 The Sequential Formula

For long-range electron transfer with a linear chain bridge, a sequential formula was developed [18] to calculate the effective coupling through the bridge. The bridge part is assumed to be a linear chain of connecting subunits, and a tight-binding Hamilto-

nian with only the nearest-neighbor interaction was assumed. For each bridge unit, the energies of its molecular orbitals and the interaction matrices with its neighboring units are needed. Since it is always possible to invert the matrix $(E\mathbf{1}-H)$ and obtain the Green's function for short bridge chains, the sequential formula was derived by assuming that the Green's function is known for a chain with one less bridge unit. In application, the resulting recursive equations are iterated until the desired length of the bridge is obtained [18].

For simplicity of notation, the following description assumes a uniform chain bridge. The generalization to bridges with different units is sketched in the Appendix. It is also assumed that the bridge has n units, and each unit has m molecular orbitals. For example, if the bridge is a long alkane chain, the bridge unit can be assigned as one CH_2, so n is the number of methylene units in the bridge and m now equals 6. The Hamiltonian and the Green's function are $6n \times 6n$ matrices in this case. These matrices can be divided into $n \times n$ blocks, with each block representing a 6×6 matrix. For H, such blocks describe the interaction between bridge units. We will focus our attention on the $(1,n)$ and (n,n) block of the Green's function, denoted by $G^{(n)}_{(1,n)}$ and $G^{(n)}_{(n,n)}$, respectively. The former is needed for calculating bridge-mediated coupling strength (i.e., for the second term of the right-hand side in Eq. (2.3)), and the latter is needed for iterating the sequential formula.

For a uniform chain bridge, the tight-binding Hamiltonian can be expressed by choosing the molecular orbitals of each unit as the basis. The quantities needed are the energy of the molecular orbitals of a single unit, $\{\varepsilon_1, \varepsilon_2, \cdots, \varepsilon_m\}$, and the interaction between adjcent units, denoted by $\mathbf{v}$, which is a $m \times m$ matrix. Define

$$\Delta = E\mathbf{1} - \mathbf{e}, \tag{2.13}$$

with $\mathbf{e}$ being a diagonal matrix with the energies of the molecular orbitals of the

bridge unit as its diagonal matrix elements:

$$\mathbf{e} = \begin{pmatrix} \varepsilon_1 & 0 & \cdots & 0 \\ 0 & \varepsilon_2 & \cdots & 0 \\ \vdots & \vdots & \ddots & \vdots \\ 0 & 0 & \cdots & \varepsilon_m \end{pmatrix}. \tag{2.14}$$

and E is the energy of the electron being transferred. An auxiliary quantity N_n was defined as

$$N_n \equiv \Delta G^{(n)}_{(n,n)}. \tag{2.15}$$

where $G^{(n)}_{(n,n)}$ is the (n, n) block of the Green's function. The $(1, n)$ block of the Green's function can now be obtained through the sequential formula [18]:

$$N_n = (\mathbf{1} - \mathbf{v}^T \Delta^{-1} N_{n-1} \mathbf{v} \Delta^{-1})^{-1}. \tag{2.16}$$

and

$$G^{(n)}_{(1,n)} = G^{(n-1)}_{(1,n-1)} \mathbf{v} \Delta^{-1} N_n. \tag{2.17}$$

The initial conditions for the above recursive equations, $G^{(2)}_{1,2}$ and $N_2 (= \Delta G^{(2)}_{2,2})$, can be obtained by taking the corresponding block matrices of

$$G^{(2)} = (E\mathbf{1} - H^{(2)})^{-1} \tag{2.18}$$

where $H^{(2)}$ is the Hamiltonian of two bridge units,

$$H^{(2)} = \begin{pmatrix} \mathbf{e} & \mathbf{v} \\ \mathbf{v}^T & \mathbf{e} \end{pmatrix}. \tag{2.19}$$

For calculating $G^{(n)}_{(1,n)}$ of a homogeneous bridge, only the energies of the molecular orbitals of a single unit, $\mathbf{e}$, and the interaction matrix between adjcent units, $\mathbf{v}$, are needed. They can be obtained by quantum chemistry calculations. In the present work, both $\mathbf{e}$ and $\mathbf{v}$ are obtained from the extended Hückel calculation (Section 2.3.1).

To calculate the effective coupling matrix element H_{Dk}^{eff} between the ferrocene-containing group and the gold electrode, assuming that direct couplings exist only between the first bridge unit and the donor orbital, and between the last bridge unit and the acceptor (metal electrode) orbital, Eq. (2.3) may be rewritten as:

$$H_{Dk}^{\text{eff}} = V_{D,1} G_{(1,n)}^{(n)} V_{n,k}. \tag{2.20}$$

The direct coupling between donor and acceptor has been assumed to be negligible, and $V_{D,1}$ and $V_{n,k}$ denote interaction between donor state and the molecular orbitals in the first bridge unit and between those in the nth bridge unit and the state $|\vec{k}\rangle$ of the metal electrode, respectively. For a bridge with more than one orbital on each site, $V_{D,1}$ denotes a row vector, $G_{(1,n)}^{(n)}$, a matrix, and $V_{n,k}$, a column vector.

With Eqs. (2.11), (2.16), (2.17) and (2.20) the averaged coupling strength $\overline{|H_{Dk}|^2}$ can be obtained, and together with Eqs. (2.9) and (2.10), the ET reaction rate can be estimated.

2.3 Application

In this section, we present the results of the calculation for the systems of ferrocenyl-carboxyl alkanethiol (**I**) and ferrocenyl alkanethiol (**II**) attached on gold electrodes, using the equations discussed in Section 2.2.

2.3.1 The Calculation

The geometry of the molecules used in the present work is depicted in Fig. 2.1. The geometry of alkanethiol is based on that of Klien and coworkers [23] who employed a molecular dynamics calculation on this self-assembled monolayer system. The alkanethiol chain is tilted 25° with respect to the normal of the metal electrode plane. The geometries of the ferrocenylcarboxyl group and the ferrocenyl group are from the crystal structure of similar molecules [24]. The orientation of these groups are chosen among the possible configurations that do not cause an overlap of neighboring

alkanethiol chains, and, for the case of ferrocenylcarboxyl group, the geometry used has a reasonable closest atom-to-atom distance (1.6 Å) to the neighboring alkanethiol chains.

The tight-binding Hamiltonian is obtained from the extended Hückel program [15], except that all the interactions beyond nearest neighbors are ignored and the overlap integrals are considered within each bridge unit only. The molecular orbitals of individual bridge units are obtained by solving the secular equation of each unit. For the energy level distribution to fit better the experimental band stucture measurements [25, 26], the MO energies of a CH_2 unit are adjusted. The details of the adjustment were given in the previous work [18]. The S atom is included in the first CH_2 unit. The detail of using the sequential formula according to this modification is included in the Appendix.

The wave functions used for the Au(111) surface are linear combinations of atomic s-orbitals obtained with the tight-binding approximation [27], and to evaluate Eq. (2.10), the coupling strengths of 60 wave vectors ($\vec{k}$) randomly sampled over the Fermi surface were calculated and averaged to obtain $\overline{|H_{Dk}|^2}$.

The energy of the electron, E in Eqs. (2.13) and (2.18), is determined by a method described in Section 1.3.2 of Chapter 1 (Ref. [18]). If the zero of the energy scale is defined as an electron being placed just outside the surface of the material in vacuum, then the energy of the electron in the Fermi surface of the metal electrode equals $-\Psi_m$, where Ψ_m denotes the work function of the metal. Similarly, the energy of the electron at the HOMO of an alkane chain is $-\Psi_B$, if Ψ_B is defined as the ionization potential of the molecule. For the electron in the transition state with the exchange current condition being imposed, the analysis in Ref. [18] gives

$$\Delta E(q^\dagger) = -eE^0_{(abs)} + \frac{e}{2}(\psi^0_m - \psi^0_s) + \Psi_B - \Delta\epsilon_i, \tag{2.21}$$

for the energy difference between the transition state and the virtual state where an electron is placed in the ith bridge orbital. In Eq. (2.21), $E^0_{(abs)}(= \Psi_m/e + (\psi^0_m - \psi^0_s))$ is the absolute potential with its reference state being an electron at rest in vacuum

close to the surface of the solution, as discussed by Trasatti in Ref. [28]. ψ_m and ψ_s are the electric *outer* potentials (also called *Volta potential*) for the metal and for the solution, accordingly. ψ_m^0 and ψ_s^0 are the corresponding standard potentials. It has been assumed, in deriving Eq. (2.21), that the electric outer potential inside the alkanethiol monolayer is the average of the potential in metal and that in solution. $\Delta\epsilon_i$ is defined as the energy difference between the ith bridge orbital and the HOMO energy level, i.e., $E_{Bi} - E_B(\mathrm{HOMO})$. Therefore, $-(\Psi_B - \Delta\epsilon_i)$ can be regarded as the shifted energy of the ith bridge orbital in which the energy of HOMO is placed at $-\Psi_B$. If E is defined as

$$E = -eE_{(abs)}^0 + \frac{e}{2}(\psi_m^0 - \psi_s^0) \tag{2.22}$$

then $\Delta E(q^\dagger)$ in Eq. (2.21) has the form of

$$E - (\text{energy of the } i\text{th bridge orbital}).$$

Therefore, here E can be regarded as the energy of the electron. So now Eq. (2.22) can be used to obtain the E in Eqs. (2.13) and (2.18).

For molecule **I**, if the standard potential of the system is taken as 0.08 V above the Ag/(1 mM $AgClO_4$, 1 M $HClO_4$) reference electrode [3], then the absolute potential $E_{(abs)}^0$ is about 5.13 V [28]. The formal potentials reported by Walczak *et al.* [29], by Popenoe *et al.* [30] and by Collard *et al.* [31] for similar systems agree with the above value within 0.1 V (Ref. [2(a)], Table 5). Together with the work function of Au(111) surface, 5.31 eV [32], we obtain -0.18 V for the potential difference, $\psi_m^0 - \psi_s^0$. So the energy for the electron in the transition state is -5.22 eV in this case.

For molecule **II**, the formal potentials in 1 M $HClO_4$ solution are reported as 0.2 V (vs. Ag/AgCl/sat.KCl) by Chidsey *et al.* [33], also about 0.2 V (vs. Ag/AgCl/sat.KCl) by Row and Creager [34], and 0.22 V (vs. SSCE) by Uosaki *et al.* [35]. If an averaged value of 0.43 V with respect to the standard hydrogen electrode is taken, the absolute potential of the system is about 4.87 V [28] and therefore the energy for the electron

in the transition state is estimated to be -5.09 eV.

2.3.2 Results

The coupling strength ($\overline{|H_{Dk}|^2}$) calculated using the sequential formula for both molecules **I** and **II** are shown in Fig. 2.2 and Table 2.1. The iteration of the sequential formula can be performed to an even longer chain ($n = 50$ or more) with good numerical precision. It can be seen that for longer bridge chains, there is an excellent exponential decay, while for shorter chains, the decay is modulated with an initial oscillation. Fitting the electronic coupling of the long chains ($n = 20$ to 50) with a term proportional to $\exp(-\beta n)$ yields $\beta = 1.05/\mathrm{CH_2}$ for both molecules **I** and **II**. β in the units of $\mathrm{\AA}^{-1}$ can be estimated by dividing the above values by 1.28 $\mathrm{\AA/CH_2}$, which is the projection of a C-C bond length on the axis of translational symmetry of the alkane chain [36], or by 1.53 $\mathrm{\AA/CH_2}$ for the C-C bond length, for a "through bond" decay constant.

The density of states of gold at the Fermi surface (ρ_f) was estimated from the low temperature specific heat measurement, 0.3/eV/atom [37], for the comparison of rate constants in the following section.

2.4 Discussion

2.4.1 Comparison to Experimental Measurements

The calculated coupling constants ($\overline{|H_{Dk}|^2}$) can be compared to the experimental rate constant using Eqs. (2.9) and (2.10). Using 0.3/eV/atom [37] as the ρ_f, the rate constants are calculated with the λ's reported in Refs. [3, 4, 6, 7]. The results are listed in Table 2.2. It is seen that the results of our calculation roughly agree with the experimental data within one order of magnitude, except with that measured by Smalley *et al.* [7] for $n = 8$ of molecule **I**. The λ for $n = 8$ is measured to be slightly larger than others (Table 2.2) which makes the magnitude of $\exp(-\lambda/4k_BT)$ smaller by a factor of two or three at the room temperature. The calculated coupling strength

(Fig. 2.2 and Table 2.1) for $n = 8$ is also smaller than that for $n = 9$ (see Section 2.4.2 for a discussion on this result).

In Ref. [7] the authors reported $\beta = 1.21 \pm 0.05/CH_2$ for molecule **I** (ester-linked) for the reaction rates. The pre-exponential factor P_n also shows a linear dependence in a semi-log plot for $n \geq 8$, giving a slope of $-1.27 \pm 0.1/CH_2$. A linear fit of the logarithm of the calculated coupling strengths for $n = 5$ to 9 gives $\beta = 1.20/CH_2$, and that for $n = 8$ to 16 yields $\beta = 1.03/CH_2$. On the other hand, Carter and coworkers [6] reported $1.44/CH_2$ for the pre-exponential factor for $n = 8, 12, 16$. The exponential fit of calculated coupling strength on the three chain lengths gives $\beta = 0.98/CH_2$. There is seen to be an underestimation of the length dependence in our calculation. In the results of our calculation for molecule **I**, the even-numbered short chains have a smaller coupling strength than that inferred from the averaged linear fit. This fact can be explained by the dephasing of the coupling through a multiple-band bridge (Section 2.4.2).

For the directly-linked molecule (**II**), the bridge is the same as that for **I**, the energy of the electron is displaced by only 0.13 eV and the length dependence is expected to be almost the same for long chains. Exponential fit gives $\beta = 1.05/CH_2$ for long chains ($n = 20$ to 50), while for short chains ($n = 5$ to 15), it is as large as $1.45/CH_2$. The latter is the same as that arising from the second smallest exponential factor in the multi-band analysis of the bridge. The details are given below.

2.4.2 The Oscillation in Short Chains

It is seen, in Fig. 2.2, that the calculated coupling strengths have a single exponential dependence on chain length n for very long chains, and a slightly faster decay with an oscillation for the shorter, experimentally accessible chains. Therefore, it is desirable to understand the behavior of chain length dependence for the shorter chains.

The iteration of the sequential formula (Eqs. (2.16) and (2.17)) gives the chain length dependence in the calculation. Equation (2.16) is a first order nonlinear difference equation for matrices $\{N_n\}$. For an off-resonance situation, N_n approaches a

constant matrix for large n. For both molecules studied in the present work, there is little variation in iterating the matrices $\{N_n\}$ numerically, starting from $n = 3$. So from Eq. (2.17), the Green's function that describes the coupling through the bridge, $G^{(n)}_{(1,n)}$, now becomes

$$G^{(n)}_{(1,n)} \cong G^{(n-1)}_{(1,n-1)} \mathbf{v}\Delta^{-1} N, \text{ for } n \geq 3, \tag{2.23}$$

where N denotes the constant matrix N_n approaches, or,

$$G^{(n)}_{(1,n)} \cong G^{(2)}_{(1,2)} (\mathbf{v}\Delta^{-1} N)^{n-2}, \text{ for } n \geq 3. \tag{2.24}$$

If we assume that the eigenvalues of $\mathbf{v}\Delta^{-1}N$ are $\{\lambda_1, \lambda_2, \cdots, \lambda_6\}$, then the effective coupling between the donor group and a state $|\vec{k}\rangle$ in the metal, H^{eff}_{Dk}, given by Eq. (2.20), is seen to be a linear combination of $\{\lambda_1^n, \lambda_2^n, \cdots, \lambda_6^n\}$. When n is large, the eigenvalue that has the largest modulus dominates over all the others since those with smaller eigenvalues become much smaller when raised to a large power n. So H^{eff}_{Dk} shows an exponential dependence on the chain length for large n. On the other hand, for small n's, those eigenvalues that are smaller in magnitude might largely affect the coupling.

A plot for the absolute values of eigenvalues of $\mathbf{v}\Delta^{-1}N$ versus E, the energy of the transferred electron, is shown in Fig. 2.3, for the alkanethiol bridge. The magnitude of the largest two eigenvalues are represented with circles and dots. The open circles represent positive numbers while the dots, negative eigenvalues. It is seen that for the energies calculated, the two eigenvalues that are the largest in magnitude always have the opposite sign. Therefore, the linear combination of powers of those eigenvalues may show an oscillation between even and odd n's, arising from the cancellation (or addition) of either even or odd powers of the two eigenvalues. The smaller calculated coupling strengths for the even n's of molecule **I** and for the odd n's of molecule **II** are because of this effect. Also, the smaller eigenvalue may dominate the decay trend among short chains, leading to a larger β in fitting the coupling strength to $\exp(-\beta n)$.

In the present work the bridge is regarded to be a sequence of linearly connected

units and each unit has several molecular orbitals. The linear combinations of those orbitals that constitute the eigenvectors of matrix $\mathbf{v}\Delta^{-1}N$ offer "decoupled paths" for the electron tunneling, and the interference between the paths due to the phase difference in the tunneling amplitude (eigenvalues of $\mathbf{v}\Delta^{-1}N$) gives an oscillatory dependence on chain length for the overall effective coupling (both H_{Dk}^{eff} and the averaged $\overline{|H_{Dk}|^2}$).

For the ester-linked ferrocenylcarboxyl alkanethiol molecule (**I**), at $E = -5.22$ eV, the two eigenvalues with the largest magnitudes of $\mathbf{v}\Delta^{-1}N$ are 0.591 and -0.485. If the averaged coupling strength, $\overline{|H_{Dk}|^2}$, is fitted to be proportional to $\exp(-\beta n)$, those corresponding β's given by those eigenvalues would be $1.05/\text{CH}_2$ and $1.45/\text{CH}_2$ respectively. (Because of the amplitude squared in $\overline{|H_{Dk}|^2}$, β equals $-2\log|\text{eigenvalues}|$.) For the directly linked ferrocenyl alkanethiol (**II**), the eigenvalues are 0.593 and -0.484, which correspond to $1.04/\text{CH}_2$ and $1.45/\text{CH}_2$ for the decay constants (β). There is only little difference in the eigenvalues of $\mathbf{v}\Delta^{-1}N$. Consequently, the β's are similar. Almost the same values of β are also obtained by linearly fitting the calculated $\log\overline{|H_{Dk}|^2}$ with respect to n for long chains ($n = 20$ to 50) of both molecules **I** and **II**. For the short chains ($n = 5$ to 15) of **II**, the fitted $1.45/\text{CH}_2$ is also the same as the one calculated from the second largest eigenvalue.

In calculating H_{Dk}^{eff} using Eq. (2.20), the weighting coefficients of the eigenvalues are determined by the coupling column or row matrices $V_{D,1}$ and $V_{n,k}$. They depend on the geometry and orientation of the ferrocene-containing groups and the alkanethiol chains on the gold surface. This explains the different length dependence of coupling strengths for short chains even though the β and the underlying eigenvalues are almost the same. In the range of experimentally accessible n's, the calculated coupling strengths are seen to be strongly influenced by the smaller eigenvalues of $\mathbf{v}\Delta^{-1}N$. Therefore, the underestimation of β for the ferrocenylcarboxyl alkanethiol system implies that the chosen geometry for the electroactive group is probably not very close to the actual one. There is possibly a distribution of the conformation of the electroactive groups, so a more realistic approach should include an average over possible conformations. In such calculations, the amplitude of the oscillation

in electronic coupling strength is expected to be smaller, and the β for experimentally accessible chain lengths is expected to be between those from the two largest eigenvalues, 1.05 and 1.45/CH_2.

2.4.3 Remarks on the Tight-Binding Approximation

The calculation using the sequential formula is based on a tight-binding Hamiltonian constructed from the extended-Hückel basis set. However, matrix elements and overlap integrals from the extended-Hückel program are not always the best choice for the tight-binding model. In our calculation we found that the band gap for a linear chain polyethylene obtained in this tight-binding model was too small (it is about 6.2 eV) compared with that from experiment (8–9 eV [26]). The band structure of a linear polyethylene from the tight-binding model also does not resemble that from the full extended-Hückel calculation, and the latter has been shown to be surprisingly close to experimental valence band structure [25]. *Ab initio* calculations on superexchange coupling strengths have concluded that nearest neighbor coupling is not the major coupling scheme for the donor/acceptor orbitals investigated [12]. The disagreement of band structures of polyethylene calculated from the tight-binding model and the full extended-Hückel[18] has also confirmed the influence of long-range coupling. As an empirical model, the difficulty is resolved by adjusting the MO energies of the CH_2 unit in order to obtain a more realistic band gap, as described in detail in Ref. [18]. In applying this method to other systems, the tight-binding Hamiltonian for the bridge part used should fit band structure measurements.

As a single-electron molecular orbital theory, extended-Hückel calculation has provided an efficient and quite correct description on hydrocarbon chains [25]. The tight-binding approximation is a further simplification, providing an alternative method that is analytically accessible and possible for making use of experimental data on the positions of energy levels. The present work shows that, even with such a simplified model Hamiltonian, a careful consideration of the position of energy levels can still provide a fairly good description on the superexchange coupling strengths.

In the present tight-binding model, the coupling through neighboring alkanethiol chains in the self-assembled monolayer and the direct coupling between the ferrocene-containing groups and the gold electrode are not considered. For the same geometry of the ferrocenylcarboxyl group as shown in Fig. 2.1, the vertical distance from the Fe atom to the gold surface for molecule **I** with n=6, is about 12 Å. Therefore, it is believed to be a very small direct coupling for the molecules listed in Table 2.2. The effect of coupling through other alkanethiol chains were studied in the previous work [18] by a full extended Hückel calculation. There is seen to be little effect on the neighboring alkanethiol chains, in which the shortest atom-to-atom distance between the ferrocenylcarboxyl group and the neighboring alkanethiol chains is 1.6 Å. Based on the above studies, it is believed that for $n \geq 5$, the electronic coupling between the ferrocene-containing groups and the gold electrode is mostly from the coupling through the bridge.

2.5 Conclusions

The sequential formula Eqs. (2.16) and (2.17) can be used to calculate the bridge-mediated electronic coupling for a long range electron transfer reaction. It is shown that the calculation gives reasonable estimation of coupling strengths. The length dependence factors, β, are slightly smaller than those from experiments. The mathematical structure of the sequential formula also provides a tool for realizing the physical picture of electron tunneling through a multi-band bridge. From such analysis, it is concluded that the length dependence for the shorter chains ($n \leq 20$) can be better estimated if the actual geometries, or the distribution of the geometries, of the ferrocene-containing groups can be used in the calculation.

Acknowledgments

The author would like to thank Professor R. A. Marcus for many insightful discussions. Discussions with Professor Stephen W. Feldberg and Dr. Yuri Georgievskii

were also very helpful. It is a pleasure to acknowledge the support of National Science Foundation, the Office of Naval Research and NEDO (Japan).

Appendix A: Generalization to Bridges with Different Units

For bridges composed of different units, the energies of molecular orbitals in each unit is used to form the matrix $\mathbf{e}$ and should be denoted by $\mathbf{e}_n$ for the nth unit. The interaction matrix between $n-1$ and nth units is denoted by $\mathbf{v}_{(n-1,n)}$, which is a square or a rectangular block of the tight-binding Hamiltonian. The definition of N_n now becomes (corresponding to Eq. (2.15))

$$N_n \equiv \Delta_n G^{(n)}_{(n,n)}, \tag{2.25}$$

and the sequential formula (Eqs. (2.16) and (2.17)) is now

$$N_n = (\mathbf{1} - \mathbf{v}^T_{(n-1,n)} \Delta^{-1}_{n-1} N_{n-1} \mathbf{v}_{(n-1,n)} \Delta^{-1}_n)^{-1}. \tag{2.26}$$

and

$$G^{(n)}_{(1,n)} = G^{(n-1)}_{(1,n-1)} \mathbf{v}_{(n-1,n)} \Delta^{-1}_n N_n. \tag{2.27}$$

The initial condition has the similar definition, for the Hamiltonian formed by the first and second bridge units,

$$H^{(2)} = \begin{pmatrix} \mathbf{e}_1 & \mathbf{v}_{(1,2)} \\ \mathbf{v}^T_{(1,2)} & \mathbf{e}_2 \end{pmatrix} \tag{2.28}$$

and Eq. (2.18) is used. For the present work, the group SCH_2 is considered as the first bridge unit. So the above initial condition is used, but for the iteration for additional CH_2 units, Eqs. (2.16) and (2.17) are used.

References and Notes

[1] For example. G. M. Whitesides and P. E. Laibinis. Langmuir 6 (1990) 87; L. H. Dubois and R. G. Nuzzo. Annu. Rev. Phys. Chem. 43 (1992) 437 and references cited therein.

[2] (a) For a recent review on the electrochemistry of self-assembled monolayers. H. O. Finklea. Electroanal. Chem. 19 (1996) 109. and references cited therein. (b) Experimental investigations of electron transfer across self-assembled monolayers on electrode surfaces include those of R. J. Forster and L. R. Faulkner. J. Am. Chem. Soc. 116 (1994) 5444; ibid. 116 (1994) 9411; M. S. Ravenscroft and H. O. Finklea J. Phys. Chem. 98 (1994) 3843; Z. Q. Feng, S. Imabayashi. T. Kakiuchi and K. Niki. J. Elec. Chem. 394 (1995) 149.

[3] C. E. D. Chidsey, Science 251 (1991) 919; ibid. 252 (1991) 631.

[4] J. N. Richardson, S. R. Peck, L. S. Curtin, L. M. Tender, R. H. Terrill, M. T. Carter, R. W. Murray, G. K. Rowe and S. E. Creager. J. Phys. Chem. 99 (1995) 766.

[5] A. M. Becka and C. J. Miller, J. Phys. Chem. 96 (1992) 2657.

[6] M. T. Carter, G. K. Rowe, J. N. Richardson. L. M. Tender. R. H. Terrill and R. W. Murray, J. Am. Chem. Soc. 117 (1995) 2896.

[7] J. F. Smalley, S. W. Feldberg, C. E. D. Chidsey, M. R. Linford, M. D. Newton and Y. P. Liu, J. Phys. Chem. 99 (1995) 13141.

[8] H. M. McConnell, J. Chem. Phys. 35 (1961) 508; the single band problem is also solved and discussed in detail by K. F. Herzfeld, J. Chem. Phys. 10 (1942) 508.

[9] V. Mujica, M. Kemp and M. A. Ratner, J. Chem. Phys. 101 (1994) 6849; ibid, 6856; M. Kemp, V. Mujica and M. A. Ratner, J. Chem. Phys. 101 (1994) 5172;

M. Kemp, A. Roitberg, V. Mujica, T. Wanta and M. A. Ratner, J. Phys. Chem. 100 (1996) 8349.

[10] J. W. Evenson and M. Karplus, J. Chem. Phys. 96 (1992) 5272; J. W. Evenson and M. Karplus, Science 262 (1993) 1247.

[11] D. N. Beratan and J. J. Hopfield, J. Am. Chem. Sec. 106 (1984) 1584; D. N. Beratan, J. N. Onuchic and J. J. Hopfield, J. Chem. Phys. 86 (1987) 4488.

[12] C. A. Naleway, L. A. Curtiss and J. R. Miller, J. Phys. Chem. 95 (1991) 8434; L. A. Curtiss, C. A. Naleway and J. R. Miller, ibid. 97 (1993) 4050; C. Liang and M. D. Newton, ibid. 96 (1992) 2855; ibid. 97 (1993) 3199.

[13] (a) For studies involving large scale Green's function calculations, see, for example, S. S. Skourtis, J. J. Regan and J. N. Onuchic J. Phys. Chem. 98 (1994) 3379; A. A. S. da Gama, J. Theoret. Biol. 142 (1990) 251; M. A. Ratner, J. Phys. Chem. 94 (1990) 4877; J. Malinsky and Y. Magarshak, J. Phys. Chem. 92 (1992) 2849. (b) for other methods for long range ET, see, for example, A. Kuki and P. G. Wolynes, Science 236 (1987) 1647; L. S. Conrad, K. V. Mikklesen, M. K. Nielsen and J. Ulstrup, Inorg. Chem. 29 (1990) 2808; S. F. Sneddon and C. L. Brooks, J. Am. Chem. Soc. 114 (1992) 8220; J. M. Gruschus and A. Kuki, J. Phys. Chem. 97 (1993) 5581; A. Okada, T. Kakitani and J. Inoue, J. Phys. Chem. 99 (1995) 2946, among others.

[14] A. A. Stuchebrukhov, Chem. Phys. Lett. 225 (1994) 55; A. A. Stuchebrukhov and R. A. Marcus, J. Phys. Chem. 99 (1995) 7581.

[15] R. Hoffmann J. Chem. Phys. 39 (1963) 1397.

[16] P. Siddarth and R. A. Marcus, J. Phys. Chem. 94 (1990) 2985, 8430; 96 (1992) 3213; 97 (1993) 13078; S. Larsson J. Am. Chem. Soc. 103 (1981) 4034; H. Ou-Yang, B. Källebring and R. A. Marcus, J. Chem. Phys. 98 (1993) 7405.

[17] H. Ou-Yang, B. Källebring and R. A. Marcus, J. Chem. Phys. 98 (1993) 7565.

[18] C.-P. Hsu and R. A. Marcus, J. Chem. Phys. in press.

[19] The matrix elements of the effective coupling is shown to be that of the transfer operator T in chapter 4 of: E. N. Economou, Green's Functions in Quantum Physics, 2nd ed., (Springer-Verlag, Berlin, 1990).

[20] R. A. Marcus and N. Sutin, Biochim. Biophys. Acta. 811 (1985) 265.

[21] For integrating over the electronic energy levels in the metal the weighting function in Eq. (6) of R. A. Marcus, J. Chem. Phys. 43 (1965) 679 is used, noting that only the second two factors there vary much with the ϵ in Eq. (6) there.

[22] The averaged coupling, $\overline{|H_{Dk}|^2}$, has units of (energy)^2(wave vector)$^{-3}$ or (energy)^2(volume)^1 because of the normalization of $|\vec{k}\rangle$ described earlier, while ρ_f is the density of states at the Fermi surface, with units of (energy)$^{-1}$(wave vector)^3, or equivalently, (energy)$^{-1}$(number of atoms)$^{-1}$.

[23] J. Hautman and M. L. Klein, J. Chem. Phys. 91, 4994 (1989). The sequential formula assumes a translational symmetry on the alkane chain, so the averaged bond angles of the alkanethiol chain are used.

[24] International Union of Crystallography, Structure Reports 20 (1956) 550; 35B (1970) 550; 33B (1968) 536; 38B (1972) 146.

[25] K. Seki, N. Ueno, U. O. Karlsson, R. Engelhardt and E. E. Koch, Chem. Phys. 105 (1986) 247; Ch. Zubrägel, F. Schneider, M. Neumann, G. Hähner, Ch. Wöll and M. Grunze, Chem. Phys. Lett. 219 (1994) 127.

[26] K. J. Less and E. G. Wilson, J. Phys C: Solid State Phys. 6 (1973) 3110; M. Fujihira and H. Inokuchi, Chem. Phys. Lett. 17 (1972) 554.

[27] For treating the electronic matrix elements, a method similar to that in Ref. [17] is used.

[28] S. Trasatti, Electrochimica Acta 35 (1990) 269; S. Trasatti, Pure Appl. Chem. 58 (1986) 955. In the latter work, the absolute potential of the standard hydrogen electrode was given as 4.44 V.

[29] M. M. Walczak, D. D. Popenoe, R. S. Deinhammer, B. D. Lamp, C. Chung and M. D. Porter, Langmuir 7 (1991) 2687.

[30] D. D. Popenoe, R. S. Deinhammer and M.D. Porter, Langmuir 8 (1992) 2521.

[31] D. M. Collard and M. A. Fox, Langmuir 7 (1991) 1192.

[32] CRC Handbook of Chemistry and Physics, D.R.Lide, ed., 73rd ed. (CRC Press, 1992-93).

[33] C. E. D. Chidsey, C. R. Bertozzi, T. M. Putvinski and A. M. Mujsce, J. Am. Chem. Soc. 112 (1990) 4301.

[34] G. K. Rowe and S. E. Creager, Langmuir 7 (1991) 2307.

[35] K. Uosaki, Y. Sato and H. Kita, Langmuir 7 (1991) 1510.

[36] The distances from the Fe atom to the center of the triple hollow site of Au surface atoms which the S atom is placed above, for the present geometries, are calculated. They show good linear dependences on n, the number of methylene units. For molecule **I**, the distance increases 1.28 ± 0.091 Å for each CH_2, on the average, while for molecule **II**, it is 1.28 ± 0.37 Å/CH_2. Since the distances are 8.3 Å for molecule **II** and 11 Å for molecule **I**, for $n = 3$, the above fluctuations (0.37 Å or 0.091Å) are negligible. For the same n, the distances of molecule **I** is about 2.59 ± 0.096 Å longer than molecule **II**, on the average.

[37] A. P. Cracknell and K. C. Wong, The Fermi Surface, Its Concept, Determination and Use in the Physics of Metals (Clarendon Press, Oxford, 1973). The γ factors reported on p. 169, based on the specific heat measurements, are *per mole* quantities. They are then converted into density of states in the units of $(\text{energy})^{-1}(\text{number of atoms})^{-1}$.

Figure 2.1: The geometry of the molecules calculated in the present work: Part **I** is for $(\eta^5\text{-}C_5H_5)Fe(\eta^5\text{-}C_5H_4)CO_2(CH_2)_{16}S$ on the gold surface. and part **II** is for $(\eta^5\text{-}C_5H_5)Fe(\eta^5\text{-}C_5H_4)(CH_2)_{16}S$. The surface gold atoms are placed on the $z = 0$ plane and the origin is placed at one of the triple hollow sites and the S atom is placed above it. The y-axis is chosen to be the direction of the tilting of the alkane chains. It is also parallel to one of the lines connecting nearest neighbors of gold atoms on this (111) plane. The units in the coordinates are Å.

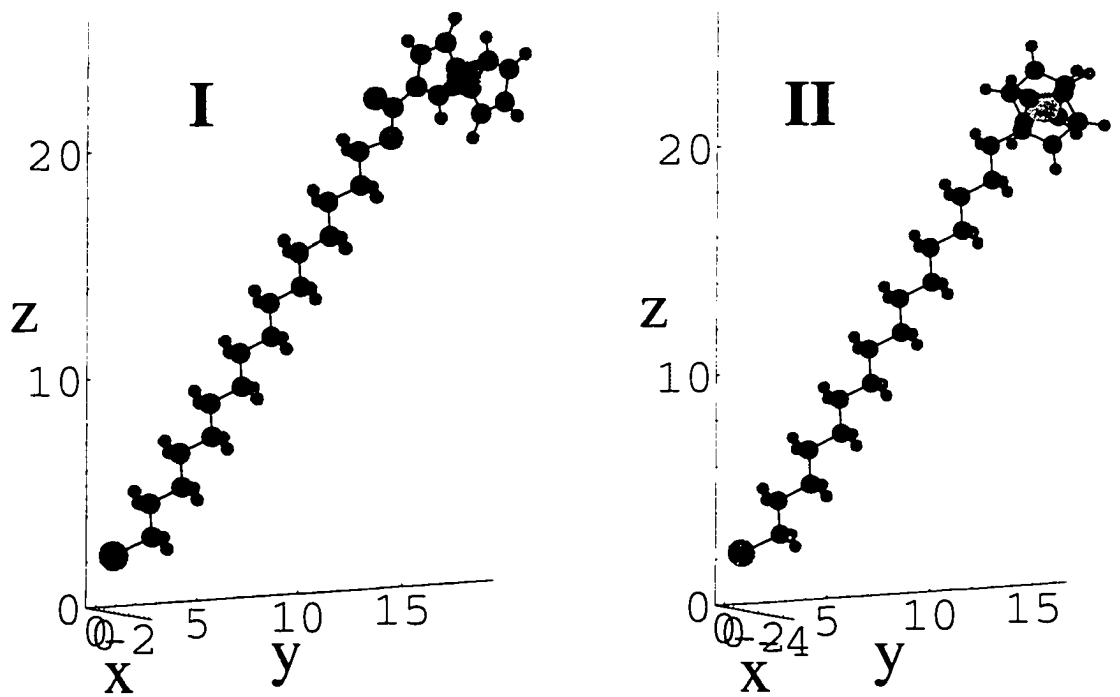

Figure 2.2: A plot for $\log_e \overline{|H_{Dk}|^2}$ versus number of methylene units in the bridge. "•" denotes that for molecule **I** (Cp-Fe-Cp-CO_2-alkanethiol). "o" is the result for molecule **II** (Cp-Fe-Cp-alkanethiol).

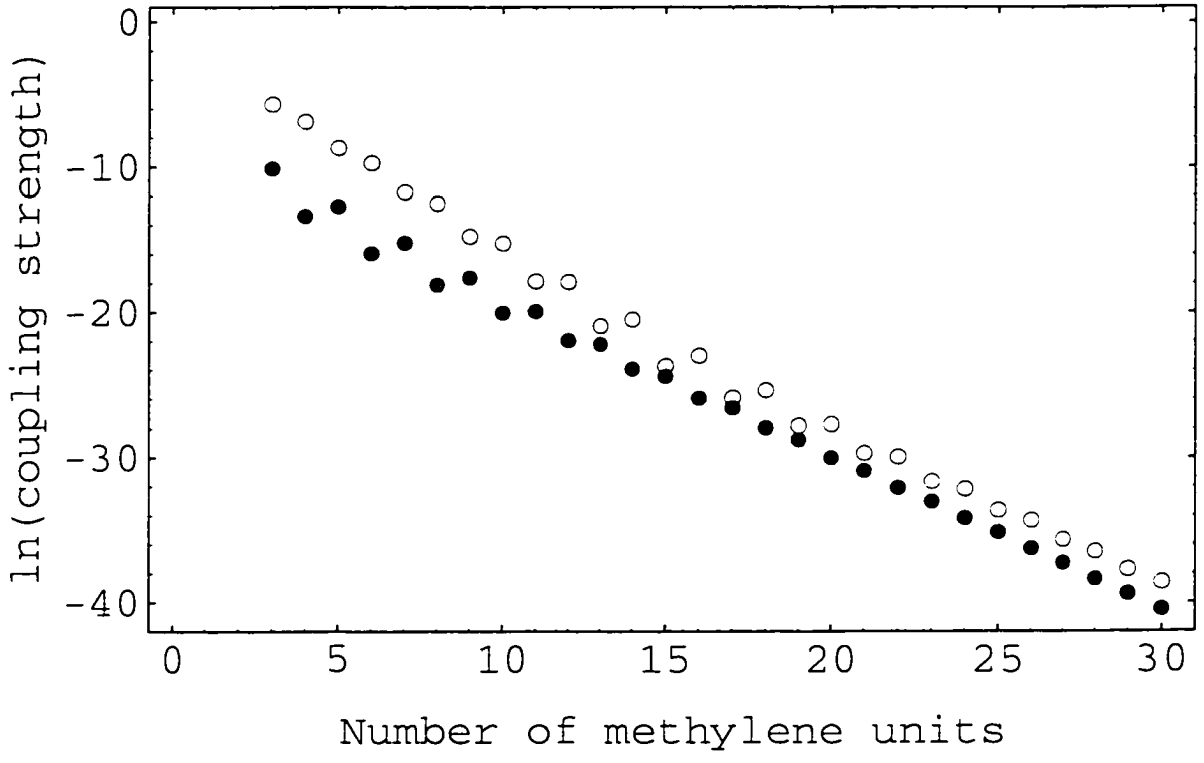

Figure 2.3: The absolute value of the eigenvalues of $\mathbf{v}\Delta^{-1}N$ vs. E, the energy of the electron being transferred, where N is the large n limit of N_n for the off-resonance cases. For each energy calculated, the largest two eigenvalues are plotted according to their signs. "o" denotes the positive eigenvalues, and "•" is for negative ones. Other smaller eigenvalues are denoted by "+," regardless of their signs. The range of E calculated is in the band gap between the valence and conduction bands of the tight-binding Hamiltonian for the long chain alkane molecules [18, 26].

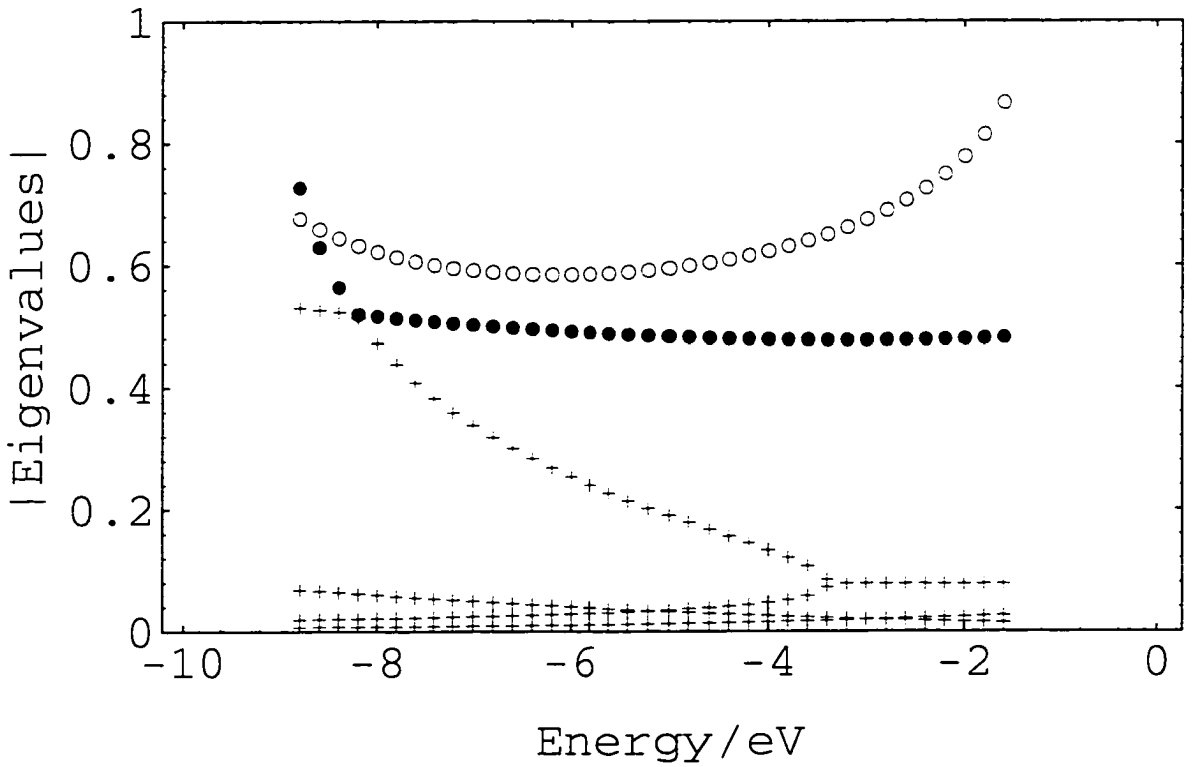

Table 2.1: The effective coupling strengths ($\overline{|H_{Dk}|^2}$) for $n = 3$ to 16.

n	$CpFeCpCO_2(CH_2)_nSH^a$	$CpFeCp(CH_2)_nSH^a$
3	4.07×10^{-5}	3.42×10^{-3}
4	1.56×10^{-6}	1.04×10^{-3}
5	3.01×10^{-6}	1.67×10^{-4}
6	1.21×10^{-7}	6.04×10^{-5}
7	2.50×10^{-7}	8.23×10^{-6}
8	1.38×10^{-8}	3.71×10^{-6}
9	2.25×10^{-8}	3.89×10^{-7}
10	2.00×10^{-9}	2.41×10^{-7}
11	2.19×10^{-9}	1.76×10^{-8}
12	2.93×10^{-10}	1.67×10^{-8}
13	2.28×10^{-10}	8.06×10^{-10}
14	4.12×10^{-11}	1.26×10^{-9}
15	2.48×10^{-11}	5.05×10^{-11}
16	5.55×10^{-12}	1.04×10^{-10}

[a] The units for the coupling strengths are (eV^2atom)[22].

Table 2.2: The experimental and the theoretically estimated ET rate constants.

n	λ.eV	$k^{(0)}$(exp), s^{-1}	Ref.	$k^{(0)}$(calc), s^{-1}[f]
		$CpFeCpCO_2(CH_2)_nSH$ (**I**)		
5	0.70[a]	1.6×10^6,[c]	[7]	1.6×10^6
6	0.84[a]	2.4×10^5,[c]	[7]	1.5×10^5
7	0.86[a]	1.7×10^5,[c]	[7]	2.5×10^5
8	0.96[a]	3.4×10^4,[c]	[7]	5.0×10^2
9	0.91[a]	1.1×10^4,[c]	[7]	1.3×10^3
8	0.95[a]	0.21[d]	[4]	0.011
16	0.85[b]	1.25[c]	[3]	0.62
8	0.95[a]	4070[e]	[6]	230
12	0.89[a]	35.5[e]	[6]	9.4
16	0.80[a]	0.16[e]	[6]	0.49
		$CpFeCp(CH_2)_nSH$ (**II**)		
8	0.96[a]	2.0[d]	[4]	2.4

[a] From the temperature dependence of rate constant (Arrhenius plot).
[b] From the overpotential dependence of rate constant.
[c] T = 25°C.
[d] T = 140 K.
[e] Extrapolated in the Arrhenius plot to T = 273 K.
[f] Rate constants calculated with the λ's listed and ρ_f =0.3/eV/atom [37], the density of states of gold at the Fermi surface.

Chapter 3 Time-Dependent Stokes Shift and its Calculation from Solvent Dielectric Dispersion Data

Chao-Ping Hsu, Xueyu Song[†] and R. A. Marcus

A. A. Noyes Laboratory of Chemical Physics, 127-72

California Institute of Technology, Pasadena, CA 91125

(Reprinted with permission from *J. Phys. Chem. B*, **101**(14), pp.2546 - 2551.

Abstract

The time-dependent solvation correlation function (the "*Stokes shift response function*"), which describes the solvent response to a sudden change in the charge distribution of a solute molecule, is calculated here directly from experimentally measured dielectric dispersion data, $\epsilon(\omega)$, of the solvent. In the calculation a reaction field with the dielectric continuum assumption is used. This simple model is applied to the experimental results of Jimenez *et al.* for photoexcited coumarin and water as a solvent, and encouraging agreement is obtained using the experimental data on $\epsilon(\omega)$.

[†]Present address: Department of Chemistry, University of California, Berkeley, CA 94720

3.1 Introduction

The dynamics of polar solvents has been a topic of recent interest in physical chemistry and has frequently been studied in charge redistribution processes in many chemical reactions [1–20]. Experimentally, the time-dependent fluorescent shift (the *Stokes shift*) has been measured over different time scales and for a variety of polar solvents [2–8]. In typical Stokes shift experiments a chromophore solute in a polar solvent is first excited by a pump pulse, and then the time-dependent fluorescence spectrum of the solute is recorded. For studies with coumarin or other dye molecules (e.g., refs [3–8]), the excited state of the solute has a different charge distribution from that in the ground state. There is expected to be little intramolecular vibrational motion excited when, as appears to be the case for some of these molecules, the geometry or vibration frequencies of the solute molecules is barely changed. In those cases, instead of vibrational Franck-Condon factors or of frictional effects due to a geometrical change of the solute (e.g., isomerization), the dynamics is dominated by the electrostatic interaction with the solvent, and then dielectric relaxation plays the major role in the relaxation process.

Recent theoretical developments [9–20] have provided physical insight into the solvation dynamics. Solvation correlation functions calculated from the Debye form, the Davidson-Cole and the Cole-Cole forms were shown to exhibit significant differences [9]. Based on similar calculations and comparisons with experiments, it was suggested that it would be useful to obtain higher frequency dielectric data for a better description of $S(t)$, the solvation correlation function [8]. The effect of molecular shape has also been discussed [10]. Much attention has also been devoted to treating the spatial dependence of dielectric response function, $\epsilon(\boldsymbol{k}, \omega)$, which includes the molecular nature of solvent [11, 12]. The dynamical mean spherical approximation theory has been influential; the comparison with experimental results is at present qualitatively satisfactory [13, 14]. A molecular hydrodynamic theory [15, 16] has been applied to water solvation dynamics with a model dielectric response function [16, 17]. Good agreement between the experimental and calculated solvation corre-

lation function was obtained and the role of intermolecular O···O stretching mode was stressed [17]. Molecular dynamics calculations have provided information on how polar solvents change the reaction rate [18] and the role played by various shells of solvent molecules [9, 19]. Such calculations have also given results in satisfactory agreement with the dynamical Stokes shift experiments [7]. The short-time solvation dynamics has also been interpreted in terms of an *instantaneous normal modes* analysis of molecular dynamics simulations [20]. In another study, the ultrafast relaxation of the Stokes shift was related to the optical Kerr effect measurement using a Brownian oscillator model and assumptions on the spectral density [21], and showed an encouraging agreement for the description of fast dynamics of the solvent.

In the present work the time-dependent solvation correlation function is calculated using the entire dielectric spectral response function $\epsilon(\omega)$ [22], instead of molecular models for the solvent. It will be seen that reasonable agreement with the experimental time-dependent Stokes shift is obtained using the measured $\epsilon(\omega)$ [23, 24] without explicitly considering the spatial dependence of dielectric relaxation, i.e., $\epsilon(\boldsymbol{k}, \omega)$. The two solute-solvent models given in Section 3.2 are dielectric continuum models with a dipole in a spherical cavity and an ellipsoid filled with dipole density [10, 25], with the induced charge on the boundary. The former is the usual *Onsager's cavity model* [26]. Comparison of these two models with each other and with the experimental results in Ref. [7] is given and discussed in Section 3.3, followed by concluding remarks in Section 3.4.

3.2 Calculation of Solvation Correlation Function

The Stokes shift response function $S(t)$ is defined in the terms of the experimental measurements as

$$S(t) = \frac{\nu(t) - \nu(\infty)}{\nu(0) - \nu(\infty)} \tag{3.1}$$

where $\nu(t)$ is the frequency of the fluorescence maximum at time t. If there is little internal vibrational excitation of the solute in the transition, then the time dependence

of $\nu(t)$ arises mainly from the time-dependent solvation energy, $\Delta E^{\text{solv}}(t)$, resulting from the change in the charge distribution of solute induced by the photoexcitation at $t = 0$. $S(t)$, also termed a "solvation correlation function," can be rewritten as:

$$S(t) = \frac{\Delta E^{\text{solv}}(t) - \Delta E^{\text{solv}}(\infty)}{\Delta E^{\text{solv}}(0) - \Delta E^{\text{solv}}(\infty)}. \tag{3.2}$$

In the following section $\Delta E^{\text{solv}}(t)$ is related to the dielectric dispersion $\epsilon(\omega)$ by assuming that the solvation energy is the electrostatic interaction energy between the solute and the surrounding solvent.

3.2.1 Dielectric Continuum Models

For the case where the charge distribution of the solute is a point dipole moment, $\boldsymbol{\mu}$, the energy of interaction of the dipole with the solvent, $E^{\text{solv}}(t)$, is

$$E^{\text{solv}}(t) = -\boldsymbol{\mu}(t) \cdot \mathbf{R}(t) \tag{3.3}$$

where $\mathbf{R}(t)$ is the reaction field at time t due to the surrounding solvent acting on the solute dipole. The reaction field $\mathbf{R}(t)$ can be obtained from linear response theory:

$$\mathbf{R}(t) = \int_{-\infty}^{t} dt' \boldsymbol{r}(t - t') \boldsymbol{\mu}(t') \tag{3.4}$$

where $\boldsymbol{r}(t - t')$ is a response function and, in general, a tensor. Causality requires that $\boldsymbol{r}(t) = 0$ for $t < 0$. The Fourier transform is introduced

$$\tilde{f}(z) = \int_{-\infty}^{\infty} dt f(t) e^{-izt}, \tag{3.5}$$

where z can be generalized to be a complex variable. Usually there is a range for $\text{Im}(z)$ where $\tilde{f}(z)$ is analytic [27]. The inverse of Eq. (3.5) is given by the standard expression

$$f(t) = \frac{1}{2\pi} \int_C dz e^{izt} \tilde{f}(z) \tag{3.6}$$

where C is a suitable contour which goes from $-\infty$ to ∞ if projected onto the real axis and stays inside the region where $\tilde{f}(z)$ is analytic. Using the convolution theorem, Eq. (3.4) yields

$$\tilde{\mathbf{R}}(z) = \tilde{\boldsymbol{r}}(z)\tilde{\boldsymbol{\mu}}(z). \tag{3.7}$$

We consider now a model system where it is assumed that the solute is treated as a spherical cavity with the dipole placed at the center. To obtain the appropriate equation for $\tilde{\boldsymbol{r}}(z)$, both for this model of the solute and for any other, it is necessary to solve the time-dependent electrostatic problem for the system. The dielectric displacement, $\mathbf{D}_i$, in any phase i is related to the electric field there, $\mathbf{E}_i$, and the dielectric polarization $\mathbf{P}_i$ by [28]

$$\mathbf{D}_i(\mathbf{r}, t) = \mathbf{E}_i(\mathbf{r}, t) + 4\pi\mathbf{P}_i(\mathbf{r}, t). \tag{3.8}$$

In linear response theory,

$$\mathbf{P}_i(\mathbf{r}, t) = \int_{-\infty}^{t} dt' \alpha_i(t - t')\mathbf{E}_i(\mathbf{r}, t') \tag{3.9}$$

where it is assumed that the polarizability of the region α_i is local in space. For a two-phase system, $i = 1, 2$, the boundary conditions at the (1,2) interface are that the normal components, $\mathbf{D}_i^{\perp}(\mathbf{r}, t)$ are equal when there is no interfacial charge density, and the parallel components $\mathbf{E}_i^{\parallel}(\mathbf{r}, t)$ are also equal [29]. Taking the Fourier transform of Eq. (3.9) and of these boundary conditions, we have [30]

$$\tilde{\mathbf{P}}_i(\mathbf{r}, z) = \tilde{\alpha}_i(z)\tilde{\mathbf{E}}_i(\mathbf{r}, z) \tag{3.10}$$

and

$$\tilde{\mathbf{D}}_1^{\perp}(\mathbf{r}, z) = \tilde{\mathbf{D}}_2^{\perp}(\mathbf{r}, z), \quad \tilde{\mathbf{E}}_1^{\parallel}(\mathbf{r}, z) = \tilde{\mathbf{E}}_2^{\parallel}(\mathbf{r}, z). \tag{3.11}$$

From Eq. (3.10) we have

$$\tilde{\mathbf{D}}_i(\mathbf{r}, z) = \epsilon_i(z)\tilde{\mathbf{E}}_i(\mathbf{r}, z), \quad i = 1, 2 \tag{3.12}$$

where the frequency-dependent dielectric constant $\epsilon_i(z)$ is

$$\epsilon_i(z) = 1 + 4\pi\tilde{\alpha}_i(z), \qquad i = 1, 2. \tag{3.13}$$

Equations (3.11) and (3.12) are the same as the static equations and so the solution of static boundary value problem applies here. Using the standard reaction field expression [25, 31], one thus obtains for the case of a point dipole in a sphere,

$$\tilde{r}(z) = \frac{2}{a^3}\frac{\epsilon(z) - 1}{2\epsilon(z) + 1}, \tag{3.14}$$

where a, the radius of the cavity, represents the size of the solute. Since a normalization appears in calculating $S(t)$ in Eq. (3.2), any constant factor cancels, and so the final response function is independent of a. Equations (3.7) and (3.14), with z replaced by ω, were used in Ref. [31] and termed there a *quasi-static boundary-value* calculation. An explicit derivation of the equations is given above and the method can be applied to any other model for the solute.

We consider the case where the optical excitation of the solute molecule occurs, in effect, instantaneously and that the dipole moment of the molecule is changed from $\boldsymbol{\mu}_g$ to $\boldsymbol{\mu}_e$ at time $t = 0$. Thus, the dipole moment of the solute $\boldsymbol{\mu}(t)$ can be written as

$$\boldsymbol{\mu}(t) = \boldsymbol{\mu}_g + \theta(t)(\boldsymbol{\mu}_e - \boldsymbol{\mu}_g), \tag{3.15}$$

where $\theta(t)$ is the unit step function. Therefore, Eq. (3.4) yields

$$\mathbf{R}(t) = r_s\boldsymbol{\mu}_g + \int_{-\infty}^{t} dt' r(t - t')\theta(t')\Delta\boldsymbol{\mu}, \tag{3.16}$$

where, using Eq. (3.14) [32],

$$r_s \equiv \tilde{r}(0) = \int_{-\infty}^{t} dt' r(t - t') = \frac{2}{a^3}\frac{\epsilon_s - 1}{2\epsilon_s + 1}. \tag{3.17}$$

Here, $\Delta\boldsymbol{\mu} \equiv \boldsymbol{\mu}_e - \boldsymbol{\mu}_g$ and ϵ_s is the static dielectric constant of the solvent. The

first term in Eq. (3.16) describes the reaction field arising from $\boldsymbol{\mu}_g$, and the second term is the change in $\mathbf{R}(t)$ due to the sudden change of dipole at time $t = 0$. The former equals the static reaction field $r_s\boldsymbol{\mu}_g$, since before the excitation the solvent is in equilibrium with the ground state dipole moment.

At time t, if the molecule suddenly fluoresces, and so reverts to the ground state, the dipole moment is changed back to $\boldsymbol{\mu}_g$ and the solvent has an immediate reaction arising from the optical frequency dielectric constant, ϵ_{op}. If $\mathbf{R}_f(t)$ denotes the reaction field immediately after this instantaneous reaction of the solvent, then

$$\mathbf{R}_f(t) = \mathbf{R}(t) - r_{\text{op}}\Delta\boldsymbol{\mu} \tag{3.18}$$

where $\mathbf{R}(t)$ is the value just prior to this fluorescence, given by Eq. (3.16), and

$$r_{\text{op}} = \frac{2}{a^3}\frac{\epsilon_{\text{op}} - 1}{2\epsilon_{\text{op}} + 1}. \tag{3.19}$$

The resulting solvation energy difference between the excited state and the ground state molecule, at time t, is now

$$\begin{aligned}\Delta E^{\text{solv}}(t) &= E_e^{\text{solv}}(t) - E_g^{\text{solv}}(t) = -\boldsymbol{\mu}_e \cdot \mathbf{R}(t) + \boldsymbol{\mu}_g \cdot \mathbf{R}_f(t) \\ &= -\boldsymbol{\mu}_g \cdot (r_{\text{op}} + r_s)\,\Delta\boldsymbol{\mu} + \Delta E(t).\end{aligned} \tag{3.20}$$

where

$$\Delta E(t) = -(\Delta\mu)^2 \int_{-\infty}^{t} dt' r(t - t')\theta(t'). \tag{3.21}$$

In Eq. (3.20), only the second term is time-dependent and so the first term cancels in calculating $S(t)$ in Eq. (3.2).

The Fourier transform of $\Delta E(t)$ can be obtained using the complex Fourier transform of $\theta(t)$,

$$\int_{-\infty}^{\infty} \theta(t)e^{-izt}dt = \left[\frac{e^{-izt}}{-iz}\right]_{t=0}^{\infty} = \frac{1}{iz}, \quad \text{if } \text{Im}(z) < 0. \tag{3.22}$$

Therefore, from the convolution theorem,

$$\Delta\tilde{E}(z) = -\frac{(\Delta\mu)^2}{iz}\tilde{r}(z), \tag{3.23}$$

where z denotes $(\omega - i\eta)$ with ω real and η being a small positive number [33]. Taking the inverse transform of $\Delta\tilde{E}(z)$, we have, using the results in appendix A,

$$\begin{aligned} \Delta E(t) &= -\frac{(\Delta\mu)^2}{2\pi}\int_C dz e^{izt}\frac{1}{iz}\tilde{r}(z) && (3.24)\\ &= -\frac{4(\Delta\mu)^2}{a^3\pi}\int_0^\infty d\omega \frac{\cos\omega t}{\omega}\mathrm{Im}\left[\frac{\epsilon(\omega)-1}{2\epsilon(\omega)+1}\right] - (\Delta\mu)^2 r_s, \quad \text{for } t \geq 0. && (3.25)\end{aligned}$$

The contour of integration, C, in Eq. (3.24) denotes a path parallel to but slightly below the real axis in the complex z plane. The solvation correlation function $S(t)$ can be calculated using Eqs. (3.2), (3.20) and (3.25). The optical response has already been included in Eq. (3.18) and so the ∞ in Eq. (3.25) actually denotes a high frequency, ω_{op}, below the optical absorption band and the Im $\epsilon(\omega)$ is essentially zero at ω_{op}. The integration over z in Eq. (3.24) is discussed in appendix A, and remarks on the relation between the optical response and the upper limit of the frequency range of Eq. (3.25) are made in appendix B.

The effect of molecular shape was also studied here by considering an ellipsoid model: if an ellipsoid filled with homogeneous dipole density is used to represent the solute, the solution for the reaction field $\mathbf{R}$ is given in Section 20 of Ref. [25] and in Ref. [10]. For any frequency ω, it is the same as in Eq. (3.7) except for a different response function $\tilde{\boldsymbol{r}}(\omega)$:

$$\tilde{\boldsymbol{r}}(\omega) = \begin{pmatrix} f_a & 0 & 0 \\ 0 & f_b & 0 \\ 0 & 0 & f_c \end{pmatrix}, \tag{3.26}$$

where

$$f_i = \frac{3}{abc}\frac{A_i(1-A_i)[\epsilon(\omega)-1]}{\epsilon(\omega)+[1-\epsilon(\omega)]A_i}, \quad i = a, b, c, \tag{3.27}$$

and A_a, A_b, A_c are ellipsoidal shape factor integrals [25]. Tables and the relation of

these shape factors to elliptic functions are given in Ref. [34]. The expression for the solvation energy ($\Delta E^{\rm solv}(t)$) is similar to that in Eq. (3.20) except that now $\boldsymbol{r}$ is a tensor instead of a scalar r:

$$\Delta E(t) = \Delta\boldsymbol{\mu} \cdot \int_{-\infty}^{t} dt' \boldsymbol{r}(t-t')\theta(t') \cdot \Delta\boldsymbol{\mu}. \tag{3.28}$$

The expression for $\Delta\tilde{E}(z)$ given by Eq. (3.23) becomes

$$\Delta\tilde{E}(z) = -\frac{1}{iz}\Delta\boldsymbol{\mu} \cdot \tilde{\boldsymbol{r}}(z) \cdot \Delta\boldsymbol{\mu}. \tag{3.29}$$

The inverse Fourier transform of this equation yields $\Delta E(t)$:

$$\Delta E(t) = -\frac{2}{\pi}\Delta\boldsymbol{\mu} \cdot \int_0^{\infty} d\omega \frac{\cos\omega t}{\omega} \mathrm{Im}\tilde{\boldsymbol{r}}(\omega) \cdot \Delta\boldsymbol{\mu} - \Delta\boldsymbol{\mu} \cdot \tilde{\boldsymbol{r}}(0) \cdot \Delta\boldsymbol{\mu} \tag{3.30}$$

which is then used to calculate $S(t)$. If the above expressions are applied to a *sphere* filled with homogeneous dipole density ($A_a = A_b = A_c = 1/3$), the expression for $\Delta E(t)$ is the same as that given by Eq. (3.25) for the dipole in a sphere model.

3.2.2 Results

The above models are now applied to the system of coumarin 343 (C343) dissolved in water [7]. The results of a numerical calculation, using Eqs. (3.2), (3.20) and (3.25) and the $\epsilon(\omega)$ of water at T=298 K [23, 24], are plotted in Fig. 3.1. As in Ref. [22], in the low frequency region ($\omega \leq 3.0 \times 10^{11}$ rad s^{-1}, about 1.6 cm^{-1}) [35], Debye's formula is used,

$$\epsilon(\omega) = \epsilon_i + \frac{\epsilon_s - \epsilon_i}{1 + i\omega\tau_D}, \tag{3.31}$$

with $\tau_D = 8.2$ ps, $\epsilon_s = 78.3$ and $\epsilon_i = 4.21$. For the frequency range $\omega = 3.0 \times 10^{11}$ to 7.2×10^{14} rad s^{-1}, a spline fit was used for both the real and imaginary parts of $\epsilon(\omega)$. The upper limit of the integration is 7.2×10^{14} rad s^{-1}, which is approximately 3800 cm^{-1}. The optical dielectric constant ($\epsilon_{\rm op}$) was assumed to be 1.8. The same numerical answer was obtained for the integration in Eq. (3.25) either using the

Fast Fourier Transform (FFT) subroutines or the direct numerical integration. This agreement confirms the quality of the present calculation. The plot of the calculated $S(t)$ is compared in Figs. 1 and 2 with the $S(t)$ obtained from the experimentally fitted parameters of experimental data in Ref. [7].

For an oblate ellipsoid with $a/b = a/c = 0.4$ and with the change of dipole $\Delta\boldsymbol{\mu}$ is parallel to one of the long axes, $\Delta E(t)$ was calculated by the inverse Fourier transform of Eq. (3.29) and then $S(t)$ is obtained from Eqs. (3.2) and (3.20). The dimensions of the ellipsoid were chosen to approximate the shape of the coumarin ion [4]. For this case the ellipsoidal shape factors are [34]: $A_a = 0.588$, $A_b = A_c = 0.206$. The results of calculation are plotted in Fig. 3.2.

3.3 Discussion

We see from Figs. 1 and 2 that this simple continuum model of solute and solvent gives a time-dependent Stokes shift reasonably close to that observed in the experiment. There may or may not be a difference of behavior at very short times ($\sim$ 50 fs) in Fig. 1 between the experimental and calculated curves. In the experiments [7], the cross-correlation of the pump pulse and the gate pulse is reported to be 100-110 fs (full width at half maximum).

It is perhaps surprising that the simple model works as well as it does, and it will be interesting to see whether similar agreement is obtained for other solvents. Because the dielectric dispersion $\epsilon(\omega)$ of the solvent contains a broad range of frequencies in its response, it is not surprising that the calculated response function, like the experimental, is far from being a single exponential. The entire dielectric dispersion spectrum of $\epsilon(\omega)$ includes the low frequency part, which is well-described by the Debye formula, and the high frequency part which contains various contributions from inter- and intra-molecular vibrational modes of the solvent. The former contributes to the long-time behavior, whose characteristic behavior is diffusional, while the latter is more "reversible" and determines the short-time behavior.

Many studies on solvation dynamics (e.g., Ref. [5, 8–10, 14, 17, 31, 39–41]) use an

analytic form for $\epsilon(\omega)$ which includes various of models for the low frequency part and damped oscillations for higher frequency region. Horng *et al.* [5] has included a low frequency Debye model and two or three damped oscillators at higher frequencies for acetonitrile and methanol and has obtained a reasonably good $S(t)$ for acetonitrile. In the interesting work by Nandi *et al.* [17] excellent agreement between the experimental and calculated $S(t)$ was obtained, though the model provided for water did not quite resemble the experimental $\epsilon(\omega)$. Loring *et al.* [39] calculated the fluorescence and hole burning lineshape with a molecular theory using a Debye model for $\epsilon(\omega)$ in obtaining the results. Jarzeba *et al.* [8] showed that simple continuum models, such as single or multiple component Debye models or the Cole-Davidson model, accurately predicted the averaged solvation time but not the shape of $S(t)$, and they suggested that it would be useful to have higher frequency dielectric data included. Their suggestion is indeed confirmed by our present calculation.

We used a spline fit for the discrete data of $\epsilon(\omega)$. Thereby, there were no adjustable parameters and a direct connection was made between $\epsilon(\omega)$ and $S(t)$. Any analytical model that provides reasonably good description of the $\epsilon(\omega)$ spectrum would of course give essentially the same $S(t)$. However, we believe that directly using the experimental dielectric dispersion data with a simple continuum model provides a transparent way of introducing the solvation dynamics, especially for the possible cases where model dielectric theories do not provide a satisfactory description of $\epsilon(\omega)$.

The model used in Fig. 3.1 is the dipole in a spherical cavity in a solvent dielectric continuum, while that used in Fig. 3.2 is the ellipsoid with a homogeneous dipole density. The rate of decay of $S(t)$ with t for the latter is slightly faster than that for the former. There is seen to be little effect of changing the shape of solute from a sphere to an ellipsoid. Results (not shown) were also obtained for the $S(t)$ when the dipole is replaced by a single charge. In that case, the solvent response $r(\omega)$ in Eq. (3.14) is replaced by $(1 - 1/\epsilon(\omega))$. One then finds that the results in Fig. 3.2 for the ellipsoid filled with a uniform dipole density lie between those for the dipole in a sphere in Fig. 3.1 and those for a charge in a sphere. This result is not unexpected, since the ellipsoid filled with a homogeneous dipole density which is parallel to the

long axis has net charges distributed at the surface at both ends of the long axis. The latter would behave more or less like two not quite separated regions of charge density and so be the intermediate between a charge and a point dipole in its behavior.

In the results of the present calculation, the small peaks of recurrence in Figs. 3.1 and 3.2 show a "reversibility" of the motion, with the shortest period being about 44 fs, which corresponds to roughly 760 cm^{-1} in frequency. The absorption band in that region has been assigned to a "libration," namely, oscillation of the water molecule in the force field of its neighbors [25]. The other bands with higher frequencies in $\epsilon(\omega)$ do not yield any significant recurrence from the rapid initial decay of $S(t)$, due to their contribution to $\epsilon(\omega)$ being very small and, to a lesser extent, due to the $1/\omega$ factor in the integrand. Thereby, these resonance bands contribute only a small portion of the rapid initial decay (cf. Fig. 3.3). Nandi *et al.* [17] pointed out the importance of the intermolecular O$\cdots$O stretching mode, which constitutes the 193 cm^{-1} band in $\epsilon(\omega)$ and corresponds to 170 fs as its recurrence period. In Fig. 3.3 there is a small shoulder located between 150 and 200 cm^{-1} arising from such motion. In Figs. 3.1 and 3.2, the (broader) recurrence peak at about 0.2 ps can be regarded as a mixed result of this lower frequency band and the librational motion, and the rate of decay is seen to slow down at this region, for both the experimental and the calculated $S(t)$.

A molecular dynamics (MD) simulation of rigid water showed a similar pattern of recurrence in $S(t)$ [7], and supports the idea that the principal reversible mode is intermolecular. In that MD work the amount of initial decay is, out of the total calculated $S(t)$, roughly 10% less than our result in Fig. 3.1. Part of this difference may arise from the effect of the rapidly dephased intramolecular modes of water, which occurs in our calculation: It includes all dispersive contributions, unlike the MD result, since a rigid model for the individual water molecules was used in the latter. Both the MD study and the present result show the importance of including the moderately high frequency intermolecular components of dielectric response spectrum on the dynamics in sub-picosecond time scale, in addition to including the Debye region.

In Figs. 3.1 and 3.2 it is seen that $S(t)$ for an oblate ellipsoid with its dipole

"lying" in the plane of the molecule decays only slightly faster than it does for a sphere. Recalling that the sphere model also applied to a homogeneous dipole density model, we also see in this comparison that the molecular shape affects $S(t)$ only a little, within the approximation of using a dielectric continuum. For a more complete description of the solvation dynamics, in addition to satisfying the boundary condition at the solute-solvent interface, the spatial dependence of the dielectric constant [11, 36] would also be taken into account.

When the smooth decay of our theoretically calculated $S(t)$ after 0.5 ps is fitted by an exponential function, the results in Fig. 3.1 correspond to a lifetime of 810 fs. This number agrees well with the slowest exponential component in Ref. [7] obtained by fitting to the experimental data, namely, 880 fs. On the other hand, the Debye model (Eq. (3.31)) describes a single exponential relaxation process: For the sphere cavity model, the relaxation time for $S(t)$ obtained from the Debye formula is $\tau_D(2\epsilon_i + 1)/(2\epsilon_s + 1)$ (e.g., Ref. [31]), which is 490 fs. The Debye model is a good description of $\epsilon(\omega)$ for $\omega = 0$ to about 3.0×10^{11} rad s^{-1}. For frequencies higher than that, the measured $\epsilon(\omega)$ begins to deviate from Debye's formula. Thereby, a decay occurring according to the Debye formula is expected to occur only after 3 ps. The current lifetime fit for $t = 0.5$ to 2 ps is not, we have just seen, the Debye 490 fs, and represents a mixed result from both the Debye model and the spline fit of dielectric dispersion for higher frequencies.

3.4 Conclusion

The solvation correlation function can be calculated by including the entire spectrum of dielectric dispersion data $\epsilon(\omega)$ up to the optical region. Using simple dielectric continuum models that neglect the molecular property of the solvent, our results show that the correlation function obtained give a reasonable description for the time-dependent Stokes shift measurement.

Acknowledgements

It is a pleasure to acknowledge the support of this research by the National Science Foundation and by the Office of Naval Research. This article is dedicated to the memory of a long-time friend, Heinz Gerischer, whom one of us had the pleasure of knowing for almost forty years. Heinz was a generous and thoughtful individual whose impact on electrochemistry is enormous.

Appendix A: Analysis for Equation (3.24)

Equation (3.24) can be rewritten as

$$\Delta E(t) = -\frac{\Delta\mu^2}{2\pi}\int_C dz \frac{\tilde{r}(z)}{iz} e^{izt} \tag{3.32}$$

$$= -\frac{\Delta\mu^2}{2\pi}\int_C dz \frac{\tilde{r}(z)-\tilde{r}(0)}{iz} e^{izt} - \frac{\Delta\mu^2}{2\pi}\int_C dz \frac{\tilde{r}(0)}{iz} e^{izt} \tag{3.33}$$

where C denotes the a contour that is parallel but slightly below the real axis. The second of the integrals in Eq. (3.33) can be shown, using the residue theorem, to equal $2\pi\tilde{r}(0)\theta(t)$. We note that $\tilde{r}(z)$ is analytic on the real axis [33], and $\tilde{r}(z=0)$ is a real number [32]. The integrand in the first integral does not possess a pole at $z = 0$, since

$$\frac{\tilde{r}(z)-\tilde{r}(0)}{z} = \left[\frac{d\tilde{r}(z)}{dz}\right]_{z=0} + O(z), \quad z \to 0. \tag{3.34}$$

and $d\tilde{r}(z)/dz$ has no singularity at $z = 0$. We may therefore allow the contour C for the first integral in Eq. (3.33) to coincide with the real axis. Denoting the real and imaginary part of $\tilde{r}(\omega)$ by $\tilde{r}'(\omega)$ and $\tilde{r}''(\omega)$, respectively, i.e., $\tilde{r}(\omega) = \tilde{r}'(\omega) + i\tilde{r}''(\omega)$, and noting that $\tilde{r}(-\omega) = \tilde{r}^*(\omega)$, which follows because $r(t)$ is real, we then find

$$\int_C dz \frac{\tilde{r}(z)-\tilde{r}(0)}{iz} e^{izt} = 2\int_0^\infty d\omega \frac{\tilde{r}''(\omega)}{\omega}\cos\omega t + 2\int_0^\infty d\omega \frac{\tilde{r}'(\omega)-r_s}{\omega}\sin\omega t. \tag{3.35}$$

Therefore, Eq. (3.33) yields

$$\Delta E(t) = -\frac{\Delta\mu^2}{\pi}\left[\int_0^\infty d\omega \frac{\tilde{r}''(\omega)}{\omega}\cos\omega t + \int_0^\infty d\omega \frac{\tilde{r}'(\omega) - r_s}{\omega}\sin\omega t + \pi r_s \theta(t)\right]. \quad (3.36)$$

Another useful property is obtained by noting that $\Delta E(t) = 0$ for $t < 0$ (Eq. (3.21)). The first integrand in Eq. (3.36) is an even function of t while the second is an odd function. Since the sum of them yields zero for negative t, they must be equal for positive t. Thus, the calculation for $\Delta E(t)$ can be performed by integrating either of the two terms in Eq. (3.36). In the present work, the first term was used because $r''(\omega)$ goes to zero as ω goes to the optical limit in an integration region and so it is numerically easier to calculate. We can write,

$$\Delta E(t) = -\frac{2\Delta\mu^2}{\pi}\int_0^\infty d\omega \frac{\tilde{r}''(\omega)}{\omega}\cos\omega t - \Delta\mu^2 r_s, \quad \text{for } t \geq 0. \quad (3.37)$$

which yields Eq. (3.25).

The second term of Eq. (3.36) can be better evaluated, if desired, as follows:

$$\int_0^\infty d\omega \frac{\tilde{r}'(\omega) - r_s}{\omega}\sin\omega t = \int_0^\infty d\omega \frac{\tilde{r}'(\omega) - r_{\text{op}}}{\omega}\sin\omega t + \int_0^\infty d\omega \frac{r_{\text{op}} - r_s}{\omega}\sin\omega t \quad (3.38)$$

$$= \int_0^\infty d\omega \frac{\tilde{r}'(\omega) - r_{\text{op}}}{\omega}\sin\omega t + \pi\left(\theta(t) - \frac{1}{2}\right)(r_{\text{op}} - r_s). \quad (3.39)$$

The first term now has a finite range of ω and so is numerically easier to calculate than the left-hand side of Eq. (3.38).

Appendix B: Remark on the Optical Response Contribution

At time $t = 0$, the first term in Eq. (3.37) would formally become

$$-\frac{2\Delta\mu^2}{\pi}\int_0^\infty d\omega\frac{\tilde{r}''(\omega)}{\omega} = \Delta\mu^2\tilde{r}'(0) = \Delta\mu^2 r_s. \tag{3.40}$$

Equation (3.40) follows from the Kramers-Kronig relationship [37, 38] when the upper limit is really $+\infty$ (and not $\omega_{\rm op}$). Equation (3.36) then gives $\Delta E(0) = 0$. However, practically the integration is cut off at a frequency ($\omega_{\rm op}$) in the range between the response arising from nuclear motions ($0 < \omega < \omega_\nu$) and the electronic polarization ($\omega_{\rm el} < \omega < \infty$). Because of the large separation of the two frequency regions (e.g., $\omega_\nu \sim 10^3{\rm cm}^{-1}$ while $\omega_{\rm el} \sim 10^5{\rm cm}^{-1}$), the $\tilde{r}''(\omega)$ from the fast electronic polarization gives approximately a constant contribution $r_{\rm op}$ to $\tilde{r}'(\omega)$ over the lower frequency region ($0 < \omega < \omega_\nu$) [38]. That constant can be obtained from the Kramers-Kronig relation:

$$\begin{aligned} r_{\rm op} &= \tilde{r}'(\omega_{\rm op}) = \frac{2}{\pi}P\int_0^\infty d\omega\frac{\omega\tilde{r}''(\omega)}{\omega_{\rm op}^2-\omega^2} \\ &\simeq \frac{2}{\pi}\left[\int_0^{\omega_\nu} d\omega\frac{\omega\tilde{r}''(\omega)}{\omega_{\rm op}^2-\omega^2} + \int_{\omega_{\rm el}}^\infty d\omega\frac{\omega\tilde{r}''(\omega)}{\omega_{\rm op}^2-\omega^2}\right] \qquad (3.41) \\ &\simeq 0 - \frac{2}{\pi}\int_{\omega_{\rm el}}^\infty d\omega\frac{\tilde{r}''(\omega)}{\omega} \simeq -\frac{2}{\pi}\int_{\omega_{\rm op}}^\infty d\omega\frac{\tilde{r}''(\omega)}{\omega}. \qquad (3.42) \end{aligned}$$

where P denotes principal part of and where it has been assumed that there is negligible absorption in the frequency interval $(\omega_\nu, \omega_{\rm el})$, so $\tilde{r}''(\omega)$ is practically zero there. In obtaining Eq. (3.42), the large separation of the two frequency regions in the integrations allows us to assume $\omega_\nu \ll \omega_{\rm op} \ll \omega_{\rm el}$, and so $\omega_{\rm op}^2$ and ω^2 dominate in the denominators of the first and second integrals, respectively, in Eq. (3.41).

If the upper limit in Eq. (3.40) were replaced by ω_{op}, it would become

$$-\frac{2\Delta\mu^2}{\pi}\int_0^{\omega_{op}} d\omega \frac{\tilde{r}''(\omega)}{\omega} = -\frac{2\Delta\mu^2}{\pi}\left(\int_0^{\infty} d\omega \frac{\tilde{r}''(\omega)}{\omega} - \int_{\omega_{op}}^{\infty} d\omega \frac{\tilde{r}''(\omega)}{\omega}\right) = \Delta\mu^2(r_s - r_{op}). \tag{3.43}$$

where we have used Eqs. (3.40) and (3.42).

Thus, in $\Delta E(t)$, there is expected to be an initial drop which is faster than the time-resolution set by this cut-off frequency ω_{op}, due to the electronic polarization:

$$\Delta E(t = 0^+) = -\Delta\mu^2 r_{op}. \tag{3.44}$$

We see from the above equation that when the $\Delta E(t)$ is calculated using ω_{op} instead of ∞ in Eq. (3.37) as the upper limit of integration, the $\Delta E(t)$ starts from a value $\Delta E(0^+)$ that arises from the electronic polarization. $\Delta E(t)$ eventually goes to a static interaction energy, $\Delta E(t \to +\infty)$, which equals to $-\Delta\mu^2 r_s$ (Eq. (3.37)). Thus, the changes in $\Delta E(t)$ after the initial brief time interval, 0^+, describe the solvational energy that arises from the nuclear response of the solvent.

References and Notes

[1] Nee, T.-W.; Zwanzig, R., *J. Chem. Phys.* **1970**, *52*, 6353. van der Zwan, G.; Hynes, J. T., *J. Chem. Phys.* **1982**, *76*, 2993.

[2] Ware, W. R.; Lee, S. K.; Brant, G. J.; Chow, P. P. *J. Chem. Phys.* **1971**, *54*, 4729. Okamura, T.; Sumitani, M.; Yoshihara, K. *Chem. Phys. Lett.* **1983**, *94*, 339. Su, S.-G.; Simon, J. D., *J. Phys. Chem.* **1987**, *91*, 2693.

[3] Jarzęba, W.; Walker, G. C.; Johnson, A.E.; Kahlow, M. A.; Barbara, P. F., *J. Phys. Chem.* **1988**, *92*, 7039;

[4] Maroncelli, M.; Fleming, G. R., *J. Chem. Phys.* **1987**, *86*, 6221.

[5] Horng, M. L.; Gardecki, J. A.; Papazyan, A.; Maroncelli, M., *J. Phys. Chem.* **1995**, *99*, 17311. Gardecke, J.; Horng M. L.; Papazyan, A. Maroncelli, M., *J. Mol. Liq.* **1995**, *65-6*, 49.

[6] Maroncelli, M., *J. Chem. Phys.*, **1997**, *106*, 1545; Kumar, P. V.; Maroncelli, M., *J. Chem. Phys.* **1995**, *103*, 3038.

[7] Jimenez, R.; Fleming, G. R.; Kumar, P. V.; Maroncelli, M. *Nature* **1994**, *369*, 471.

[8] Jarzeba, W.; Walker, G. C.; Johnson, A. E.; Barbara, P. F. *Chem. Phys.* **1991**, *152*, 57.

[9] Maroncelli, M.; Castner, E. W. Jr.; Bagchi, B.; Fleming, G. R., *Faraday Discuss. Chem. Soc.* **1988**, *85*, 199.

[10] Castner, E. W. Jr.; Fleming, G. R.; Bagchi, B. *Chem. Phys. Lett.* **1988**, *143*, 270.

[11] Wolynes, P. G., *J. Chem. Phys.* **1987**, *86*, 5133. Rips, I.; Klafter, J.; Jortner, J. *J. Chem. Phys.* **1988**, *88*, 3246; *ibid.* **1988**, *89*, 4288. Nichols, III A. L.; Calef, D. F., *J. Chem. Phys.* **1988**, *89*, 3783.

[12] Raineri, F. O.; Resat, H.; Perng, B.-C.; Hirata, F.; Friedman, H. L., *J. Chem. Phys.* **1994**, *100*, 1477. Zhou, Y.; Friedman, H. L.; Stell, G., *J. Chem. Phys.* **1989**, *91*, 4885. Fried, L. E.; Mukamel, S., *J. Chem. Phys.* **1990**, *93*, 932; Loring, R. F.; Mukamel, S., *J. Chem. Phys.* **1987**, *87*, 1272. Bagchi, B.; Chandra, A., *J. Chem. Phys.* **1989**, *90*, 7338.

[13] Maroncelli, M.; Fleming, G. R., *J. Chem. Phys.* **1988**, *89*, 875.

[14] Kahlow, M. A.; Jarzęba, W.; Kang, T. J.; Barbara, P. F., *J. Chem. Phys.* **1989**, *90*, 151.

[15] Bagchi, B.; Chandra, A., *Adv. Chem. Phys.* **1991**, *80*, 1. Bagchi, B., *Annu. Rev. Phys. Chem.* **1989**, *40*, 115.

[16] Roy, S.; Bagchi, B., *J. Chem. Phys.* **1993**, *99*, 9938.

[17] Nandi, N.; Roy, S.; Bagchi, B., *J. Chem. Phys.* **1995**, *102*, 1390.

[18] Gertner, B. J.; Whitnell, R. M.; Wilson K. R.; Hynes, J. T. *J. Am. Chem. Soc.* **1991**, *113*, 74.

[19] Maroncelli, M.; Fleming, G. R., *J. Chem. Phys.* **1988**, *89*, 5044.

[20] Ladanyi, B. M.; Stratt, R. M., *J. Phys. Chem.* **1995**, *99*, 2502; *ibid.* **1996**, *100*, 1266.

[21] Cho, M.; Rosenthal, S. J.; Scherer, N. F.; Ziegler, L. D.; Fleming, G. R., *J. Chem. Phys.* **1992**, *96*, 5033.

[22] Song, X.; Marcus, R. A., *J. Chem. Phys.* **1993**, *99* , 7768.

[23] Hasted, J. B., *Aqueous Dielectrics*; Chapman and Hall: London, 1973.

[24] Asfar, M. N.; Hasted, J. B., *Infrared Phys.* **1978**, *18*, 835. Hasted, J. B.; Husain, S. K.; Frescura, F. A. M.; Birch, J. R. *Infrared Phys.* **1987**, *27*, 11. Hale, G. M.; Querry, M. R., *Applied Optics* **1973**, *12*, 555.

[25] Böttcher, C. J. F., *Theory of Electric Polarization*, Vol. 1; Elsevier: Amsterdam, 1983.

[26] Onsager, L., *J. Am. Chem. Soc.* **1936**, *58*, 1486.

[27] For example, Mathews, J.; Walker, R. L. *Mathematical Methods of Physics*, 2nd ed.; W. A. Benjamin: New York; 1970; pp. 246–247. Titchmarsh, E. C., *Introduction to the Theory of Fourier Integrals*, 2nd ed.; The Clarendon Press: Oxford, 1948; pp. 4–6.

[28] For example, Kubo, R.; Toda, M.; Hashitsume, N. *Statistical Physics*, Springer-Verlag: New York, 1983; Vol. II, p. 120. Ginzburg, V. L. *The Propagation of Electromagnetic Waves in Plasmas*, 2nd ed.; Pergamon Press: Oxford, 1970; pp. 4–7.

[29] For example, Jackson, J. D., *Classical Electrodynamics*, 2nd ed.; Wiley: New York, 1975.

[30] Since all the time-dependent physical quantities, $\mathbf{P}_i(\mathbf{r},t)$, $\mathbf{E}_i(\mathbf{r},t)$, and $\mathbf{D}_i(\mathbf{r},t)$, are real, $\alpha_i(t)$ is also real. Thus, when $z = \omega$, a real variable, the Fourier transform $\tilde{\alpha}_i(\omega)$ has the property, $\tilde{\alpha}_i(-\omega) = \tilde{\alpha}_i^*(\omega)$, where $\tilde{\alpha}_i^*$ is the complex conjugate of $\tilde{\alpha}_i$. From Eqs. (3.13) and (3.14), it is also true that $\epsilon_i(-\omega) = \epsilon_i^*(\omega)$ and $r(-\omega) = r^*(\omega)$.

[31] Bagchi, B.; Oxtoby, D. W.; Fleming, G. R. *Chem. Phys.* **1984**, *86*, 257.

[32] We note, from Eq. (3.5), that $\tilde{r}(0) = \int_{-\infty}^{\infty} r(t)dt = \int_0^{\infty} r(t)dt$ since $r(t) = 0$ for $t < 0$ and note that $\int_{-\infty}^{t} r(t-t')dt' = \int_0^{\infty} r(t'')dt''$. Also, $\tilde{r}(0)$ is a real number since $r(t)$ is a real function of t.

[33] Since $r(t)$, the response function, goes to zero exponentially as t goes to $+\infty$, and it equals zero for negative t's (causality), its corresponding transform $\tilde{r}(z)$ is analytic both on the real axis and in the lower half complex plane of z (cf. Eq. (3.5)).

[34] Osborn, J. A., *Phys. Rev.* **1945**, *67*, 351; Stoner, E. C., *Phil. Mag.* **1945**, *36*, 803.

[35] In Ref. [22] the boundary used for switching from Debye's formula to the spline fit was 1.0×10^{11} rad s^{-1}. Changing that number to the current 3.0×10^{11} rad s^{-1} does not change the result of calculation presented in this work.

[36] Song, X.; Chandler, D.; Marcus, R. A. *J. Phys. Chem.* **1996**, *100*, 11954.

[37] For example, McQuarrie, D. A., *Statistical Mechanics*; Harper & Row: New York, 1976; pp. 498-499.

[38] Böttcher, C. J. F.; Bordewijk ,P., *Theory of Electric Polarization*, Vol. 2; Elsevier: Amsterdam, 1973.

[39] Loring, R. F.; Yan, Y. J.; Mukamel S., *J. Chem. Phys.* **1987**, *87*, 5840.

[40] van der Zwan, G.; Hynes, J. T., *J. Phys. Chem.* **1985**, *89*, 4181.

[41] Neumann, M., *J. Chem. Phys.* **1986**, *85*, 1567.

Figure 3.1: Calculated $S(t)$ (solid line) for a dipole in a sphere using Eq. (3.25). The dashed line depicts the experimental result from Ref. [7]. The latter is a fit to their experimental data with one narrow Gaussian and two exponential functions.

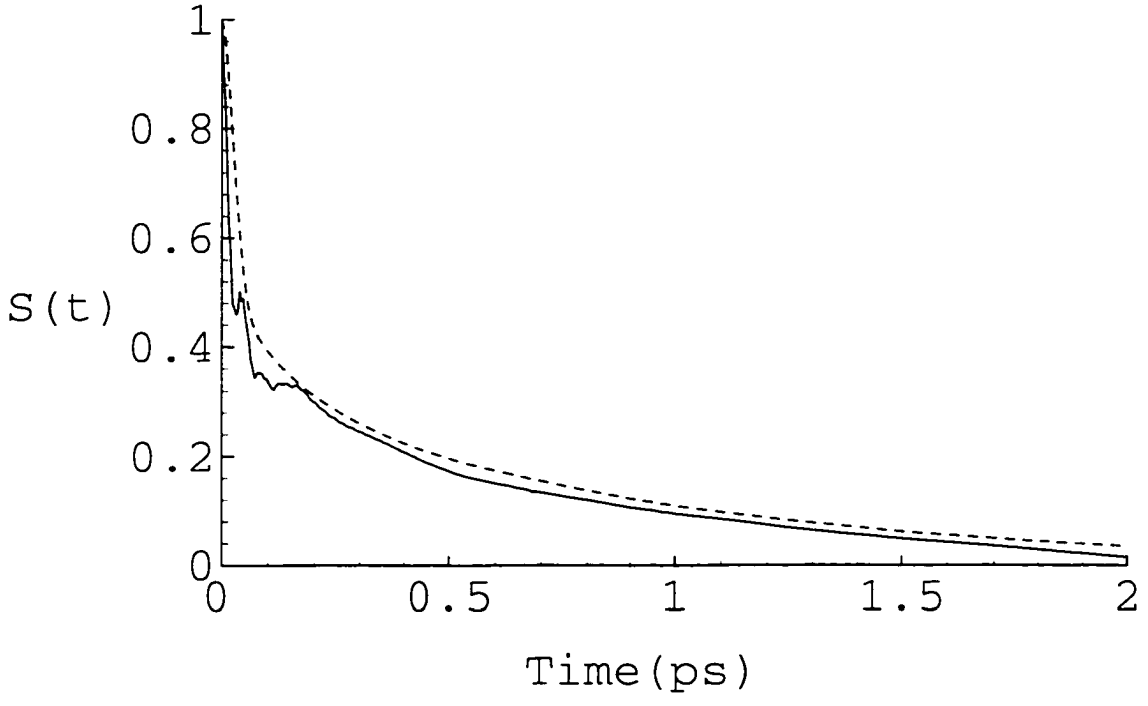

Figure 3.2: Calculated $S(t)$ (solid line) for a model of an ellipsoid solute using Eqs. (3.26) and (3.29). The ellipsoid has $a : b : c = 0.4 : 1 : 1$ with the dipole moment lying on b or c axis. The dashed line is the experimental result, which is the same as that in Fig. 3.1.

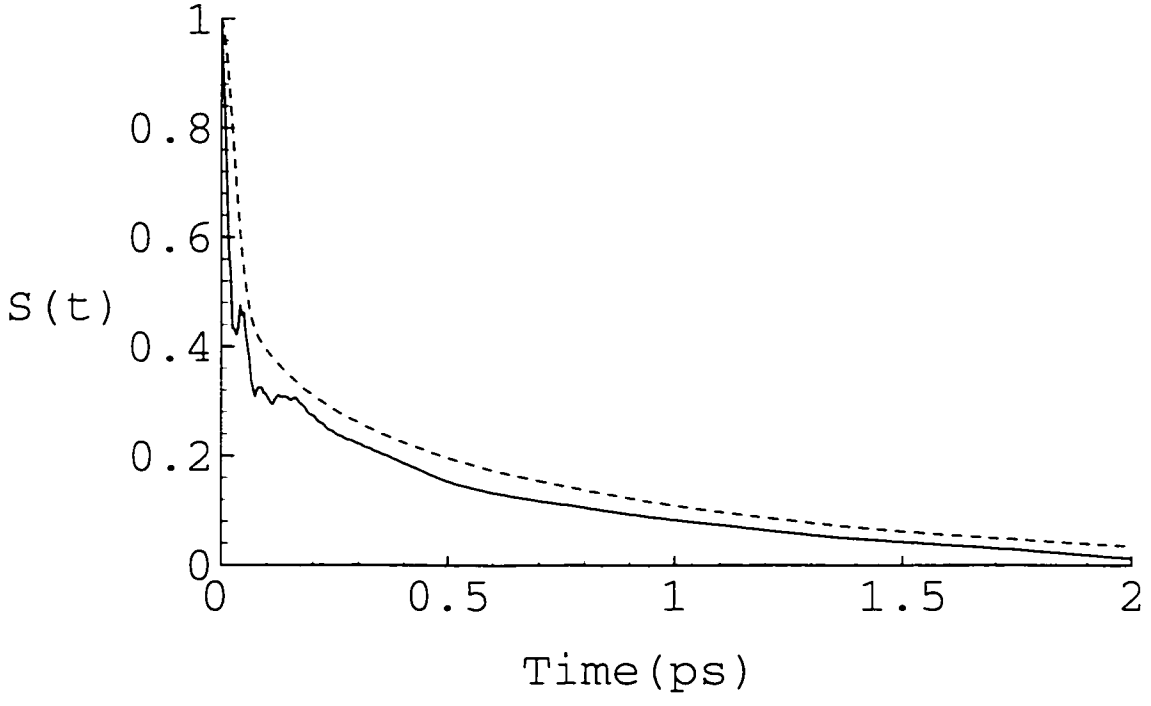

Figure 3.3: The imaginary part of the quantity, $[(\epsilon(\omega)-1)/(2\epsilon(\omega)+1)]/\omega$, which is proportional to the term that is cosine transformed in Eq. (3.25), for the dipole in a sphere cavity. Circles denote the data points calculated from experimental $\epsilon(\omega)$. The zero frequency limit of this quantity, estimated from the Debye formula (Eq. (3.31)), is -0.073 ps rad^{-1}. It is seen that the contribution of the intramolecular vibrational bands is quite small compared to that of the librational mode at about 800 cm^{-1}. The units of the ordinate are ps rad^{-1}.

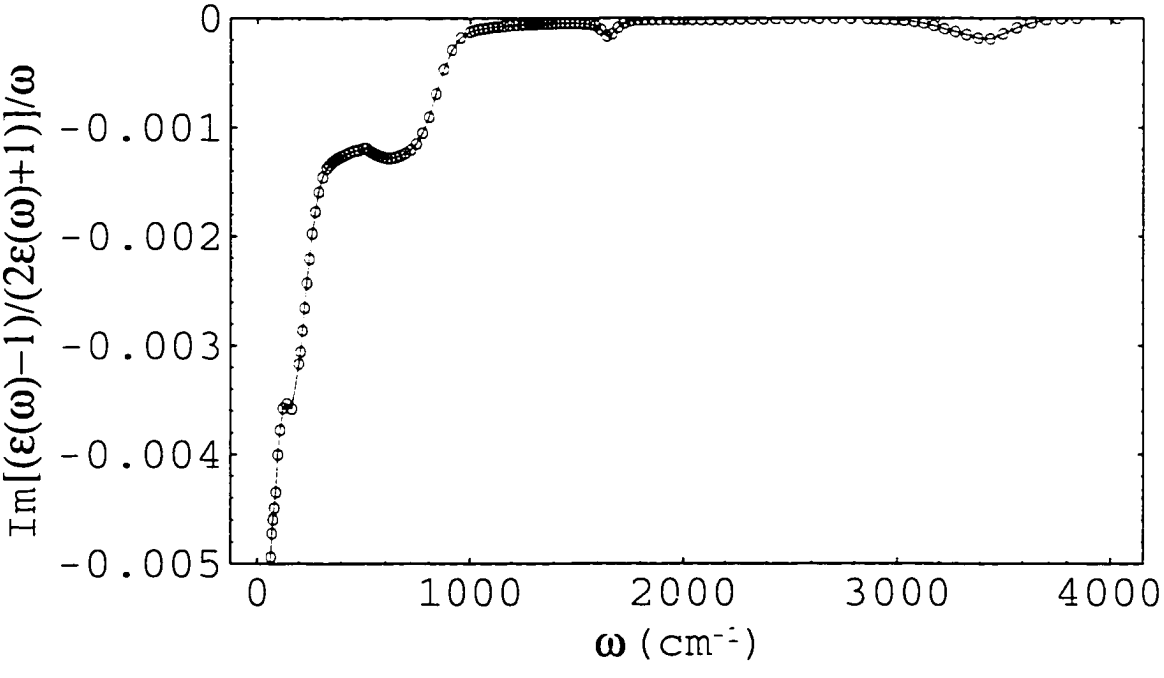

Chapter 4 Dynamic Stokes Shift in Solution: Effect of Finite Pump Pulse Duration

Yuri Georgievskii, Chao-Ping Hsu, and R. A. Marcus

Division of Chemistry and Chemical Engineering, Noyes Laboratory of Chemical Physics, Mail Code 127-72, California Institute of Technology, Pasadena, CA 91125

(Reprinted with permission from *J. Chem. Phys.*, in press.

Abstract

The time-evolution of the fluorescence spectrum of a dissolved chromophore excited by an ultrafast pump pulse is considered. The average value of the energy difference of the solute in its excited and ground states is used to describe the relaxation of the maximum of the transient fluorescence spectrum to its equilibrium value (dynamic Stokes shift, DSS). A simple formula for the normalized DSS is obtained which generalizes an earlier standard classical expression and includes the effect of a pump pulse of finite duration. As an example, dielectric dispersion data are used for a dipolar solute in water to estimate the quantum correction to the standard DSS expression. The correction is negligible when the frequency of the pump pulse is close to the maximum in the absorption spectrum, but a deviation from the standard formula can be expected for the pump pulse tuned to a far wing of the absorption band of the chromophore. An expression is given for this deviation.

4.1 Introduction

The solvation dynamics of dipolar and ionic solutes in polar solvents has attracted considerable attention in recent years, e.g., Refs. [1–7]. This interest reflects the importance of the solvent dynamics in many chemical and physical processes in the condensed phase [8–11]. Transient nonlinear spectroscopy has been one main tool for tracing the ultrafast dynamics of solvation [12–14]. The loss of coherence between the ground and excited electronic states, which is caused by the solute-solvent interaction, is closely related to solvation dynamics. The photon echo technique [15–22] and pump-probe spectroscopy [23–26] have both been used to separate the inhomogeneous (slow) broadening of the spectral line associated with a particular electronic transition from the homogeneous (fast) electronic dephasing. Several new experimental techniques have been developed to trace electronic dephasing with femtosecond resolution [27–31]. In a different, but related approach, the optical Kerr effect has been used to study subpicosecond dynamics of the solvent as a whole [32-35].

Most of the experimental data on solvation dynamics in polar solvents have been obtained using a time-resolved fluorescence method with upconversion [36–46]. The energy difference in the ground and excited electronic states of the solute is manifested through $\nu(t)$, the frequency of the fluorescence spectral maximum of the molecule. Its time-evolution (dynamic Stokes shift, DSS) reflects the solvation dynamics of the electronically excited solute. At the current level of resolution, a DSS experiment permits a scanning of the solvent dynamics on a time scale ranging from less than 100 femtoseconds for fast relaxing solvents like water [2] up to nanoseconds for 'slow' solvents [47]. For strongly coupled systems the time-resolved fluorescence experiments [36–47] have been more extensively compared with theory and with computer simulations than photon echo [15–22, 27–31] or optical Kerr effect measurements [32–35].

To interpret the results of a DSS measurement, it is usually assumed that the photoexcitation, i.e., the transition forming the molecule in the excited electronic state, occurs much faster than any relaxation of the solvent and so the excited molecule would appear initially in a solvent which is in equilibrium with the ground state of

the molecule [48]. It is also usually assumed that the solvent dynamics that is related to the evolution of the transient fluorescence spectrum can be described classically and that quantum effects in the solvent dynamics can be neglected.

Recent ultrafast DSS measurements [2, 36–38] have shown that the considerable part of relaxation ($\geq 50\%$) in many solvents composed of small molecules occurs on a very short time scale ($\leq$ 100 fs), which becomes comparable to the pump pulse duration. Under these conditions the validity of the assumption that the state of the solvent immediately after the excitation is the same as before is no longer strictly valid. In the present article an estimate is made of the effect of the finite pump pulse duration on this time-development of the Stokes shift and of the extent to which the quantum dynamics of the solvent can modify the usual classical result. A model is described in Section 4.2, and the dynamic Stokes shift is calculated in Section 4.3, initially for an instantaneous pulse (Section 4.3.1) and then for a pulse of finite duration (Section 4.3.2). A physical interpretation of the principal equations is given in Section 4.4, and a summary is given in Section 4.5.

4.2 The Model

For treating the solvent dynamics, several approaches come to mind. In one of these linear response theory is used, as Ovchinnikov and Ovchinnikova did [49] in their application of the quantum field theoretical method of Abrikosov *et al.* [50]. In a similar spirit, Mukamel and coworkers [51–53] used a cumulant expansion, based on second-order perturbation theory to treat systems which in molecular terms have nonlinear interactions. Neither treatment uses a molecular harmonic oscillator model. An approach which is, at first glance, quite different from these in validity, is the use of a molecular oscillator model - the well known spin-boson Hamiltonian [54]. It gives results which are formally the same [55] as those obtained by the other two methods, when the number of oscillators N allowed to become infinite. This agreement is not accidental. Rather, it bears some analogy to the representation of a nonperiodic function by a Fourier integral, when the latter is regarded as the limit as N tends

to ∞ of a Fourier series representation of the function. We have chosen to use this spin-boson Hamiltonian approach, and then allowing N to tend to ∞, because of its simplicity, although either of the other two methods could have been used instead to to obtain the key equations, Eqs. (4.47) and (4.48). We note that these equations do not, for the above reason, contain any properties specific to molecular harmonic oscillators.

In the harmonic oscillator approach (with finite N, which at the end is allowed to become infinite), the solvent Hamiltonian H_g in the ground electronic state can be written as [54, 56–68]

$$H_g = \sum_j \frac{1}{2}(P_j^2 + \omega_j^2 Q_j^2) + U_g, \tag{4.1}$$

where ω_j, Q_j, and P_j are the frequencies, coordinates, and momenta of the 'normal modes', respectively (mass-weighted coordinates). When the resulting change of electronic state after an electronic transition leads only to shifts of the normal modes but not to changes in their frequency, the solvent Hamiltonian H_e in the excited electronic state can be written as [54, 56–68]

$$H_e = \sum_j \frac{1}{2}[P_j^2 + \omega_j^2(Q_j + \frac{c_j}{\omega_j^2})^2] + U_e. \tag{4.2}$$

where the coefficients c_j uniquely characterize the shifts of equilibrium positions of the normal modes. The difference of the minima of the potential energies $\Delta U = U_e - U_g$ in the excited and ground electronic states, respectively, coincides with the free energy difference for this harmonic oscillator model.

A comment is relevant here about the role of intramolecular solute modes. In most experiments relatively large molecules (mostly dye molecules) with many nuclear degrees of freedom are used as solute probes [5], molecules in which the equilibrium nuclear configuration in the excited electronic state is different from the one in the ground electronic state. Vibrational modes of such solutes, changes in the ring modes in aromatic systems, for example, contribute considerably to the static Stokes shift and must be included in any model. The harmonic approximation for intramolecular

modes is often used for electron transfer and other nonadiabatic electronic transitions [57, 58]. One can then assume that the sum in Eqs. (4.1) and (4.2) is not only over the solvent modes but also over the intramolecular solute modes, neglecting any change in their frequencies as a result of the electronic transition.

To describe the solvent dynamics related to the spectroscopy of the solute , it is now customary to treat the energy difference of the excited and ground electronic states as a collective coordinate [51-53]

$$X = H_e - H_g = \sum_j c_j Q_j + \Delta U + \lambda, \tag{4.3}$$

where the 'solvent reorganization energy' λ is given in the harmonic oscillator model by

$$\lambda = \sum_j c_j^2 / 2\omega_j^2. \tag{4.4}$$

The coordinate X corresponds to the optical frequency of the vertical electronic transition at any specified values of the nuclear coordinates of the solvent. It can be referred to as a generalized 'solvation coordinate'. A similar idea was used earlier in electron transfer theory [60-65]. Statistical and temporal properties of the solvation coordinate are primarily responsible for the spectroscopic properties of the solute. It is convenient to separate X into a constant part and a fluctuation,

$$X = \langle X \rangle + \Delta X, \tag{4.5}$$

where the average is taken over a thermal equilibrium distribution in the ground electronic state of the solute,

$$\langle \ldots \rangle = \mathrm{Tr}[\ldots \rho_0], \quad \rho_0 = e^{-\beta H_g} / \mathrm{Tr} e^{-\beta H_g}, \quad \beta = 1/k_B T. \tag{4.6}$$

For the model in Eqs. (4.1) and (4.2), the average value of X is equal to

$$\langle X \rangle = \Delta U + \lambda. \tag{4.7}$$

4.3 Dynamic Stokes Shift Calculation

4.3.1 Instantaneous Pump Pulse

As noted earlier it is usually assumed that the solvent state does not change during the photoinduced electronic excitation of the solute molecule. A sudden change of the electronic state of the molecule can then be viewed as switching on the potential X at $t = 0$. The constant energy change, $\langle X \rangle$, which does not influence the solvent dynamics, can be omitted. The average value [averaged as in Eq. (4.22) given below] of a dynamical variable will be denoted by the bar over that variable. The average value of the solvation coordinate variation ΔX can then be obtained as a linear response to the 'applied external force', which is a unit step function $-\theta(t)$ ($\theta(t) = 0$ if $t < 0$, and 1 for $t > 0$),

$$\overline{\Delta X}(t) = -\int_{-\infty}^{t} \alpha(t - t')\theta(t')dt' = -\int_{0}^{t} \alpha(\tau)\, d\tau. \tag{4.8}$$

The generalized susceptibility $\alpha(t)$ is given in linear response theory in terms of a correlation function of the solvation coordinate [66],

$$\alpha(t) = -\frac{1}{i\hbar}\langle[\Delta X_g(t), \Delta X_g(0)]\rangle. \tag{4.9}$$

where the square brackets denote the commutator, the subscript g in ΔX_g denotes a dynamical evolution of ΔX that proceeds with the Hamiltonian H_g, i.e., $\Delta X_g(t) = \exp(iH_g t/\hbar)\Delta X \exp(-iH_g t/\hbar)$, and the thermal averaging is performed using the ground electronic state of the solute, as in Eq. (4.6). Introducing a correlation function of the solvation coordinate,

$$C(t) = \langle \Delta X_g(t)\Delta X_g(0)\rangle, \tag{4.10}$$

Eq. (4.9) can be rewritten as [67]

$$\alpha(t) = -\frac{2}{\hbar}\mathrm{Im}[C(t)]. \tag{4.11}$$

Equations (4.8)-(4.11) are valid for arbitrary molecular Hamiltonians H_g and H_e but assuming a linear response approximation. It is difficult to formulate a rigorous, quantitative criterion of applicability of linear response theory, and do not presuppose any molecular harmonic oscillator model. However, numerical simulations [1, 4, 37, 68–73] have shown that in most cases for all but very small solutes the linear response theory is applicable even for values of ΔX which are much larger than its thermal fluctuation. Equation (4.9) is also applicable in classical mechanics, in the same approximation, when the commutator $[.....]/i\hbar$ is interpreted as the Poisson bracket [66].

To characterize the time-evolution of the fluorescence spectrum the mean optical frequency $\nu(t)$ at time t could be used [74],

$$h\nu(t) = \overline{X}(t), \tag{4.12}$$

where $h = 2\pi\hbar$ is Planck's constant. The frequency ν depends on the properties of the solute molecule as well as on those of the solvent. Commonly, instead, a dimensionless solvent response function $S(t)$ is used to characterize the solvent-related aspect of the Stokes shift evolution [48],

$$S(t) = \frac{\nu(t) - \nu(\infty)}{\nu(0) - \nu(\infty)}. \tag{4.13}$$

In classical mechanics Eq. (4.9) is substituted by [66]

$$\alpha(t) = -\beta \frac{d}{dt} C_{cl}(t), \tag{4.14}$$

where $C_{cl}(t)$ is the classical correlation function of the solvation coordinate

$$C_{cl}(t) = \langle \Delta X_g(t) \Delta X_g(0) \rangle_{cl}. \tag{4.15}$$

In the latter the averaging is over the equilibrium classical statistical ensemble appropriate to the ground electronic state of the solute. Substituting Eq. (4.14) into

Eq. (4.8) and then into Eq. (4.13), one obtains

$$S(t) = C_{cl}(t)/C_{cl}(0). \tag{4.16}$$

This result is widely used in numerical simulations [1, 4, 37, 68–73] to describe the time-evolution of the Stokes shift in terms of the classical correlation function of the solvation coordinate [cf. Eqs. (4.8) and (4.19)]. It does not assume that the motion is harmonic.

For the harmonic oscillator model in Eqs. (4.1) and (4.2), the correlation function of the solvation coordinate, Eq. (4.10), is given by [75]

$$C(t) = \hbar \sum_j \frac{c_j^2}{2\omega_j} [\coth(\beta\hbar\omega_j/2)\cos\omega_j t - i\sin\omega_j t]. \tag{4.17}$$

In the classical limit, $\hbar \to 0$, Eq. (4.17) is reduced to the following expression:

$$C_{cl}(t) = \beta^{-1} \sum_j \frac{c_j^2}{\omega_j^2} \cos\omega_j t \tag{4.18}$$

From Eqs. (4.11) and (4.17) one obtains $\alpha(t)$ for the harmonic oscillator model:

$$\alpha(t) = \sum_j \frac{c_j^2}{\omega_j} \sin\omega_j t. \tag{4.19}$$

Substituting Eq. (4.19) into Eq. (4.8) and then into Eq. (4.13), one obtains

$$S(t) = \Delta(t), \tag{4.20}$$

where

$$\Delta(t) = \frac{1}{2\lambda} \sum_j \frac{c_j^2}{\omega_j^2} \cos\omega_j t. \tag{4.21}$$

The function $\Delta(t)$, which coincides with the normalized classical correlation function $C_{cl}(t)$ [cf. Eq. (4.16)], vanishes when $t \to \infty$, and, as one can see from its definition and Eq. (4.4), equals unity at $t = 0$.

Equations (4.16) and (4.20) allow one to relate the solvent response function, Eq. (4.13), to the correlation function, Eq. (4.15) of the solvation coordinate for an instantaneous pump pulse. Equation (4.16), which is valid for a generic nonlinear system, looks more general than Eqs. (4.20) and (4.21). It is worth noting, however, that if one *defines* coefficients c_j of the *effective harmonic oscillator model* in Eq. (4.2) in such a way that the correlation function $C_d(t)$, Eq. (4.15), of the nonlinear system is fitted with suitable choice of c_j's to Eq. (4.18), then Eqs. (4.16) and (4.20) become identical (see the discussion below).

We are not aware of any success in generalizing the above procedure to the case where the electronic transition of the molecule cannot be viewed as instantaneous. Accordingly, we describe next a different approach, a density matrix method which can be used to treat the solvent dynamics for the case of an arbitrary duration of the pump pulse. Conceptually, it is close to the method used by Mukamel and coworkers [51, 52, 53], but the execution is different. When the pulse is instantaneous, the results will be shown to reduce to those given by the previous method, Eqs. (4.8) and (4.19).

4.3.2 Pump Pulse of Finite Duration

We introduce the density matrix of the solvent $\rho(t)$, which is evolving on a potential energy surface involving the excited electronic state of the solute. The average value of the solvation coordinate $\overline{X}(t)$ at the time t after the excitation can then be written as

$$\overline{X}(t) = \mathrm{Tr}[X\rho(t)], \tag{4.22}$$

where $\rho(t) = \exp(-iH_e t/\hbar)\rho(0)\exp(iH_e t/\hbar)$.

This expression for $\overline{X}(t)$ can be rewritten in an equivalent form:

$$\overline{X}(t) = \mathrm{Tr}[X_e(t)\rho(0)], \tag{4.23}$$

where the subscript e means that the evolution of X proceeds with the Hamiltonian

H_e, $X_e(t) = \exp(iH_e t/\hbar) X \exp(-iH_e t/\hbar)$. It is shown in Appendix A that for the model in Eqs. (4.1) and (4.2), the following relation is satisfied:

$$X_e(t) = X_g(t) + 2\lambda[\Delta(t) - 1], \tag{4.24}$$

where $\Delta(t)$ is given by Eq. (4.21).

For comparison with our later results, we first consider the case that the density matrix $\rho(t)$ of the solvent does not change during the electronic transition ("instantaneous pump pulse"). In this case $\rho(0) \simeq \rho_0$, the equilibrium solvent distribution corresponding to the ground electronic state of the solute [cf. Eq. (4.6)]. Using Eqs. (4.7), (4.23) and (4.24), one immediately obtains

$$\overline{X}(t) = \Delta U + \lambda[2\Delta(t) - 1], \tag{4.25}$$

and, as a consequence, obtains Eq. (4.20) upon using Eqs. (4.12) and (4.13).

For a pump pulse of finite duration, the actual density matrix of the solvent ρ immediately after electronic excitation of the solute will differ from the ρ_0 defined in Eq. (4.6). To calculate the density matrix $\rho(t)$, the process of the excitation now needs to be considered explicitly. To this end we introduce the common assumptions that the pump pulse radiation field $E(t)$ can be described classically and that the dipole approximation can be used for its interaction with the solute [51]:

$$H_{int}(t) = \frac{E(t) + E^*(t)}{2}\hat{\mu}, \quad \hat{\mu} = \mu(|e><g| + |g><e|), \tag{4.26}$$

where the electric field is treated as linearly polarized along the x-axis $E(t) = E_x(t)$. It is also assumed that $E(t)$ has a relatively narrow spectrum, so one can write it in a quasi-harmonic form,

$$E(t) = E_0(t) \exp(-i2\pi\nu_0 t), \tag{4.27}$$

where $E_0(t)$ is a function changing slowly with time. The asterisk in Eq. (4.26) denotes the complex-conjugate.

The transition dipole moment of the solute along the x axis is $\mu = \mu_0 n_x$, where n_x is the directional cosine of the transition dipole moment along the x axis, and is treated as a constant. It may be noted that the last assumption is usually referred to a spatially fixed solute (Condon approximation) and, strictly speaking, is not applicable to a moving solute. However, one dynamical effect, that of the solute reorientation, which is frequently modeled as rotational diffusion [48], is rather small on a time scale of the processes considered in the present article, especially for large dye solute molecules which are commonly used in these experiments and whose orientational diffusion is relatively slow: A relative change of the transition dipole moment due to the solute diffusional reorientation can be estimated as $\delta\mu/\mu_0 \sim \sqrt{Dt}$, where D is the rotational diffusion coefficient and t is the relaxation time. Substituting an estimate from Ref. [48] $D = 5\ 10^8\ \mathrm{s}^{-1}$ and taking $t = 1$ ps, $\delta\mu/\mu_0$ is estimated to be of the order of 2% which is probably at least as good as the other approximations. Thereby, the effect of the solute reorientation can be treated statically, averaging the final result over all possible solute orientations at the end of the calculation.

The orientation of the solute influences only the amplitude of the corresponding perturbation Hamiltonian, both for the excitation pulse [cf. Eq. (4.26)] and for the resulting fluorescence spectrum [52]. As a result, the solute orientation does not influence the shape of the transient fluorescence spectrum but only its directional properties. The dependence of the fluorescence intensity on the direction of observation and on the fluorescence polarization direction is considered in Appendix B for completeness.

To find the density matrix of the solvent $\rho(t)$ with the solute in the excited electronic state, second-order time-dependent perturbation theory with H_{int} as a perturbation must be used. Under the rotating wave approximation, the expression for $\rho(t)$ is given by [12]

$$\rho(t) = \frac{\mu^2}{4\hbar^2} \int_{-\infty}^{+\infty} \int_{-\infty}^{+\infty} dt' dt'' E^*(t') E(t'') e^{-i(t-t'')H_e/\hbar} e^{-it''H_g/\hbar} \rho_0 e^{it'H_g/\hbar} e^{i(t-t')H_e/\hbar}. \tag{4.28}$$

Here and below we assume that the fluorescence signal is observed when the pump

pulse is already over. If, instead, the pump and upconverting pulses overlap, the observed signal cannot be interpreted as a pure fluorescence, but contains also a Raman scattering component [12]. The $\rho(t)$ in Eq. (4.28) is a part of the "solvent+solute" system total density matrix, which is diagonal over the excited electronic state of the solute. Since we neglect nonradiative electronic transitions of the solute, the time-evolution of $\rho(t)$ can be considered separately. We will normalize $\rho(t)$ for convenience. The normalized $\rho(t)$, i.e., such that $\mathrm{Tr}[\rho(t)] = 1$, is given by

$$\rho(t) = \frac{1}{v_0}\int_{-\infty}^{+\infty}\int_{-\infty}^{+\infty} dt'dt'' E^*(t')E(t'')e^{-i(t-t'')H_e/\hbar}e^{-it''H_g/\hbar}\rho_0 e^{it'H_g/\hbar}e^{i(t-t')H_e/\hbar}. \tag{4.29}$$

where

$$v_0 = \int_{-\infty}^{+\infty}\int_{-\infty}^{+\infty} dt'dt'' E^*(t')E(t'')R(t'-t''). \tag{4.30}$$

$$R(\tau) = \langle e^{-i\tau H_e/\hbar}e^{i\tau H_g/\hbar}\rangle. \tag{4.31}$$

where $\langle \ldots \rangle$ denotes thermal average, Eq. (4.6). The function $R(\tau)$ coincides with the normalized correlation function of the operator for the transition dipole moment $\hat{\mu}$, and its Fourier transform gives the absorption lineshape [76]. The correlation function $R(\tau)$ is expressed in terms of the (quantum) correlation function of the solvation coordinate, Eq. (4.10), as [76]

$$R(\tau) = \exp[-\frac{i}{\hbar}\tau\langle X\rangle - \frac{1}{\hbar^2}\int_0^{\tau} d\tau' \int_0^{\tau'} C(\tau'-\tau'')\,d\tau'']. \tag{4.32}$$

If the pulse is infinitely short, which formally corresponds to using $E(t) \propto \delta(t)$, then $\rho(t) \to \rho(0) = \rho_0$, at $t \to +0$, a situation discussed above.

Equations (4.22), (4.12), (4.13), and (4.29)-(4.32) provide a basis for calculating the time-evolution of the Stokes shift for an arbitrary pump pulse. Using Eq. (4.29) the average value of the solvent coordinate X at time t can be represented in the form:

$$\overline{X}(t) = \frac{1}{v_0}\int_{-\infty}^{+\infty}\int_{-\infty}^{+\infty} dt'dt'' f(t|t',t'')E^*(t')E(t''), \tag{4.33}$$

where the integral kernel $f(t|t',t'')$ is given by

$$f(t|t',t'') = \mathrm{Tr}[X_e(t-t')e^{-i(t'-t'')H_e/\hbar}e^{i(t'-t'')H_g/\hbar}\rho_0]. \tag{4.34}$$

A straightforward but somewhat cumbersome calculation given in Appendix C yields the following expression for this kernel:

$$\begin{aligned} f(t|t',t'') &= R(t'-t''))\{\lambda[\Delta(t-t')+\Delta(t-t'')]-\lambda+\Delta U+ \\ &\quad i\sum_j \frac{c_j^2}{\omega_j^2}\coth(\beta\hbar\omega_j/2)\sin[\omega_j(t''-t')/2]\cos[\omega_j(t-t''/2-t'/2)]\}. \end{aligned} \tag{4.35}$$

It is easily seen that in the short pump pulse limit Eq. (4.35) reduces to a previous result, Eq. (4.25). Really, in this limit the integration times t' and t'' can be set to zero in all terms in braces. As a result, the expression for f takes a simple form: $f(t|t',t'') = R(t'-t'')[2\lambda\Delta(t)-\lambda+\Delta U]$. Upon substituting this expression into Eq. (4.33), Eq. (4.25) immediately follows.

In the harmonic oscillator model, the solute-solvent interaction is characterized by the 'normal mode shifts' c_j in Eq. (4.2). Physically important, however, are not so much the c_j's themselves but their combination in the well known form, the spectral density function $J(\omega)$ of the solvent modes [54],

$$J(\omega) = \frac{\pi}{2}\sum_j (c_j^2/\omega_j)\delta(\omega-\omega_j), \tag{4.36}$$

where $\delta(\omega)$ denotes the Dirac delta function. Using the spectral density function allows one most naturally go to the limit $N=\infty$. If the number of harmonic modes is finite, then $J(\omega)$ is the sum of finite number of delta functions. In the limit $N\to\infty$ $J(\omega)$ is transformed to a regular continuous function. Using the definition of the spectral density function, the expressions for the reorganization energy λ, for $\Delta(t)$, and for the correlation function $C(t)$, Eqs. (4.4), (4.21), and (4.17), can be

written as

$$\lambda = \frac{1}{\pi}\int_0^\infty d\omega \frac{J(\omega)}{\omega}, \quad \Delta(t) = \frac{1}{\pi\lambda}\int_0^\infty d\omega \frac{J(\omega)}{\omega}\cos\omega t, \tag{4.37}$$

and

$$C(t) = \frac{\hbar}{\pi}\int_0^\infty d\omega J(\omega)[\coth(\beta\hbar\omega/2)\cos\omega t - i\sin\omega t]. \tag{4.38}$$

Equation (4.35) can be rewritten using the definition of $J(\omega)$ as

$$\begin{aligned} f(t|t',t'') &= R(\tau)\{\lambda[\Delta(t-T-\tau/2)+\Delta(t-T+\tau/2)]-\lambda+\Delta U+ \\ &\quad -i\frac{2}{\pi}\int_0^\infty d\omega \frac{J(\omega)}{\omega}\coth(\beta\hbar\omega/2)\sin(\omega\tau/2)\cos\omega(t-T)\}. \end{aligned} \tag{4.39}$$

where we have also changed the integration variables:

$$\tau = t' - t'', \quad T = (t''+t')/2. \tag{4.40}$$

Equation (4.39) has been derived using the harmonic oscillator model. Eqs. (4.1) and (4.2). However, as was noted in the introduction in Section 4.2, this equation and other equations which follow from it have a broader validity and can be applied to a nonlinear system too. To this end, one has to redefine the spectral density function $J(\omega)$, which occurs in Eq. (4.39), because Eq. (4.36), which was used as a definition of $J(\omega)$, is no longer valid for the nonlinear system. The easiest way of doing this, leading to Eq. (4.41) below, is to use the harmonic oscillator model to relate the spectral density function to the imaginary part of the quantum correlation function of the solvation coordinate, Eq. (4.38). (It is important to use a *quantum* correlation function because for a generic nonlinear system, in contrast to a harmonic one, there is no simple relation between the classical and quantum correlation functions.) Applying the inverse Fourier transform to the imaginary part of Eq. (4.38), one obtains:

$$J(\omega) = \frac{2}{\hbar}\int_0^\infty \mathrm{Im}[C(t)]\sin\omega t\, dt \tag{4.41}$$

where $C(t)$ is given by Eq. (4.10). Equation (4.39), with $J(\omega)$ given by Eq. (4.41), can also be derived more generally by following Mukamel's type of argument [51],

without introducing any molecular harmonic oscillator model.

To proceed further analytically with Eqs. (4.33) and (4.39), we assume for a moment that the correlation function $C(t)$ which enters into $R(t)$, Eq. (4.32), can be approximated by its value at zero time,

$$C(t) \simeq C(0). \tag{4.42}$$

While this approximation is always qualitatively correct, it neglects the important contribution to the absorption spectrum which arises from the solute's high-frequency vibrational modes. These effects will be taken into account later in Eqs. (4.56) and (4.58).

Substituting Eq. (4.42) into Eq. (4.32), one obtains:

$$R(\tau) = \exp[-C(0)\tau^2/2\hbar^2 - i\langle X\rangle\tau/\hbar], \tag{4.43}$$

where $\langle X\rangle$ is given by Eq. (4.7). Assuming that the main contribution to the correlation function $C(t)$, Eq. (4.38), arises from low frequency modes (classical modes), one can use an estimate for $C(0)$ [cf. Eqs. (4.37) (4.38)].

$$C(0) \sim 2\lambda/\beta. \tag{4.44}$$

Equations (4.43) and (4.44) define the important time-scale τ_c over which the correlation function $R(\tau)$, Eq. (4.31), is essentially different from zero:

$$\tau_c = \hbar\sqrt{\beta/\lambda}. \tag{4.45}$$

The correlation function $R(\tau)$ limits the important time difference τ in Eq. (4.39) to being less than τ_c. Within such times the sine under the integral in Eq. (4.39) can be replaced by its argument $\omega\tau/2$ and τ can also be neglected in the arguments of the

functions $\Delta(t - T \pm \tau/2)$, giving as a result:

$$f(t|t', t'') = R(\tau)\{2\lambda\Delta(t - T) - \lambda + \Delta U - i\hbar^{-1}\tau \mathrm{Re}[C(t - T)]\}. \tag{4.46}$$

where we have used the expression for $C(t)$, Eq. (4.38). Substituting Eq. (4.46) and a quasi-harmonic representation for the pump pulse, Eq. (4.27), into Eqs. (4.30) and (4.33), one arrives at the following expression for $\overline{X(t)}$:

$$\overline{X}(t) = \frac{\int_{-\infty}^{\infty} dT |E_0(T)|^2 K(t - T)}{\int_{-\infty}^{\infty} dT |E_0(T)|^2}. \tag{4.47}$$

where

$$K(t) = \frac{\int_{-\infty}^{\infty} d\tau \exp(i2\pi\nu_0\tau) R(\tau)\{2\lambda\Delta(t) - \lambda + \Delta U - i\hbar^{-1}\tau \mathrm{Re}[C(t)]\}}{\int_{-\infty}^{\infty} d\tau \exp(i2\pi\nu_0\tau) R(\tau)}. \tag{4.48}$$

In derivation of Eqs. (4.47) and (4.48) we again neglected the small time difference τ in $E_0(T \pm \tau/2)$, which changes slowly with time. The last assumption implies that the pulse duration τ_p is much longer than the correlation time τ_c, Eq. (4.45).

$$\tau_p \gg \tau_c. \tag{4.49}$$

Equation (4.49) is typically satisfied for a system at a room temperature with strong solute-solvent interaction and for a pump pulse with $\tau_p \geq 50$ fs.

From Eq. (4.47) one can see that the DSS resulting from a long pump pulse is given by convolution of the pulse shape and the function $K(t)$ given by Eq. (4.48). This function describes a DSS which corresponds to a pulse which is much longer than the correlation time τ_c, Eq. (4.45), but still shorter than any time-scale, relevant to the solvent dynamics. To calculate $K(t)$ we first use the Gaussian approximation for $R(\tau)$, Eq. (4.43). Substituting Eq. (4.43) into Eq. (4.48) and integrating over τ one obtains

$$K(t) = \Delta U - \lambda + 2\lambda\Delta(t) + h\Delta\nu_0\Delta_1(t), \tag{4.50}$$

where $\Delta\nu_0$ is the central frequency shift of the pump pulse ν_0 relative to the maximum

of the absorption spectrum,

$$\Delta\nu_0 = \nu_0 - (\Delta U + \lambda)/h. \tag{4.51}$$

The function $\Delta_1(t)$ is the quantum analog of the normalized classical correlation function $\Delta(t)$ [Eq. (4.37)],

$$\Delta_1(t) = \frac{\mathrm{Re}[C(t)]}{C(0)}. \tag{4.52}$$

$\Delta_1(0) = 1$, and $C(t)$ is given by Eq. (4.38). It is convenient for comparison later with Eq. (4.73) to rewrite the DSS for a short pulse, Eq. (4.50), in a different form:

$$\overline{X}(t) - \overline{X}(\infty) = 2\lambda\Delta(t) + h\Delta\nu_0\Delta_1(t). \tag{4.53}$$

It can be seen from this equation that the variation of the transition frequency $\Delta\nu = \nu(0) - \nu(\infty) = [\overline{X}(0) - \overline{X}(\infty)/h$ is:

$$\Delta\nu = \Delta\nu_0 + 2\lambda/h. \tag{4.54}$$

The solvent response function $S(t)$ is obtained by substituting Eq. (4.50) into Eq. (4.13):

$$S(t) = \frac{1}{1+\kappa}[\Delta(t) + \kappa\Delta_1(t)], \quad \kappa = \frac{h\Delta\nu_0}{2\lambda}. \tag{4.55}$$

Equation (4.55) gives a simple expression for the solvent response function which generalizes Eq. (4.20) and reduces to it when $\hbar \to 0$ or when pump pulse is not off-resonance ($\Delta\nu_0 = 0$). The expression in Eq. (4.55) with $\kappa = 0$ corresponds to the purely classical response of the solvent [cf. Eq. (4.20)]. The quantum correlation function $\Delta_1(t)$ and κ are responsible for the quantum effects entering into the solvent response. For a choice of $h\Delta\nu_0 \sim 2\sqrt{\lambda/\beta}$, which is the absorption linewidth, one can estimate the contribution of κ to the total solvent response as $\kappa \sim 1/\sqrt{\lambda\beta}$, which is typically small. However, particularly in the far wing on the red side, a larger $\Delta\nu_0$ can be used. We give an interpretation of Eq. (4.55) later. We note that Eqs. (4.53) and (4.55) contain no properties specific to a molecular harmonic oscillator model.

A Gaussian approximation for the correlation function $R(t)$ [use of Eq. (4.43) to represent Eq. (4.31)] may be too restrictive for a solute with a complex spectrum. Using Eq. (4.48) one readily obtains the following expression for the DSS:

$$K(t) = \Delta U - \lambda + 2\lambda\Delta(t) - \hbar^{-1}C(0)\left.\frac{d\ln[\tilde{R}(\omega)]}{d\omega}\right|_{\omega=2\pi\nu_0}\Delta_1(t), \tag{4.56}$$

where $\tilde{R}(\omega)$ is the Fourier transform of $R(t)$,

$$\tilde{R}(\omega) = \int_{-\infty}^{\infty} e^{i\omega t}R(t)dt. \tag{4.57}$$

The absorption coefficient is proportional to $\omega\tilde{R}(\omega)$ [76]. It follows from Eq. (4.56) that for a solute with a non-Gaussian absorption spectrum, even if the solvent dynamics can be described classically, i.e., if $\Delta_1(t) \simeq \Delta(t)$, then the solvent response function $S(t)$ is given by Eq. (4.20), but the variation of the transition frequency $\nu(0) - \nu(\infty)$ will differ from that predicted from the classical theory, $\Delta\nu_0 = 2\lambda/h$ [cf. Eq. (4.54)]. A generalization of the expression for κ in Eq. (4.55) for a solute with an arbitrary absorption spectrum is:

$$\kappa = -\frac{C(0)}{2\hbar\lambda}\left.\frac{d\ln[\tilde{R}(\omega)]}{d\omega}\right|_{\omega=2\pi\nu_0}. \tag{4.58}$$

One aim in the present paper is to estimate for a realistic experimental situation the change in the Stokes shift time-evolution due to the finite pump pulse duration. To estimate the Stokes shift dynamics, a realistic spectral density function $J(\omega)$ in Eq. (4.41) is needed for the solute-solvent interaction. The main contribution to the interaction of polar solutes with small-molecule polar solvents is due to long range dipole-dipole and charge-dipole interactions, together with hydrogen bonding in the case of protic solvents [77–79]. interaction in polar solvents has been described in terms of continuum models using an exponential or multiexponential dielectric response [5, 48, 80]. It has been argued by some researchers that due to inherent molecular nature of the solvation process, the continuum models ultimately fail to

explain some important features of solvation, in particular its initial, ultrafast stage. In more recent investigations, however, it was found that once one includes not only the low-frequency, diffusional part of the solvent's dielectric response but also the high-frequency, inertial part, a prominent role of the inertial motion in solvation is recovered [36, 81, 82]. In their work on the dynamic Stokes shift of coumarin 343 anion (C343) in water, Hsu *et al.* [82] obtained encouraging agreement with the experiment [2] upon using the experimental dielectric response function $\epsilon(\omega)$ for water and a continuum-based approach.

In the present paper we again use for simplicity the Onsager model for the solute, which treats the solute as a dipole in the center of a spherical cavity and the solvent as a dielectric continuum with uniform properties, surrounding the solute. The dielectric response of the solvent is assumed to be local and to be characterized by the experimental bulk dielectric response function $\epsilon(\omega)$. The spectral density $J(\omega)$ of the solvent's normal modes can be related to the dielectric function using the expression for the DSS caused by an instantaneous pump pulse. Such a DSS can readily be expressed in terms of the spectral density function using Eqs. (4.25) and (4.37),

$$\overline{X}(t) = \Delta U - \lambda + \frac{2}{\pi}\int_0^\infty d\omega \frac{J(\omega)}{\omega}\cos\omega t. \tag{4.59}$$

On the other hand, within the framework of the reaction field approach, the DSS associated to an instantaneous pump pulse is given by [82],

$$\overline{X}(t) = \Delta U - \lambda - \frac{4\Delta\mu^2}{a^3\pi}\int_0^\infty d\omega \frac{\cos\omega t}{\omega}\mathrm{Im}\left[\frac{\epsilon(\omega)-1}{2\epsilon(\omega)+1}\right]. \tag{4.60}$$

where $\Delta\mu = \mu_e - \mu_g$ is the (vector) difference of the dipole moments in the excited and ground electronic states, a is the solute cavity radius, and the minus sign in Eq. (4.60) appears when the convention is used that the imaginary part of the dielectric function $\epsilon(\omega)$ is taken to be negative. Comparing Eqs. (4.59) and (4.60), one obtains the desired expression:

$$J(\omega) = -\frac{2\Delta\mu^2}{a^3}\mathrm{Im}\left[\frac{\epsilon(\omega)-1}{2\epsilon(\omega)+1}\right]. \tag{4.61}$$

It can be shown by other methods [52, 49] using linear response theory that Eq. (4.61) holds in most general conditions for the Onsager model if one assumes that the dielectric response of the solvent is local on atomic length-scale.

Using Eq. (4.61) the solvation dynamics of the system can be estimated once the dielectric function of the solvent $\epsilon(\omega)$ is known. As an example the dielectric dispersion data for water at $T = 298$ K (Fig. 4.1) were used to calculate the spectral density of the solvent modes. Water has been used in DSS measurements [2, 42] and its dielectric response function is available at a high level of accuracy over a wide range of frequencies [83–86]. (4.55) shows that the effect of the finite pump pulse duration on the DSS depends on the difference between $\Delta(t)$ and $\Delta_1(t)$. Eqs. (4.37) and (4.52). These functions are shown in Fig. 4.2. A relative contribution of the ultrafast component to the correlation function $\Delta_1(t)$ is larger due to the 0^oK fluctuations of the quantum modes, and the oscillations with the period of 10-15 fs are much stronger. The exponential relaxation time (appropriate in the low frequency regime) is the same for both $\Delta(t)$ and $\Delta_1(t)$. This result is expected since the long time scale orientational relaxation is associated with the slow classical solvent modes.

The instrument response time (FWHM of a cross-correlation of the pump and gate pulses [87]), which characterizes the time-resolution in a measurement of the transient fluorescence also must be taken into account. It is not better than about 100 fs [36]. The correlation functions $\Delta(t)$ and $\Delta_1(t)$ were next convoluted with appropriate Gaussian shapes of both the pump pulse [cf. Eq. (4.47)] and the upconverting pulse [88], with the results given in Fig. 4.3. These convolutions make the difference between the classical and quantum correlation functions even less pronounced. Taking into account the fact that $\Delta_1(t)$ enters into the total solvent response $R(t)$ with the weight κ [Eq. (4.55)], which is generally much less than unity, one can conclude that the deviation from the standard formula [Eq. (4.20)] due to the finite pump pulse duration is small and can be neglected in most DSS experiments. Some deviation can be expected when the central frequency of the pump pulse lies in the far wing of the absorption band of the chromophore, and then the additional contribution in the correlation function $\Delta_1(t)$ to the total solvent response can be comparable with the

standard term, $\Delta(t)$. For example, a red shift of the pump pulse from the fluorescence maximum, $\Delta\nu_0 \simeq \lambda/h$, which would give the excitation probability of the order of 10% of the maximum for Coumarin 153 in ethanol, leads to $\kappa \sim 0.5$.

4.4 Physical Interpretation of Eqs. (4.53) and (4.55)

To interpret Eq. (4.53) we first obtain, in Eqs. (4.62)-(4.65) below, the distribution of the displacements Q_j of the harmonic oscillators before and immediately after the electronic transition. The probability distribution W_j of the coordinate Q_j for a single oscillator in equilibrium with the ground electronic state of the solute (the statistical state of the system before the excitation) is given by [89]

$$W_j(Q_j) = \sqrt{\frac{\omega_j \tanh(\hbar\omega_j\beta/2)}{\pi\hbar}} \exp[-\tanh(\hbar\omega_j\beta/2)\omega_j Q_j^2/\hbar]. \tag{4.62}$$

In the high temperature (low frequency) limit, this distribution reduces to the classical one:

$$W_j(Q_j) \simeq \sqrt{\frac{\omega_j^2\beta}{2\pi}} \exp(-\beta\omega_j^2 Q_j^2/2), \quad \hbar\omega_j\beta/2 \ll 1. \tag{4.63}$$

In the low temperature (high frequency) limit, it reduces to the probability distribution corresponding to the ground state of the oscillator:

$$W_j(Q_j) \simeq \sqrt{\frac{\omega_j}{\pi\hbar}} \exp(-\omega_j Q_j^2/\hbar), \quad \hbar\omega_j\beta/2 \gg 1. \tag{4.64}$$

which is much broader than the classical distribution when $\hbar\omega_j\beta/2 \gg 1$. The last property can be interpreted as the result of nuclear tunneling of the oscillator to nonclassical regions. The total distribution of all oscillators representing the solvent is given by the product of the distributions in Eq. (4.62),

$$W(\mathbf{Q}) = \prod_j W_j(Q_j). \tag{4.65}$$

The maximum of the absorption spectrum corresponds to $Q_j = 0$. If the pump pulse frequency is tuned away from the maximum of the absorption spectrum, the mean displacements $\overline{Q_j^0}$ of the jth harmonic oscillator excited by this off-resonance optical excitation immediately after the excitation deviate from their initial zero values. To find these displacements one must maximize the probability $W(\mathbf{Q})$ in Eq. (4.65) subject to the constraint that the frequency shift $\Delta\nu_0$ is kept fixed. Equations (4.3), (4.12), and (4.51) yield for this constrain:

$$h\Delta\nu_0 = \sum_j c_j Q_j. \tag{4.66}$$

Using the log $W(\mathbf{Q})$ as a function to be maximized and applying to it the method of Lagrange multipliers, we have

$$\frac{\partial}{\partial Q_j}[\sum_j \omega_j \tanh(\beta\hbar\omega_j/2)Q_j^2 - \alpha\sum_j c_j Q_j] = 0. \tag{4.67}$$

where α is a Lagrange multiplier; the following expression for the most probable values of the oscillators coordinates Q_j^0 is readily obtained:

$$Q_j^0 = \frac{\alpha}{2}\frac{c_j}{\omega_j}\coth(\beta\hbar\omega_j/2). \tag{4.68}$$

One can see that the initial displacement of the jth solvent mode Q_j^0 is larger in the quantum case, since $\tanh(\beta\hbar\omega_j/2)$ is less the corresponding classical term, $\beta\hbar\omega_j/2$, for the high frequency modes. To find the value of α which corresponds to $\Delta\nu_0$, Eq. (4.68) is introduced into Eq. (4.66):

$$\Delta\nu_0 = \alpha\sum_j \frac{c_j^2}{2h\omega_j}\coth(\beta\hbar\omega_j/2). \tag{4.69}$$

Using the expression for $C(t)$, Eq. (4.17), the following estimate for α is readily obtained:

$$\alpha = \frac{h^2\Delta\nu_0}{2\pi C(0)}. \tag{4.70}$$

Thus, the expression for the initial displacement of the jth solvent mode in this off-peak excitation can be written as

$$Q_j^0 = \frac{h^2 \Delta\nu_0}{4\pi C(0)} \frac{c_j}{\omega_j} \coth(\beta\hbar\omega_j/2). \tag{4.71}$$

This expression gives the displacements of the solvent modes relative to their minima in the ground electronic state of the solute. The time-evolution, however, proceeds in the excited electronic state. The initial displacement of the jth solvent mode relative to its minimum in the *excited* electronic state is [cf. Eqs. (4.2) and (4.75)]:

$$Q_j'^0 = \frac{c_j}{\omega_j^2} + Q_j^0 = \frac{c_j}{\omega_j^2} \left[1 + \frac{h\Delta\nu_0}{C(0)} \frac{\hbar\omega_j/2}{\tanh(\hbar\omega_j\beta/2)} \right]. \tag{4.72}$$

The first term in Eq. (4.72) describes the displacement of the jth mode when the pump pulse frequency is tuned to the maximum of the absorption spectrum. It is purely classical in the harmonic oscillator model. The second term appears when there is a detuning $\Delta\nu_0$. It is larger for the high frequency (and hence quantum) modes because of the tunneling [see the discussion after Eq. (4.68)]. The time-evolution is similar both for the quantum and classical modes and is described by the factor $\cos\omega_j t$ for the jth mode. Therefore, the DSS can be written as

$$\overline{X}(t) - \overline{X}(\infty) = \sum_j c_j Q_j'^0 \cos\omega_j t = 2\lambda\Delta(t) + h\Delta\nu_0\Delta_1(t), \tag{4.73}$$

where we have used Eqs. (4.17), (4.21), (4.52), and (4.72). Comparing Eqs. (4.73) and (4.53) one sees that they coincide. Thus, the deviation of the solvent response $S(t)$ [cf. Eq. (4.55)] from Eq. (4.20) is caused by the fact that the mean displacements $Q_j'^0$ of the high frequency modes immediately after the pump pulse are different in the quantum and classical cases.

It was assumed in the previous discussion that the high frequency solvent modes do not have time to change during the excitation. In particular, τ_p must satisfy the

condition:

$$\frac{h}{\tau_p} \geq k_B T. \tag{4.74}$$

(A high frequency mode is defined here as one whose frequency exceeds $k_B T/h$.) This condition is loosely satisfied for the pump pulse with duration $\tau_p \simeq 50$ fs at the room temperature. On the other hand, the pulse must not be too broad in the frequency domain, since otherwise the constraint $\Delta\nu_0$ =const would be meaningless. Taking into account that the spectral width is $\sqrt{\lambda/\beta}/\hbar$ one arrives at the condition given by Eq. (4.49) and discussed above.

4.5 Summary

In the present paper the effect of the pump pulse duration on the Stokes shift time-evolution was considered. It was shown that the deviation of the solvent response from the classical expression, Eq. (4.20), is due to the mean initial displacements of the high frequency solvent modes being different in the quantum and classical cases. It was found, however, that usually this effect is small and that the standard description using an infinitely short excitation pulse is then applicable. However, it was shown that a deviation can be expected when the excitation pulse frequency is tuned to the far wing of the absorption band of the chromophore. The description of the transient fluorescence spectrum in which the only parameter, the central frequency of the spectrum, is used to characterize its dynamics can omit some of the dynamical features. The other features of the spectrum such as its width and shape can contain additional information about the solvation dynamics.

Acknowledgements

It is a pleasure to acknowledge the support of the National Science Foundation and the Office of Naval Research. One of us (Y.G.) would like to acknowledge the support of the James W. Glanville Postdoctoral Scholarship in Chemistry at Caltech and support in the early stages of this research of the Rueff-Wormser Fellowship.

Appendix A: Derivation of Eq. (4.24)

To derive Eq. (4.24) shifted normal modes Q'_j can be introduced:

$$Q'_j = Q_j + \frac{c_j}{\omega_j^2}. \tag{4.75}$$

The expression for the change ΔX in the solvation coordinate X in Eqs. (4.3) and (4.5) can be rewritten in terms of Q'_j as

$$\Delta X = \sum_j c_j Q'_j - 2\lambda \tag{4.76}$$

using Eq. (4.4) for λ. The time-evolution of a shifted normal mode in the excited electronic state with the Hamiltonian H_e [Eq. (4.2)] formally coincides with a time-evolution of an unshifted harmonic oscillator and is given by

$$Q'_j(t) = Q'_j \cos\omega_j t + \frac{P_j}{\omega_j} \sin\omega_j t. \tag{4.77}$$

$\Delta X_e(t)$ can be written as

$$\Delta X_e(t) = \sum_j c_j Q'_j(t) - 2\lambda = \Delta X_g(t) + 2\lambda[\Delta(t) - 1]. \tag{4.78}$$

where we have used Eqs. (4.75)-(4.77), (4.21) and the expression for $\Delta X_g(t)$,

$$\Delta X_g(t) = \sum_j c_j [Q_j \cos\omega_j t + \frac{P_j}{\omega_j} \sin\omega_j t]. \tag{4.79}$$

Appendix B: The Directional Properties of The Transient Fluorescence

If the direction of the electric field $\mathbf{n_0}$ in the pump pulse is not collinear with the direction of the transition dipole moment of the solute $\mathbf{n}'$, a factor of $\mathbf{n_0} \cdot \mathbf{n}'$ appears in the expression for the Hamiltonian of interaction of the pump pulse with the solute

[cf. Eq. (4.26)]. Similarly, if the direction of the electric field $\mathbf{n}$ in a particular fluorescence mode is not collinear with $\mathbf{n}'$, a factor of $\mathbf{n} \cdot \mathbf{n}'$ appears in the corresponding interaction Hamiltonian. The transient fluorescence intensity is obtained as a result of the second order perturbation over the interaction with the pump pulse plus the second order perturbation over the interaction with the particular fluorescence mode [52]. The contribution to the intensity $I_{n'}$ of the transient fluorescence to the particular fluorescence mode from solutes with the given orientation $\mathbf{n}'$ of the transition dipole moment can then be written as

$$I_{n'} = (\mathbf{n_0} \cdot \mathbf{n}')^2 (\mathbf{n} \cdot \mathbf{n}')^2 I_0. \tag{4.80}$$

where I_0 depends neither on $\mathbf{n_0}$ and $\mathbf{n}$ nor on $\mathbf{n}'$. To obtain the orientational dependence of the transient fluorescence intensity I, one must average Eq. (4.81) over possible orientations of a solute molecule,

$$I = n_{0i} n_{0j} n_k n_l \overline{n'_i n'_j n'_k n'_l} I_0. \quad i, j, k, l = 1, 2, 3\,. \tag{4.81}$$

where the bar means averaging over the solute orientation and the summation over repeated indices is assumed. The tensor $\overline{n'_i n'_j n'_k n'_l}$ has to be isotropic because of the solvent isotropy. The most general form of such a tensor is

$$\overline{n'_i n'_j n'_k n'_l} = a(\delta_{i,j}\delta_{k,l} + \delta_{i,k}\delta_{j,l} + \delta_{i,l}\delta_{j,k}). \tag{4.82}$$

Summing the tensor $\overline{n'_i n'_j n'_k n'_l}$ over indices i, j and k, l and taking into account that $n'_i n'_i = 1$, one finds that $a = 1/15$. As a result, the fluorescence intensity can be written as

$$I = \frac{1}{15}[1 + 2(\mathbf{n} \cdot \mathbf{n_0})] I_0. \tag{4.83}$$

Appendix C: Derivation of Eq. (4.35)

To derive Eq. (4.35) it is convenient to treat the trace in this equation as a thermal average in the ground electronic state, Eq. (4.6), and to use the time-ordered exponential notation [90],

$$\exp_+[-\frac{i}{\hbar}\int_0^t dt' X_g(t')] = e^{itH_g/\hbar}e^{-itH_e/\hbar}. \tag{4.84}$$

The correlation function $R(t)$, Eq. (4.31), can be written in this notation as

$$R(t) = \langle \exp_+[-\frac{i}{\hbar}\int_0^t dt' X_g(t')]\rangle. \tag{4.85}$$

Using Eq. (4.24) the response function $f(t|t',t'')$ defined in Eq. (4.34) can be written as

$$f(t|t',t'') = f_1(t|t',t'') + 2\lambda[\Delta(t-t') - 1]R(t'-t''), \tag{4.86}$$

where

$$f_1(t|t',t'') = \langle X_g(t-t')\exp_+[-\frac{i}{\hbar}\int_{t''-t'}^0 d\tau X_g(\tau)]\rangle. \tag{4.87}$$

It can be shown, using a diagrammatic technique [90] for example, that for a harmonic system the function $f_1(t|t',t'')$ is equal to

$$f_1(t|t',t'') = [\langle X\rangle - \frac{i}{\hbar}\int_{t''-t'}^0 d\tau\langle \Delta X_g(t-t')\Delta X_g(\tau)\rangle]\langle \exp_+[-\frac{i}{\hbar}\int_{t''-t'}^0 d\tau X_g(\tau)]\rangle. \tag{4.88}$$

Substituting Eq. (4.17) into Eq. (4.88) and integrating over τ, the expression for $f_1(t|t',t'')$ is obtained. After the substitution into Eq. (4.86) it yields Eq. (4.35).

References and Notes

[1] R. M. Stratt and M. Maroncelli, J. Phys. Chem. **100**, 12981 (1996).

[2] R. Jimenez, G. R. Fleming, P. V. Kumar, and M. Maroncelli, Nature **369**, 471 (1994).

[3] M. Maroncelli, J. Mol. Liq. **57**, 1 (1993).

[4] E. A. Carter and J. T. Hynes, J. Chem. Phys. **94**, 5961 (1991).

[5] P. F. Barbara and W. Jarzeba, Adv. Photochem. **15**, 1 (1990).

[6] J. D. Simon, Acc. Chem. Res. **21**, 128 (1988).

[7] E. W. Castner, Jr., B. Bagchi, M. Maroncelli, S. P. Webb, A. J. Ruggiero, and G. R. Fleming, Ber. Bunsenges. Phys. Chem. **92**, 363 (1988).

[8] P. J. Rossky and J. D. Simon, Nature **370**, 263 (1994).

[9] P. F. Barbara, G. C. Walker, and T. P. Smith, Science **256**, 975 (1992).

[10] G. R. Fleming and P. G. Wolynes, Phys. Today **43**, 36 (1990).

[11] M. Maroncelli, J. MacInnis, and G. R. Fleming, Science **243**, 1674 (1989).

[12] S. Mukamel, *Principles of nonlinear optical spectroscopy* (Oxford University Press, New York, 1995).

[13] *Ultrafast Dynamics of Chemical Systems*, edited by J. D. Simon (Kluwer Academic Publishers, Dordrecht, 1994).

[14] G. R. Fleming, *Chemical Applications of Ultrafast Spectroscopy* (Clarendon Press, Oxford, 1986).

[15] T.-S. Yang, P. Vöhringer, D. C. Arnett, and N. F. Scherer, J. Chem. Phys. **103**, 8346 (1995).

[16] P. Vöhringer, D. C. Arnett, R. A. Westervelt, M. J. Feldstein, N. F. Scherer, J. Chem. Phys. **102**, 4027 (1995).

[17] E. T. J. Nibbering, D. A. Wiersma, and K. Duppen, Phys. Rev. Lett. **66**, 2464 (1991).

[18] P. C. Becker, H. L. Fragnito, J.-Y. Bigot, C. H. Brito Cruz, R. L. Fork, and C. V. Shank, Phys. Rev. Lett. **63**, 505 (1989).

[19] M. Cho, J.-Y. Yu, T. Joo, Y. Nagasawa, S. A. Passino, and G. R. Fleming, J. Phys. Chem. **100**, 11944 (1996).

[20] T. Joo and A. C. Albrecht, Chem. Phys. **176**, 233 (1993).

[21] J.-Y. Bigot, M. T. Portella, R. W. Schoenlein, C. J. Bardeen, A. Migus, and C. V. Shank, Phys. Rev. Lett. **66**, 1138 (1991).

[22] A. M. Weiner, S. D. Silvestri, and E. P. Ippen, J. Opt. Soc. Am. B **2**, 654 (1985).

[23] P. Cong, H. P. Deuel, Y. J. Yan, and J. D. Simon, J. Lumin. **60**, 699 (1994).

[24] P. Cong, Y. J. Yan, H. P. Deuel, and J. D. Simon, J. Chem. Phys. **100**, 7855 (1994).

[25] P. Cong, H. P. Deuel, and J. D. Simon, Chem. Phys. Lett. **212**, 367 (1993).

[26] H. L. Fragnito, J.-Y. Bigot, P. C. Becker, and C. V. Shank, Chem. Phys. Lett. **160**, 101 (1989).

[27] T. Joo, Y. Jia, and G. R. Fleming, J. Chem. Phys. **102**, 4063 (1995).

[28] M. Cho and G. R. Fleming, J. Phys. Chem. **98**, 3478 (1994).

[29] M. S. Pshenichnikov, K. Duppen, and D. A. Wiersma, Phys. Rev. Lett. **74**, 674 (95).

[30] P. Vöhringer, D. C. Arnett, T.-S. Yang, and N. F. Scherer, Chem. Phys. Lett. **237**, 387 (1995).

[31] C. J. Bardeen and C. V. Shank, Chem. Phys. Lett. **203**, 535 (1993).

[32] P. Vöhringer and N. F. Scherer, J. Phys. Chem. **99**, 2684 (1995).

[33] Y. G. Chang and J. E. W. Castner, J. Chem. Phys. **99**, 7289 (1993).

[34] M. Cho, S. J. Rosenthal, N. F. Scherer, L. D. Ziegler, and G. R. Fleming, J. Chem. Phys. **96**, 5033 (1992).

[35] D. McMorrow, W. T. Lotshaw, and G. A. Kenney-Wallace, IEEE J. Quantum Electron. **24**, 443 (1988).

[36] M. L. Horng, J. A. Gardecki, A. Papazyan, and M. Maroncelli, J. Phys. Chem. **99**, 17311 (1995).

[37] S. J. Rosenthal, R. Jimenez, G. R. Fleming, P. V. Kumar, and M. Maroncelli, J. Mol. Liq. **60**, 25 (1994).

[38] S. J. Rosenthal, X. Xie, M. Du, and G. R. Fleming, J. Chem. Phys. **95**, 4715 (1991).

[39] W. Jarzeba, G. C. Walker, A. E. Johnson, and P. F. Barbara, Chem. Phys. **152**, 57 (1991).

[40] M. A. Kahlow, W. Jarzeba, T. J. Kang, and P. F. Barbara, J. Chem. Phys. **90**, 151 (1989).

[41] M. A. Kahlow, T. J. Kang, and P. F. Barbara, J. Chem. Phys. **88**, 2372 (1988).

[42] W. Jarzeba, G. C. Walker, A. E. Johnson, M. A. Kahlow, and P. F. Barbara, J. Phys. Chem. **92**, 7039 (1988).

[43] M. A. Kahlow, T. J. Kang, and P. F. Barbara, J. Phys. Chem. **91**, 6452 (1987).

[44] V. Nagarajan, A. M. Brearley, T.-J. Kang, and P. F. Barbara, J. Chem. Phys. **86**, 3183 (1987).

[45] M. Maroncelli and G. R. Fleming, J. Chem. Phys. **86**, 6221 (1987).

[46] J. E. W. Castner, M. Maroncelli, and G. R. Fleming, J. Chem. Phys. **86**, 1090 (1987).

[47] Y. T. Mazurenko and V. S. Udaltsov, Opt. Spectrosc. **45**, 765 (1978).

[48] B. Bagchi, D. W. Oxtoby, and G. R. Fleming, Chem. Phys. **86**, 257 (1984).

[49] A. A. Ovchinnikov and M. Y. Ovchinnikova, Sov. Phys. JETP **29**, 688 (1969).

[50] A. A. Abrikosov, L. P. Gorkov, and I. E. Dzyaloshinski, *Methods of quantum field theory in statistical physics* (Dover Publications, New York, 1975).

[51] S. Mukamel, J. Phys. Chem. **89**, 1077 (1985).

[52] R. F. Loring, Y. J. Yan, and S. Mukamel, J. Chem. Phys. **87**, 5840 (1987).

[53] R. F. Loring, Y. J. Yan, and S. Mukamel, Chem. Phys. Lett. **135**, 23 (1987).

[54] A. J. Leggett, S. Chakravarty, A. T. Dorsey, M. P. A. Fisher, A. Garg, and W. Zwerger, Rev. Mod. Phys. **59**, 1 (1987).

[55] Mukamel pointed out that a key equation of his, Eq. 28 of Ref. [51], that is used in Raman spectra, time-dependent fluorescence, and photon echoes, and that he derived using a cumulant expansion, can also be derived using a molecular harmonic oscillator model. Similarly, the expression for the reaction rate (and reorganization energy) obtained by Ovchinnikov and Ovchinnikova [49] was obtained later by Dogonadze and coworkers using the molecular harmonic oscillator model [see, for example, J. Ulstrup, *Charge Transfer Processes in Condensed Media* (Springer-Verlag, Berlin, 1979), p.113 and references therein].

[56] V. G. Levich, Adv. Electrochem. Electrochem. Eng. **4**, 249 (1966).

[57] N. R. Kestner, J. Logan, and J. Jortner, J. Phys. Chem. **78**, 2148 (1974).

[58] P. Siders and R. A. Marcus, J. Am. Chem. Soc. **103**, 741 (1981).

[59] A. Mokhtari, A. Chebira, and J. Chesnoy, J. Opt. Soc. Am. B **7**, 1551 (1990).

[60] R. A. Marcus, Disscuss. Farad. Soc. **29**, 21 (1960).

[61] L. D. Zusman, Chem. Phys. **49**, 295 (1980).

[62] A. Warshel, J. Phys. Chem. **86**, 2218 (1982).

[63] D. F. Calef and P. G. Wolynes, J. Phys. Chem. **87**, 3387 (1983).

[64] R. A. Kuharski, J. S. Bader, D. Chandler, M. Sprik, M. L. Klein, and R. W. Impey, J. Chem. Phys. **89**, 3248 (1988).

[65] T. Fonseca, B. M. Ladanyi, and J. T. Hynes, J. Phys. Chem. **96**, 4085 (1992).

[66] R. Kubo, M. Toda, and N. Hashitsume, *Statistical physics II* (Springer, Berlin, 1995), p. 150.

[67] To obtain Eq. (4.11) from Eq. (4.9) the following property of $C(t)$ is used: $\langle \Delta X_g(0) \Delta X_g(t) \rangle = \langle \Delta X_g(-t) \Delta X_g(0) \rangle = C(-t) = C^*(t)$.

[68] J. S. Bader and D. Chandler, Chem. Phys. Lett. **157**, 501 (1989).

[69] M. Maroncelli and G. R. Fleming, J. Chem. Phys. **89**, 5044 (1988).

[70] M. Maroncelli, J. Chem. Phys. **94**, 2084 (1991).

[71] T. Fonseca and B. M. Ladanyi, J. Phys. Chem. **95**, 2116 (1991).

[72] K. Ando and S. Kato, J. Chem. Phys. **95**, 5966 (1991).

[73] J. Zhu and R. I. Cukier, J. Chem. Phys. **98**, 5679 (1993).

[74] In experiment the frequency of the fluorescence spectrum maximum is traditionally used. See, for example, M. A. Kahlow, T. J. Kang, and P. F. Barbara, J. Chem. Phys. **88**, 2372 (1988).

[75] Equation (4.17) is obtained using statistical independence of different modes, $C(t) = \sum_j c_j^2 \langle Q_j(t) Q_j(0) \rangle$, and the correlation function of a harmonic oscillator coordinate, $\langle Q_j(t) Q_j(0) \rangle = \hbar \cosh(\beta\hbar\omega_j/2 - i\omega_j t)/2\omega_j \sinh(\beta\hbar\omega_j/2)$ (cf. Eqs. (8.6)-(8.8) of Ref. [76]).

[76] M. Lax, J. Chem. Phys. **20**, 1752 (1952).

[77] C. F. Chapman, R. S. Fee, and M. Maroncelli, J. Phys. Chem. **99**, 4811 (1995).

[78] Y. Lin and C. D. Jonah, in *Ultrafast Dynamics of Chemical Systems*, edited by J. D. Simon (Kluwer Academic Publishers, Dordrecht, 1994), pp. 137–162.

[79] A. J. Benigno, E. Ahmed, and M. Berg, J. Chem. Phys. **104**, 7382 (1996).

[80] H. Sumi and R. A. Marcus, J. Chem. Phys. **84**, 4272 (1986).

[81] R. Biswas, N. Nandi, and B. Bagchi, J. Phys. Chem. B **101**, 2968 (1997).

[82] C.-P. Hsu, X. Song, and R. A. Marcus, J. Phys. Chem. B **101**, 2546 (1997).

[83] J. B. Hasted, *Aqueous dielectrics* (Chapman and Hall, London, 1973).

[84] M. N. Asfar and J. B. Hasted, Infrared Phys. **18**, 835 (1978).

[85] J. B. Hasted, S. K. Husain, F. A. M. Frescura, and J. R. Birch, Infrared Phys. **27**, 11 (1987).

[86] G. M. Hale and M. R. Querry, Appl. Optics **12**, 555 (1973).

[87] E. P. Ippen and C. V. Shank in *Ultrashort Light Pulses*, edited by S. L. Shapiro (Springer-Verlag, Berlin, 1977), p. 83.

[88] Assuming that the pump and the gate pulses have the same duration, the instrument response function is defined by the convolution of a pulse intensity function $\exp(-2 * t^2/\tau_p^2)$ with itself [87] and has a FWHM=$2\sqrt{\ln 2}\tau_p$.

[89] R. P. Feynman, *Statistical Mechanics* (W. A. Benjamin, Reading, Massachusetts, 1972), p. 51.

[90] G. D. Mahan, *Many-particle Physics* (Plenum Press, New York, 1990).

Figure 4.1: The real and imaginary parts of the dielectric function of water [83, 84, 85, 86].

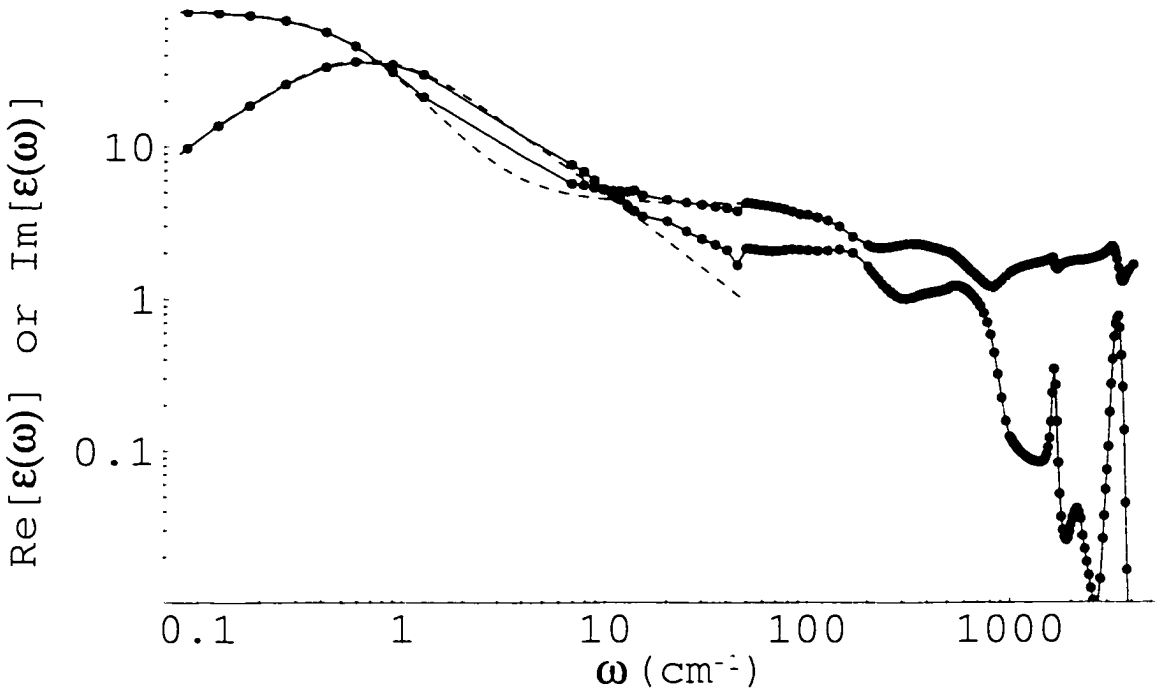

Figure 4.2: The normalized classical and quantum correlation functions. $\Delta_{cl}(t)$ [Eq. (4.21)] and $\Delta_{qu}(t)$ [Eq. (4.52)], are given by the upper and lower curves, respectively. The inset gives the results over a longer picosecond time interval. The spectral density of the solvent was calculated using the dielectric data of water and Eq. (4.61).

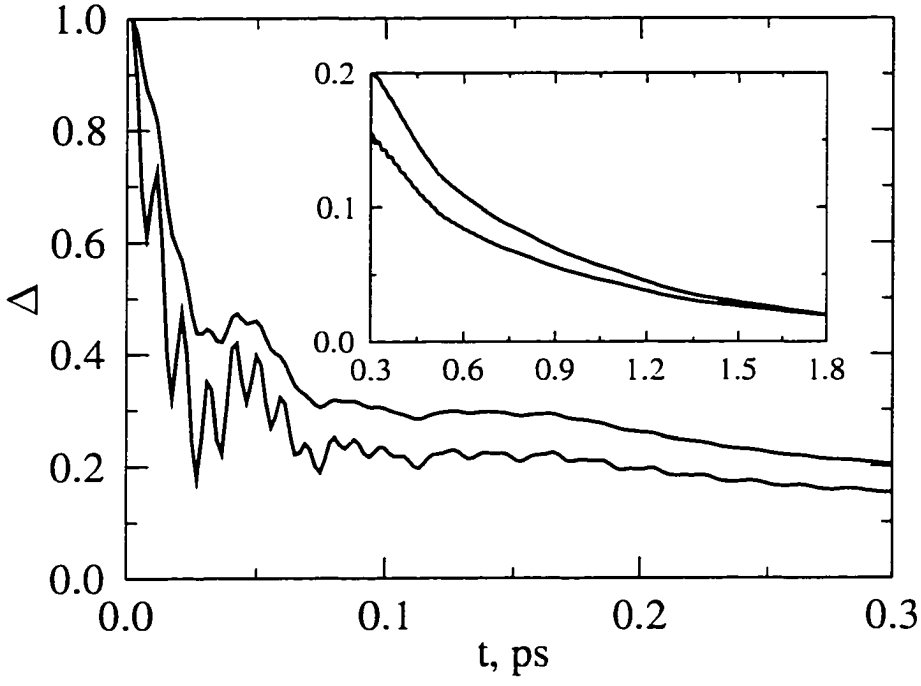

Figure 4.3: The classical (upper) and quantum (lower curve) correlation functions, $\Delta_{cl}(t)$ and $\Delta_{qu}(t)$, respectively, with finite time resolution. Convolution was performed with the Gaussian $\exp(-t^2/\tau_p^2)$, τ_p = 50 fs, which corresponds to an instrument response function of FWHM=$2\sqrt{\ln 2}\tau_p$ = 83 fs [88].

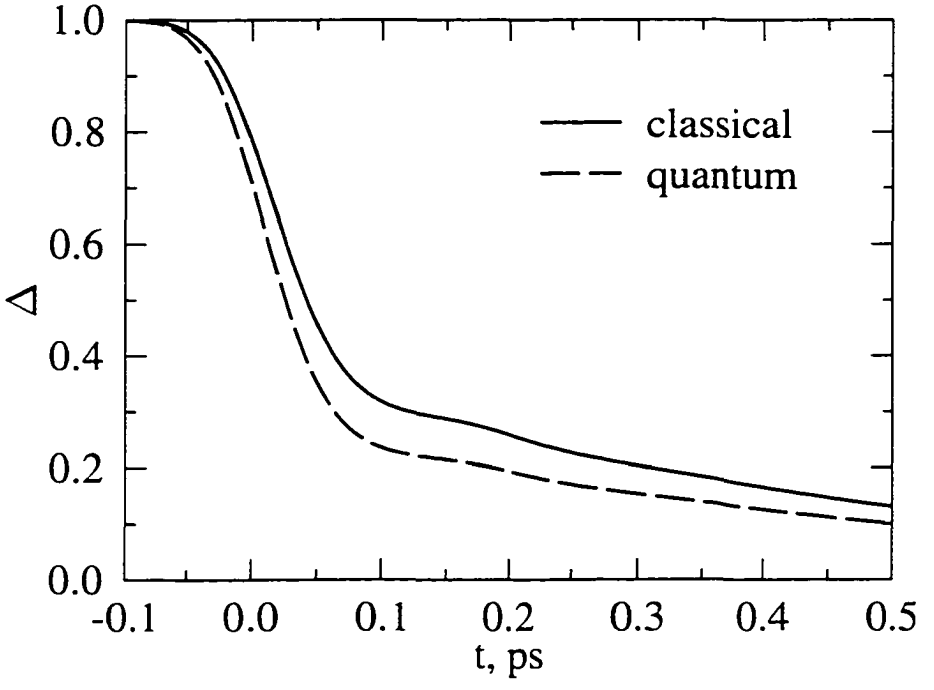

Chapter 5 The Time-Dependent Fluorescence Spectra of Large Molecules in Polar Solvents

Chao-Ping Hsu, Yuri Georgievskii and R. A. Marcus

A. A. Noyes Laboratory of Chemical Physics, 127-72

California Institute of Technology, Pasadena, California 91125

(Reprinted with permission from *J. Phys. Chem. B*, in press.

Abstract

A method is described for incorporating the vibronic transitions of a solute molecule in the calculation of the time-evolution of its fluorescence spectrum in a polar solvent. In this initial article, systems are treated in which the intramolecular vibrational relaxation is much faster than the observation delay time. The overall fluorescence spectrum is then shown to be a convolution of the steady-state absorption and emission spectra of the solute in a *nonpolar* solvent and the time-dependent emission lineshape arising only from polar interactions. Calculations are made for coumarin 153 in acetonitrile, using the dielectric dispersion data of the solvent available from experimental measurements. The results are in encouraging agreement with experimental spectra. Results are also given for the dynamic Stokes shift in methanol.

5.1 Introduction

The dynamics of polar solvents has been studied in charge redistribution processes in many chemical reactions and photo-induced processes [1–29]. Pioneering works, both in theories and experiments in nanosecond time scales, were performed by Bakhshiev, Mazurenko and their coworkers [1–4]. Experimentally, the time-dependent fluorescence shift (the *dynamic Stokes shift*) has been measured over different time scales and for a variety of polar solvents [6–15]. In typical Stokes shift experiments, a chromophoric solute dissolved in a polar solvent is first excited by a pump pulse, and the time-dependent fluorescence spectrum of the solute is then recorded. For studies with coumarin or other dye molecules (e.g., Refs. [7–15]), the excited state of the solute has a charge distribution quite different from that of the ground state. The change in charge distribution causes the polar solvent to adjust its configuration to minimize the interaction free energy. Such processes have been monitored by measuring the dynamics Stokes shift, $S(t)$,

$$S(t) = \frac{\nu(t) - \nu(0)}{\nu(\infty) - \nu(0)} \tag{5.1}$$

where $\nu(t)$ is either the peak or the averaged frequency of the transient emission spectrum.

It has been shown for coumarin 153 (C153) in polar solvents that such Stokes shift measurements can be described in terms of the polar solvation processes [9, 10, 14, 15, 21, 30]. For systems with an infinitely short pump pulse, $S(t)$ is expected to follow the normalized classical correlation function of the interaction energy between the solute and solvent [29–35]. However, when the pulse has a finite duration, it has been shown that the $S(t)$ is a linear combination of the classical and quantum correlation functions of the interaction [36], a combination in which the quantum correlation term vanishes in the limit of a very short pump pulse.

Theoretical developments [16–29] have provided much physical insight into solvation dynamics. Solvation correlation functions calculated from the Debye form,

the Davidson-Cole and the Cole-Cole forms have been shown to exhibit significant differences [16]. Based on similar calculations and comparisons with experiments it has been noted that it would be useful to obtain higher frequency dielectric data for a better description of $S(t)$, the solvation correlation function [14].

Much attention has been devoted to treating theoretically the spatial dependence of dielectric response function, $\epsilon(\boldsymbol{k}, \omega)$, which includes the molecular nature of solvent [18, 19]. The dynamical mean spherical approximation theory has been used, for example [20, 21]. A systematic comparison of the $S(t)$ predicted by dynamical mean spherical approximation theory with that in experiments was reported in Ref. [9]. It was found there that a slower dynamics is usually predicted by the dynamical mean spherical approximation theory, when the solute is modeled as a dipolar sphere. A molecular hydrodynamic theory [22, 23] has been applied to a variety of systems with a model dielectric response function. Agreement between the experimental and calculated solvation correlation function was reported for water [23, 24], alcohols[25] and acetonitrile [26]. Molecular dynamics calculations have provided information on the influence of polar solvents on the reaction rate [27] and on the role played by various shells of solvent molecules [16, 29]. The short-time solvation dynamics has also been interpreted in terms of an *instantaneous normal modes* analysis of molecular dynamics simulations [28].

The lineshape of the time-evolving emission spectrum is considered in the present work. Mukamel and coworkers have developed formal expressions for various optical processes [37–39]. In those works the transient emission spectrum was expressed in terms of a direct summation over all vibronic transitions, in which each transition is described by the time-evolution of a single transition between two vibronic states and that evolution was derived from the perturbation theory [40]. Maroncelli and coworkers [9, 41, 42] and Mazurenko [4] have provided a phenomenological description for estimating the fluorescence at time zero. At the very short time limit, it was assumed that the solvent is frozen but that the internal vibrational relaxation in the solute molecule is already complete. We recall the results here for discussion and application later:

Following Maroncelli and Mazurenko [4, 42], the zero-time fluorescence can be written as proportional to a quantity F_P given by

$$F_P(\omega, t=0; \omega_{ex}) = \omega^3 \omega_{ex} \int_{-\infty}^{\infty} d\omega'' g_{np}(\omega_{ex} - \omega'') f_{np}(\omega - \omega'') p_1(\omega'') \qquad (5.2)$$

where $g_{np}(\omega)$ describes the absorption spectrum of the solute molecule and $f_{np}(\omega)$ is the emission lineshape, both in a nonpolar solvent. The $p_1(\omega)$ describes the probability distribution of the polar solvent configurations which have a given energy difference $\hbar\omega$ between the two states of the solute molecule, sampled from the polar solvent configurations in thermal equilibrium with the *ground* electronic state of the solute molecule. Such an energy difference of the two solute electronic states is assumed to arise from the polar solute-solvent interaction. Thus, $p_1(\omega)$ would have been the absorption lineshape in polar solution, if there had been only a difference in the *polar* interactions of the ground and excited state Hamiltonians. In applying Eq. (5.2) the nonpolar reference absorption and emission spectra are used to obtain $g_{np}(\omega)$ and $f_{np}(\omega)$ [9, 41, 42]:

$$\omega g_{np}(\omega) \propto A_{np}(\omega) \qquad (5.3)$$

$$\omega^3 f_{np}(\omega) \propto F_{np}(\omega) \qquad (5.4)$$

where A_{np} is the absorption spectrum and F_{np} is the steady-state emission spectrum, for the same solute in a nonpolar reference solvent.

One might imagine that an extension of Eq. (5.2) for a phenomenological description of the time-dependent fluorescence can be written as [4]:

$$F_P(\omega, t; \omega_{ex}) = \omega^3 \omega_{ex} \int_{-\infty}^{\infty} d\omega' \int_{-\infty}^{\infty} d\omega'' g_{np}(\omega_{ex} - \omega'') f_{np}(\omega - \omega') p(\omega', t; \omega'') \qquad (5.5)$$

where $p(\omega', t; \omega'')$ is the time-evolution of a probability distribution for the energy difference of the two states of the solute that have an energy difference $\hbar\omega''$ at $t = 0$ which then drifts to $\hbar\omega'$ at time t, if only polar solute-solvent interactions were included.

This drift in the energy difference is due to the difference in charge distributions of solute in the two electronic states. Thus, $p(\omega', t; \omega'')$ can also be regarded as the time-evolution of the emission spectral lineshape (with emission frequency ω') when the pump frequency is ω'' for the two-state solute if there were only the polar interaction with the solvent. The desired properties of $p(\omega', t; \omega'')$ are:

$$p(\omega', t = 0; \omega'') = p_1(\omega'')\delta(\omega' - \omega'') \tag{5.6}$$

$$\lim_{t\to\infty} p(\omega', t; \omega'') = p_1(\omega'')p_2(\omega') \tag{5.7}$$

where the first property is needed to yield Eq. (5.2) as a special case of Eq. (5.5), and the second property means that at very long time, the spectral shifts ω' and ω'' are independent. The $p_2(\omega')$ denotes the equilibrium probability distribution of energy difference (spectral shift), sampled from solvent configurations in thermal equilibrium with the *excited* state solute charge distribution. Thus $p_2(\omega')$ is also the steady-state emission lineshape for the two-state solute when only polar interactions with the solvent are considered.

In the present work it is shown that Eq. (5.5) can be obtained from perturbation theory using Mukamel's formalism. The result provides a method for including the vibronic transitions of the dye molecule in the time-dependent fluorescence spectrum. The major physical approximation made is a time-separation of the motions. For the purpose of the present article, the nonpolar interactions between the solute and solvent as well as the intramolecular vibrational motion, are treated as instantaneous, while in the literature a Brownian oscillator model is sometimes used [37, 43]. The remaining motion is the electrostatic interaction between the solute and the polar solvent. It is assumed to provide all the measurable dynamics in the current upconversion fluorescence experiments.

The outline of the paper is as follows: The general theoretical description of the fluorescence spectrum is presented in Section 5.2.1. The separation of contributions from the above time scales of motion to the interaction energy is made in Section 5.2.2. The results of applying expressions obtained in Section 5.2 to C153 in acetonitrile,

using the dielectric continuum model with experimental $\epsilon(\omega)$ data, are given in Section 5.3. The results are discussed in Section 5.4. It has been pointed out [44] in a treatment of the dynamic Stokes shift that the inclusion of some description of the electronic polarizability of the solute [8, 11, 45] leads to an improved agreement, and that behavior is also found here. Concluding remarks are given in Section 5.5.

5.2 Theory

5.2.1 General Formalism for the Time-Evolution of the Fluorescence Spectrum

The time-evolution of the fluorescence spectrum has been treated by Mukamel and coworkers [37, 38]. With their formalism, the time-dependent emission spectrum $F(\omega, t; \omega_{ex})$, the spectral intensity at time t of the fluorescence at frequency ω when the frequency of excitation is ω_{ex}, can be calculated from the perturbation theory [40]. The solute molecule is considered to have two electronic states, $|g\rangle$ and $|e\rangle$, whose energies are dependent on both the internal vibration coordinates and the configuration of the solvent molecules. Under the Condon approximation, an explicit expression for $F(\omega, t; \omega_{ex})$ can be obtained using third-order perturbation theory for the interaction between the material and the radiation to calculate the time-evolution of the density matrix [37, 38, 40]:

$$\begin{aligned} F(\omega, t; \omega_{ex}) &= \left|\frac{E_1\mu}{\hbar^2}\right|^2 \left|\frac{E_2\mu}{\hbar^2}\right|^2 \times \\ &\quad \mathrm{Re}\int_{-\infty}^{t} dt_3 \int_{-\infty}^{t} dt_1 \int_{-\infty}^{t} dt_2 e^{i\omega(t-t_3)} e^{i\omega_{ex}(t_2-t_1)} e(t_1) e^*(t_2) R(t_1, t_2, t_3; t) \end{aligned} \tag{5.8}$$

where Re denotes the real part of the function, E_1 and E_2 are the electric field strengths of the pump pulse and the emitting light, respectively, μ is the transition dipole moment, $e(t)$ is the profile of the pump pulse, and R is a four-point correlation

function:

$$R(t_1,t_2,t_3;t) = \langle \exp_- \frac{i}{\hbar}\int_{t_2-t_1}^{t_3-t_1} \mathcal{X}(\tau_1)d\tau_1 \exp_+ \frac{-i}{\hbar}\int_0^{t-t_1} \mathcal{X}(\tau_2)d\tau_2\rangle. \tag{5.9}$$

Here, $\exp_+$ ($\exp_-$) is the time-ordered (reverse ordered) exponential function. $\langle\cdots\rangle$ indicates that the quantity is averaged over a thermal equilibrium with solute molecule in the *ground state* ($\equiv \mathrm{Tr}[e^{-\beta H_g}\cdots]$), and $\mathcal{X}$ is the difference in Hamiltonians.

$$\mathcal{X} = H_e - H_g, \tag{5.10}$$

where H_e and H_g are the Hamiltonians for the excited state and ground state solute molecule, respectively. They are dependent on both the intramolecular and intermolecular configurations. The $\mathcal{X}(\tau)$ in Eq. (5.9) is the time-evolution of $\mathcal{X}$ under the *ground* state Hamiltonian.

$$\mathcal{X}(\tau) = e^{iH_g\tau/\hbar}\mathcal{X}e^{-iH_g\tau/\hbar}. \tag{5.11}$$

Using the second order cumulant expansion [46] for R in Eq. (5.9), we have

$$\begin{aligned} &R(t_1,t_2,t_3;t) = e^{i(\Delta G^0+\lambda)(t_3-t+t_1-t_2)/\hbar}\times \\ &\exp\frac{-1}{\hbar^2}[\zeta(t_2-t_1)+\zeta^*(t-t_3)+\zeta(t-t_1)-\zeta(t_3-t_1)-\zeta^*(t-t_2)+\zeta^*(t_3-t_2)] \end{aligned} \tag{5.12}$$

with

$$\zeta(\tau) \equiv \int_0^\tau d\tau_1\int_0^{\tau_1} d\tau_2\langle X(\tau_1)X(\tau_2)\rangle \tag{5.13}$$

$$= \int_0^\tau du(\tau-u)\langle X(u)X(0)\rangle \tag{5.14}$$

and

$$X = \mathcal{X} - \langle\mathcal{X}\rangle. \tag{5.15}$$

The stationarity of the correlation function $\langle X(\tau_1)X(\tau_2)\rangle$ was used in obtaining Eq. (5.14).

The diagram corresponding to the evolution of density matrix used in obtaining Eq. (5.8) is given in Fig. 5.1. In Eq. (5.12), the terms $\zeta(t_2 - t_1)$ and $\zeta^*(t - t_3)$ are related to the lineshapes of the absorption and emission spectra, respectively [47]. The remaining four ζ terms in the exponent of $R(t_1, t_2, t_3; t)$ in Eq. (5.12) can be simplified as follows: The ranges of t_1 and t_2 are limited by the excitation pulse profile, $e(t)$, while the observation of fluorescence at time t can be much later. The time $(t - t_3)$ is limited by the decay time of $\exp[-\zeta^*(t - t_3)/\hbar^2]$. For example, for systems at room temperature (such as in Ref. [9]) with a reorganization energy λ of the order 1000 cm^{-1} arising from the polar solvation, the decay time for both $\exp[-\zeta(t_2 - t_1)/\hbar^2]$ and $\exp[-\zeta^*(t - t_3)/\hbar^2]$ is of the order of 10 fs (cf. Eq. (5.27) below). The latter limits $|t_2 - t_1|$ and $|t - t_3|$ to be of the order of 10 fs. It is then reasonable to assume, for a simplification of the exponent in Eq. (5.12), that

$$0 \approx t_1 \sim t_2 \ll t_3 \sim t. \tag{5.16}$$

Equation (5.16) implies a significant time difference between the optical absorption (at t_1, t_2) during the pulse and the subsequent fluorescence (at t_3, t) after the pulse. At the observation time t, the algebraic sum of the latter four ζ terms in Eq. (5.12), $\zeta(t - t_1) - \zeta(t_3 - t_1) - \zeta^*(t - t_2) + \zeta^*(t_3 - t_2)$, is approximated by a Taylor expansion at time t, to second order in t_1, t_2 and $(t - t_3)$:

$$\begin{aligned} & \zeta(t - t_1) - \zeta(t_3 - t_1) - \zeta^*(t - t_2) + \zeta^*(t_3 - t_2) \\ \simeq\ & 2i(t - t_3)\ \mathrm{Im}\zeta'(t) + (t_2 - t_1)(t - t_3)\ \mathrm{Re}\zeta''(t) - i(t_2 + t_1 + t - t_3)(t - t_3)\ \mathrm{Im}\zeta''(t) \end{aligned} \tag{5.17}$$

where the primes denote the first and second derivatives of $\zeta(t)$, and Re and Im denote the real part and imaginary part of the functions, respectively [48]. The first term in the right-hand side of Eq. (5.17) is the leading term of the algebraic sum of the four

ζ functions. It results in a spectral shift in the Fourier transform to the frequency domain. Thereby, those four ζ functions in the exponent of Eq. (5.12) generate the time-dependent spectral shift, among other (higher order) effects.

In the next section, we describe a way of treating the intramolecular vibrational modes of the solute molecule.

5.2.2 Treatment of the Internal Vibrational Relaxation

For a polar molecular such as C153 in a polar solvent, the ground state and excited state energies have a different dependence on the internal vibration coordinate and on the solvent configuration. The solvent part can be considered to be composed of both nonpolar and polar interactions. The nonpolar interaction arises, in part, from any difference in size or shape of the wave functions of the two electronic states, and the polar part arises from the electrostatic interaction of the solvent polarization with the different charge distribution of the ground and excited states of the solute molecules. Thereby, X can be divided into two parts:

$$X = X_s + X_f \tag{5.18}$$

where X_f arises from the intramolecular vibrations of the solute and the van der Waals type of nonpolar interaction between the solute and solvent, both treated here as fast. X_s is the part of energy difference arising from the electrostatic interaction between the solute and polar solvent, which then provides the major contribution to the dynamic Stokes shift and is assumed to respond more slowly than the X_f for the present study. For studies with higher time-resolution or for other solutes and solvents, the assumption that X_f response is instantaneous can be removed by using a model, Brownian oscillators for example [37, 43], and we may do so later for a related problem.

Assuming X_f and X_s to be statistically independent, the correlation function in

X can be separated as

$$\langle X(\tau_1)X(\tau_2)\rangle = \langle X_f(\tau_1)X_f(\tau_2)\rangle + \langle X_s(\tau_1)X_s(\tau_2)\rangle \tag{5.19}$$

The corresponding ζ function becomes

$$\zeta(t) = \zeta_f(t) + \zeta_s(t). \tag{5.20}$$

For the fast modes, $\langle X_f(t)X_f(0)\rangle$ is assumed to decay to zero before the fluorescence is observed in the experiment. Namely, we approximate the correlation function arising from such fast motions by its long time limit. Thereby, the fast mode contribution to the right-hand side of Eq. (5.17) yields $2i(t-t_3)\lambda_f/\hbar$ arising from the first term, and zero from the other two terms, where λ_f is:

$$\lambda_f \equiv -\frac{1}{\hbar}\lim_{t\to\infty} \mathrm{Im}\zeta_f'(t) \left(= -\frac{1}{\hbar}\int_0^\infty \mathrm{Im}\ \langle X_f(t)X_f(0)\rangle dt\right). \tag{5.21}$$

[The second equality in Eq. (5.21) can be seen from the definition of $\zeta(t)$ in Eq. (5.13).] With the above definition, λ_f is the reorganization energy arising from the fast modes [49]. This fast mode contribution, $2i(t-t_3)\lambda_f/\hbar$, yields a constant spectral shift $2\lambda_f/\hbar$ in the emission frequency ω when introduced into Eqs. (5.12) and (5.8).

In rewriting the time-dependent fluorescence $F(\omega,t;\omega_{\mathrm{ex}})$ in Eq. (5.8) with the separation of fast and slow modes, Eq. (5.20) is used for all six ζ functions in Eq. (5.12). The approximation given in Eq. (5.17) is used, with the terms for fast modes being simplified as described above, and the result is used to rewrite $F(\omega,t;\omega_{\mathrm{ex}})$ in Eq. (5.8). Such manipulation is followed by a rearrangement of the various terms in the exponent. Equation (5.8) can then be rewritten as

$$F(\omega,t;\omega_{\mathrm{ex}}) \propto \mathrm{Re}\int_{-\infty}^{\infty} d\tau' \int_{-\infty}^{\infty} d\tau'' e^{i\Delta\omega\tau'} e^{i\Delta\omega_{\mathrm{ex}}\tau''}\theta(\tau')\tilde{g}(\tau'')\tilde{f}(\tau')\tilde{p}(\tau',t;\tau''), \tag{5.22}$$

where $\Delta\omega \equiv \omega - (\Delta G^{\mathrm{solv}} + \lambda_s)/\hbar$, $\Delta\omega_{\mathrm{ex}} \equiv \omega_{\mathrm{ex}} - (\Delta G^{\mathrm{solv}} + \lambda_s)/\hbar$ and $\tilde{g}$, $\tilde{f}$ and $\tilde{p}$ are defined below. The equilibrium free energy difference ΔG^0 of the two states in polar

solvent has been written as the sum of the free energy difference in a *nonpolar* solvent, $\Delta G^0_{\rm np}$, and the difference in the solvation free energy $\Delta G^{\rm solv}$ between the ground and excited states of the solute. In obtaining Eq. (5.22) from Eq. (5.8), with $\tilde{p}$ defined below by Eq. (5.25), a change of variables has been introduced: $\tau' \equiv t - t_3$, $\tau'' \equiv t_2 - t_1$ and (for Eq. (5.25)) $u \equiv t_1 + t_2$. $\theta(\tau)$ is a step function that equals 1 if $\tau \geq 0$ and 0, otherwise. This step function is introduced so that the range of integration over τ' becomes $-\infty$ to ∞ instead of 0 to ∞, and so the convolution theorem of Fourier transform can then be applied [50]. The λ_s is the reorganization energy arising from the "slow modes", with a definition analogous to that in Eq. (5.21), but for the slow variable, $X_s(t)$.

The functions $\tilde{f}(\tau')$ and $\tilde{g}(\tau'')$ in Eq. (5.22) describe the fast mode contribution, and $\tilde{p}(\tau', t; \tau'')$ contains the slow mode contribution and the optical pulse shape. These functions are given by

$$\begin{aligned} \tilde{f}(\tau') &\equiv \exp[-\zeta_f^*(\tau')/\hbar^2 + 2i\tau'\lambda_f/\hbar] \exp[-i(\Delta G^0_{\rm np} + \lambda_f)\tau'/\hbar] \\ &= \exp[-\zeta_f^*(\tau')/\hbar^2 - i(\Delta G^0_{\rm np} - \lambda_f)\tau'/\hbar], \end{aligned} \tag{5.23}$$

$$\tilde{g}(\tau'') \equiv \exp[-\zeta_f(\tau'')/\hbar^2 - i(\Delta G^0_{\rm np} + \lambda_f)\tau''/\hbar], \tag{5.24}$$

and

$$\begin{aligned} &\tilde{p}(\tau', t; \tau'') \equiv \int_{-\infty}^{\infty} du\; e(\frac{u - \tau''}{2}) e^*(\frac{u + \tau''}{2}) \\ &\exp \frac{-1}{\hbar^2}[\zeta_s(\tau'') + \zeta_s^*(\tau') + 2i\tau' {\rm Im}\zeta_s'(t) + \tau'\tau'' {\rm Re}\zeta_s''(t) - i(u + \tau')\tau' {\rm Im}\zeta_s''(t)]. \end{aligned} \tag{5.25}$$

Expressions in Eqs. (5.23) and (5.24) are, respectively, the Fourier transforms of the long-time emission and absorption spectra that the system would have in the absence of the slow mode (electrostatic) interaction [51, 52]. These spectra can be approximated by the steady-state absorption and emission spectra of the same solute molecule in a *nonpolar* solvent. Application of the convolution theorem to Eq. (5.22)

then yields

$$F(\omega, t; \omega_{ex}) \propto \int_{-\infty}^{\infty} d\omega' \int_{-\infty}^{\infty} d\omega'' g(\omega_{ex} - \omega'') f(\omega - \omega') p(\omega' - \omega_0, t; \omega'' - \omega_0) \quad (5.26)$$

with $\omega_0 \equiv (\Delta G^{solv} + \lambda_s)/\hbar$. The equation above is of the form given by Eq. (5.5). The factors ω^3 and ω_{ex} are obtained by summing over the emission photon mode and converting the number of absorption photons into energy units [53].

To integrate Eq. (5.25) for the purposes of the present paper, a Gaussian optical pulse, $e(t) \sim \exp(-t^2/\tau_p^2)$, is assumed, though this assumption is a convenience rather than a necessity. When the Gaussian approximation [54],

$$\exp \frac{-1}{\hbar^2} \zeta_s(t) \approx \exp(-\lambda_s k_B T t^2/\hbar^2) \quad (5.27)$$

is used to obtain the Fourier transform of $\tilde{p}(\tau', t; \tau'')$, the result of these manipulations yields

$$p(\omega', t; \omega'') \propto \frac{1}{\sqrt{A(t)}} \exp\left[-\frac{B(t)^2}{4A(t)} - \frac{\omega''^2}{C}\right], \quad (5.28)$$

where

$$A(t) = \frac{\lambda_s k_B T}{\hbar^2} - \frac{\mathrm{Re}\zeta_s''(t)^2}{2C\hbar^4}, \quad (5.29)$$

$$B(t) = \omega' + 2\mathrm{Im}\zeta_s'(t)/\hbar^2 + \omega'' \frac{\mathrm{Re}\zeta_s''(t)}{C\hbar^2}, \quad (5.30)$$

and

$$C = \frac{2\lambda_s k_B T}{\hbar^2} + \frac{1}{\tau_p^2} \quad (5.31)$$

where the $\mathrm{Im}\zeta_s''(t) (= \mathrm{Im}\langle X_s(t) X_s(0)\rangle)$ is neglected because the imaginary part of the correlation function is much smaller than the real part. Moreover, in Eq. (5.25), $\mathrm{Im}\zeta_s''(t)$ is multiplied by factors composed of u and τ' and they are limited by the pump pulse profile and the decay time of $\exp[-\zeta_s^*(\tau')/\hbar^2]$, respectively. The latter is of the same order as the $\tau'\tau''$ in Eq. (5.25), the factor multiplying $\mathrm{Re}\zeta_s''(t)$ there. From Eq. (5.25) it can be inferred that the function $p(\omega', t; \omega'')$ is the time-evolution of the emission spectrum (with emission frequency ω') for a two-state solute that is

excited at frequency ω'', if only X_s contributed to the difference in the Hamiltonians of the two states. (Cf. the general expression for time-evolution emission spectrum in Eq. (5.8).)

Thereby, the time-dependent fluorescence spectrum can be calculated from the convolution of the steady-state absorption and emission spectra in a nonpolar solvent and the function $p(\omega', t; \omega'')$ given by Eq. (5.28). To calculate $p(\omega', t; \omega'')$, the explicit numerical values of the integrated correlation function $\zeta_s(t)$ are needed. They can be obtained from the correlation function, $\langle X_s(t)X_s(0)\rangle$, using Eq. (5.14).

For treating the correlation function, several approaches come to mind. One involves using, in effect, linear response theory, as Ovchinnikov and Ovchinnikova did [55] in their application of a quantum field theoretic method [56]. This treatment does not use a molecular harmonic oscillator model [57]. In a work by Mukamel [58], a spectral density function $J(\omega)$ was introduced from a general consideration which involves large anharmonic vibrations of molecules. A property of such spectral density function was also discussed in the context of fluctuation-dissipation theorem there [58]. From such property, the correlation function can be written in terms of its corresponding spectral density in the frequency domain [58, 59]

$$\langle X_s(t)X_s(0)\rangle = \frac{\hbar}{\pi}\int_0^\infty d\omega J(\omega)\left(\coth\frac{\beta\hbar\omega}{2}\cos\omega t - i\sin\omega t\right) \tag{5.32}$$

where $\beta \equiv 1/k_B T$. Even though the terms inside the parentheses of the integrand resemble the correlation function of a harmonic oscillator [60], Eq. (5.32) is obtained from a general consideration of the properties of correlation functions, and is not limited to any harmonic oscillator model [55, 58, 59].

The spectral density $J(\omega)$ can be related to a measurable property of the solvent, the dielectric dispersion $\epsilon(\omega)$. With the simple continuum model, the linear response theory can be applied to obtain the response function for a time-varying dipole representing the solute. Such response function is closely related to the correlation function $\langle X_s(t)X_s(0)\rangle$ needed here [59, 61]. In Ref. [55] a homogeneous boundary condition was implicitly assumed and a form of $J(\omega)$ in terms of $\epsilon(\omega)$ was obtained. For a point

dipole in a sphere cavity model, the spectral density $J(\omega)$ is [37, 62]

$$J(\omega) = -\frac{2\Delta\mu^2}{a^3}\mathrm{Im}\left[\frac{\epsilon(\omega)-1}{2\epsilon(\omega)+1}\right] \tag{5.33}$$

where $\Delta\mu$ is the change in the dipole moment of the solute in the two states, and a is the radius of the cavity. For a spherical cavity filled with dielectric material having a dielectric constant ϵ_c to account for the electronic polarizability of the solute, the corresponding expression is (compare related expressions in Refs. [8, 11, 45, 63–65]),

$$J(\omega) = -\frac{2\Delta\mu^2}{a^3}\mathrm{Im}\left[\frac{\epsilon(\omega)-1}{2\epsilon(\omega)+\epsilon_c}\right]\left(\frac{\epsilon_c+2}{3}\right). \tag{5.34}$$

which reduces to Eq. (5.33) when ϵ_c is assumed to be unity.

The correlation function of X_s can now be obtained using the above expressions for $J(\omega)$ and Eq. (5.32). The integrated correlation function $\zeta_s(t)$ is then, from Eq. (5.14), given by

$$\zeta_s(t) = \frac{\hbar}{\pi}\int_0^\infty d\omega \frac{J(\omega)}{\omega^2}\left[\coth\frac{\beta\hbar\omega}{2}(1-\cos\omega t) - i(\omega t - \sin\omega t)\right]. \tag{5.35}$$

Two functions needed in Eqs. (5.29) and (5.30) to calculate the time-dependent fluorescence spectrum are [66]

$$\mathrm{Im}\zeta_s'(t) = \frac{\hbar}{\pi}\int_0^\infty d\omega \frac{J(\omega)}{\omega}(-1+\cos\omega t) \tag{5.36}$$

$$= -\lambda_s\hbar + \frac{\hbar}{\pi}\int_0^\infty d\omega \frac{J(\omega)}{\omega}\cos\omega t \tag{5.37}$$

and

$$\mathrm{Re}\zeta_s''(t) = \mathrm{Re}\langle X_s(t)X_s(0)\rangle = \frac{\hbar}{\pi}\int_0^\infty d\omega J(\omega)\coth\frac{\beta\hbar\omega}{2}\cos\omega t. \tag{5.38}$$

They can be calculated using Fourier cosine transform subroutines. The second term of Eq. (5.37), if normalized to unity at $t = 0$, is the same as the function $\Delta_{cl}(t)$ used in Ref. [36] and has been shown to be $S(t)$, the dynamic Stokes shift function [30].

Namely,

$$S(t) = \frac{\int_0^\infty \cos\omega t J(\omega)/\omega d\omega}{\int_0^\infty J(\omega)/\omega d\omega} \tag{5.39}$$

The term $\mathrm{Re}\zeta_s''(t)$, when normalized, yields $\Delta_{qu}(t)$ in our previous work [36].

5.3 Application

Using experimental data for $\epsilon(\omega)$ for the solvents, all the correlation functions of the solvent modes needed can be calculated with the aid of Eqs. (5.33) (or (5.34)), (5.37) and (5.38). The overall spectral lineshape can be then obtained from Eqs. (5.26) and (5.28).

The dielectric dispersion $\epsilon(\omega)$ of acetonitrile has been measured for a wide frequency range. At low frequencies, J. Barthel *et al.* reported parameters for a Cole-Cole equation for frequencies lower than 89 GHz [67, 68], which corresponds roughly to 3 cm^{-1}. In the microwave and far-infrared region (frequencies up to 200 or 250 cm^{-1}) the optical constants (complex refractive indices) have been reported [69–72]. The absorption peak at about 378 cm^{-1} was measured and described in Ref.[73]. For the infrared region, there is the early work by Goplen *et al.* [74] and Bertie's recent work [75].

For the present calculation, the parameters of Cole-Cole equation in Ref. [67] are used for low frequency region. For frequencies higher than 3 cm^{-1}, we first obtain the imaginary part $k(\tilde{\nu})$ of the complex refractive index ($\hat{n}(\tilde{\nu}) = n(\tilde{\nu}) - ik(\tilde{\nu})$) from data in the literature [70, 73, 75, 76]. The absorption coefficients $\alpha(\tilde{\nu})$ reported in Refs. [70] and [73] can be converted to $k(\tilde{\nu})$ by dividing α by $2\pi\tilde{\nu}$. A cubic spline interpolation [77, 78] was then used to obtain $k(\tilde{\nu})$ for any given frequency. The Kramers-Kronig transformation [79] was used to obtain the real part of refractive index, $n(\tilde{\nu})$, from $k(\tilde{\nu})$

$$n(\tilde{\nu}) = n_\infty + \frac{2}{\pi}\mathrm{P}\int_0^\infty \frac{\tilde{\nu}' k(\tilde{\nu}')d\tilde{\nu}'}{\tilde{\nu}'^2 - \tilde{\nu}^2} \tag{5.40}$$

where P denotes the principal value of the integral, and the upper limit "∞" denotes a high frequency, where $n = n_\infty$. It has been shown [80] that to obtain $n(\tilde{\nu})$ at infrared

frequencies by integrating over $k(\tilde{\nu})$ in only infrared region, the above equation can be rewritten as

$$n(\tilde{\nu}) \approx (a_0 + a_2\tilde{\nu}^2 + a_4\tilde{\nu}^4) + \frac{2}{\pi}\mathrm{P}\int_0^{\tilde{\nu}_{\mathrm{IR}}} \frac{\tilde{\nu}' k(\tilde{\nu}')d\tilde{\nu}'}{\tilde{\nu}'^2 - \tilde{\nu}^2} \tag{5.41}$$

where the first three terms in the parentheses are a suitable approximation to the contribution from the UV absorption. For the present calculation, coefficients (a_0, a_1 and a_2) are obtained from those given in Ref. [80]. The numerical integration using Eq. (5.41) gives an $n(\tilde{\nu})$ in good agreement with the values reported in Refs. [70, 75] and [81]. The dielectric dispersion $\epsilon(\omega)$ for those frequencies equals the square of the complex refractive index, $n(\tilde{\nu}) - ik(\tilde{\nu})$, and so is now known.

The values of $\mathrm{Im}\zeta_s'(t)$ and $\mathrm{Re}\zeta_s''(t)$ are obtained using the dielectric dispersion data obtained above and Eqs. (5.33) (or (5.34)), (5.37) and (5.38). The nonpolar reference spectra are those published in Ref. [9] for C153 in 2-methyl butane. In the calculation we also need a number for $(\Delta G^{\mathrm{solv}} + \lambda_s)/\hbar$ which is the change in absorption frequency due to a change in solvent polarity. This quantity for a polar molecule is dependent on solvent polarity and the dipole moments of both states of the molecule (cf. eq 20 of Ref. [30] or eq 4.2 of Ref. [9]). In the present work 1490 cm^{-1} is used for this quantity, $(\Delta G^{\mathrm{solv}} + \lambda_s)/\hbar$, for C153 in acetonitrile [82].

The overall spectral shift due to the polar interaction is $2\lambda_s$, which is proportional to the factor $\Delta\mu^2/a^3$ in Eqs. (5.33) and (5.34). Maroncelli and Fleming have examined the steady-state Stokes shift measurements of C153 in various polar solvents and have obtained the dipole moment change as 6.0 D if the radius of the spherical cavity resembling the solute molecule is assumed to be 3.9 Å[8]. From fitting the emission spectral position calculated at $t \to \infty$ to the steady-state experimental fluoresce spectrum, we obtained a similar value, 6.1 D, as the dipole moment change for a non-polarizable solute of the same size. However, if a polarizable spherical solute model is used (Eq. (5.34)), the size of the calculated dipole is smaller for the given solvation free energy: Assuming $\epsilon_c = 2.0$ [11], the dipole moment change is estimated to be 5.1 D from the same resulting λ_s as the one calculated using nonpolarizable model

with $\Delta\mu = 6.1$ D [83]. Using this ϵ_c and $\Delta\mu$ for the polarizable model the result of the overall calculation for the time-dependent emission spectrum is compared in Fig. 5.2 with the experimental spectrum obtained from Ref. [10]. In the calculation we set $\tau_p = 50$ fs. which corresponds to 118 fs FWHM in the correlation between pulses. (The values of 112–125 fs is reported in Ref. [10].) In Fig. 5.3 the dynamic Stokes shift $S(t)$, calculated from the second term of Eq. (5.37), is plotted together with the one obtained from experiment [9].

We have also calculated a dynamic Stokes shift for methanol: Dielectric dispersion data for methanol are available for a wide range of frequencies. The parameters obtained from fitting microwave measurements to a three-term Debye model have been reported for frequencies less than 295 GHz (≈ 10 cm^{-1}) [84]. The complex refractive indices of methanol from 2 cm^{-1} to 8000 cm^{-1} have been reported in Ref. [85]. For frequencies from 2 cm^{-1} to 50 cm^{-1}, the dielectric dispersion was also measured by Kindt *et al.* [86]. A three-term Debye model fit was performed in the latter work and the dielectric dispersion results obtained from those parameters agree fairly well with the lower frequency results reported by Bertie [85]. For the present calculation a cubic spline fit of the tabulated numbers from Bertie's work was used for frequencies higher than 8 cm^{-1}. For frequencies lower than 8 cm^{-1} the three-term Debye fit reported in Ref. [84] was used.

The calculated $S(t)$ is compared in Fig. 5.4 with the experimental results of Ref. [9]. In this case the plot from dipole in a spherical cavity model is seen to deviate from that from experiment. Results from a calculation using the polarizable solute model using Eq. (5.34) with the cavity dielectric constant $\epsilon_c = 2$ are also given in Fig. 5.4, and the agreement is seen to be somewhat improved.

5.4 Discussion

There is seen to be reasonably good agreement in Fig. 5.2 between the position and spectral shapes of the calculated time-dependent spectra in acetonitrile and those from experiment, when the possible experimental uncertainties are considered, especially

at early times [32]. This result supports the idea that the dynamics observed is mainly relaxation from the polar interaction between the solute and the solvent. In a recent article on shorter times [87] the authors reported very early transient absorption and gain (spontaneous emission) spectra after a pump pulse of C153 in acetonitrile and methanol. At those short times ($\leq$ 300 fs) the gain band is red-shifted with two isosbestic points appearing successively. It has been noted [87] that such results may imply that some intramolecular process is involved in the earlier dynamics.

The time-dependence of the emission spectrum in polar solutions has long been a subject of interest. In the 1960s and 1970s, experiments were performed on the nanosecond time scale [3, 65], and the *kinetics* of the spectrum was discussed in terms of the lifetime of the excited state and the orientational relaxation of the solvent molecules. The latter was related to the dielectric dispersion, $\epsilon(\omega)$, [1, 2] and a Debye form was used for $\epsilon(\omega)$ to account for the orientation dipole relaxation [1-3, 65]. A stochastic theory was also proposed to describe the time-evolution of the spectrum [4] (cf. recent work by Maroncelli and coworkers, Refs. [41, 42]). As the techniques advanced, the dynamics in femtosecond time regime became observable and so a relaxation in the intermolecular vibrations (e.g., the librational mode for water [13, 30]) has become important in understanding the experimental results in that time region. The low frequency intramolecular vibrations in both solute and solvents may also affect the early time-evolution. By including in the dielectric dispersion, the IR frequency region, we have taken the solvent vibrational modes into account.

In the present work we have considered the case, in deriving the expressions used in calculations, that the vibrational relaxation is complete before the time of observing fluorescence. A short-range nonpolar interaction and the relaxed vibrational contribution was included in an approximate way, by using the absorption and emission spectra in a *nonpolar* solvent. For experiments with a higher time-resolution, or with techniques which are more sensitive to short-time dynamics, the solute vibrational relaxation should be considered explicitly. In the present case, it was found in Ref. [9] that almost no time-dependence of the spectral shift is observed in their observations on the fluorescence of C153 in cyclohexane, and that the transient fluorescence spec-

trum is very close to that of the steady-state fluorescence spectrum for the same system (All are Stark-shifted from the absorption spectral maximum). This result shows that in this nonpolar solvent the relaxation (for both solute and solvent) to equilibrium free energy of the excited state occurs within the time resolution (120 fs FWHM instrumental response [9]) of the experiment, and so supports the assumption of fast relaxing internal modes made in the present study. The assumption itself provides a major simplification and permits the simple application of expressions for a two-level problem to a real system.

In the present calculation, there are two undetermined quantities which are inferred from experimental spectra. One is $(\Delta G^{\text{solv}} + \lambda_s)/\hbar$, the difference between averaged absorption spectra in polar and in nonpolar solvents. For the present study, a value of this quantity was chosen so as to yield agreement between the calculated and the reported (estimated) zero-time fluorescence spectrum in Ref. [10]. The other undetermined quantity, $\Delta\mu^2/a^3$, is proportional to λ_s, and so is proportional to the overall dynamic spectral shift. The latter is also related to the width of $p(\omega', t; \omega'')$ (Eq. (5.29)). However, the width of this $p(\omega', t; \omega'')$ has only a small influence on the lineshape of final convoluted spectrum, $F(\omega, t; \omega_{\text{ex}})$, because of the large Franck-Condon vibrational contribution to the width. Thereby, the quantity $\Delta\mu^2/a^3$ can be estimated solely from the spectral shift arising from the polar interaction, namely, the frequency difference of the zero-time emission spectrum and the steady-state fluorescence spectrum in the polar solvent. With the nonpolarizable model, the change in dipole moment is estimated to be 6.1 D, using the peak frequency difference of the zero-time estimated emission spectrum and the steady-state emission spectrum in methanol reported in Refs. [32] and [9], respectively. This result agrees, as noted earlier, with the 6.0 D estimated in Ref. [8] from the steady-state experimental spectrum using the same nonpolarizable model.

The calculated dynamic Stokes shift result for acetonitrile, shown in Fig. 5.3, has an oscillation period of about 0.3 ps, which arises from a strong far-infrared absorption at about 100 cm^{-1}. The results in Fig. 5.3 with polarizable solute are quite close to those reported in a recent work [88], calculated from a theory which

the authors developed for the longitudinal linear dielectric response of polarizable solvents with given shape and charge distribution. (That theory includes a $\boldsymbol{k}$ spatial dependence.) No such oscillation is reported in the experimental data, but the latter depend on the time-resolution of the technique and the data processing used. In Ref. [9] it is indicated that the deconvolution of an instrumental response function has been performed on the raw emission intensity data. It would be interesting to see if such an oscillatory correlation function can be observed in experiments with finer time-resolution, such as that in photon echoes [89].

The dynamic Stokes shift results for methanol are shown in Fig. 5.4 and display an appreciable discrepancy when compared with experiment [9]. It is seen there that the inclusion of ϵ_c to represent polarizability of solute improves somewhat the agreement of experiment and theory [11, 44]. Since we use the simple dielectric continuum in describing the solvent, and extend the frequency range to include IR frequencies, the entire response of the *bulk* solvent to a change in electric field is considered. Using other theoretical methods, namely, the dynamical MSA theory and the molecular hydrodynamic theory, the following results have been obtained for polar solvents:

In Ref. [9] it was shown that in the case of methanol, a calculated $S(t)$ using a model for the dielectric dispersion with the far infrared dielectric response included is significantly faster than the measured dynamic Stokes shift from experiment. In the same work the authors compared the dynamics calculated from the dynamical MSA theory [18], which includes a spatial dependent dielectric response, with the experimental $S(t)$. They concluded that the dynamical MSA theory gives results that are slower than those from simple continuum model which is used in the present work. For most of the cases studied in Ref. [9], the dynamical MSA theory predicts a dynamical behavior slower than the experimental one for C153 if a dipolar hard sphere is used to represent the solute. On the other hand, when the neutral dipolar solute was modeled as an ion, an improved agreement was obtained in applying the dynamical MSA theory. However, a charge distribution appropriate to the actual one should, of course, be used in comparing with the experimental $S(t)$.

In a recent article, Bagchi and coworkers applied their molecular hydrodynamic

theory, which includes rotational and translational contributions of solvent polarization relaxation, to monohydroxy alcohols. They reported the calculated *dipolar* solvation to be slightly slower than the experimental observation. Again, when the neutral dipolar C153 solute is hypothetically modeled as an ion in their model calculations, there is better agreement between the calculated and experimental $S(t)$ [25].

We have investigated the effect of pulse width by changing the pulse duration τ_p of Gaussian pulses from the limit of very short pulses to the limit of pulses which are much longer than the dephasing time ($\hbar/\sqrt{\lambda_s k_B T}$) (but still shorter than the fluorescence observation time), by taking the limits of small and large τ_p in the expressions in Eqs. (5.29) and (5.30). Results of calculations of these two limiting cases showed negligible changes in the widths in the emission spectra (of the order of 10 cm^{-1} for acetonitrile). The small effect of the pulse widths can be understood as follows: As shown in Section 5.2.2 and Eq. (5.26), the overall time-dependent spectrum is a convolution of $p(\omega', t; \omega'')$ and the steady-state absorption and emission spectra in a nonpolar solvent. The absorption and emission spectra in the nonpolar solvent have a large width, largely due to the quantized in-plane aromatic ring vibrations, which serve as a frame for the spectra that is filled in by absorption or emission due to the lower frequency modes. While in a more detailed study the correct shape of pulse profile could be used, and it may lead to a change in $p(\omega', t; \omega'')$ (Eq. (5.25)), it is not expected to be able to change the overall spectrum $F(\omega, t; \omega_{ex})$ significantly after the convolution with the large-width reference nonpolar absorption and emission spectra.

For the same reason, the lineshape information obtained from the function $p(\omega', t; \omega'')$ is mostly buried in the convolution with the large-width reference spectra. As seen in Eqs. (5.28) and (5.29), the spectral evolution of a single transition has its spectral width controlled by the quantum correlation function (the expression in Eq. (5.38)). However, after convolution with the broad reference absorption and emission spectra, the effect of spectral width of single transition is quite small in the final result. Thus, the quantum solvent effect cannot be easily retrieved from the final spectral lineshape for such systems. The time-evolution of fluorescence spectral band widths

were measured and reported for C153 in dimethyl sulfoxide (DMSO) [9] and for 1,1',3,3,3',3'-hexamethylindotricarbocyanine (HITC) in ethanol [90]. With the advances in techniques in obtaining data with an improved time-resolution and with a continuum spectral measurement, it should be possible to address more closely the evolution of emission band width and other details of the lineshape in terms of solvation dynamics and molecular properties.

5.5 Conclusion

A theory of time-dependent fluorescence spectrum for a polar solute in polar solvents is formulated and applied to C153 in acetonitrile in the present study. The dynamics of the fast motion of intramolecular vibration and the nonpolar collision-like interaction is assumed to be the same in nonpolar solvents and polar solvents and such motion is seen to decay rapidly. Polar solvents provide additional electrostatic interaction whose dynamics is slower and is observed in the experiments. Based on this assumption, we have developed a method for including the vibronic transitions of the dye molecule in the time-dependent fluorescence spectrum, and the results for C153 in acetonitrile are close to experimental ones.

Since it is now possible to estimate the overall time-dependent spectrum, a presentation of the data for the time-evolution fluorescence spectrum in numerical form, rather than only a fitted analytic functional form, would remove the added approximation of the fitting.

Acknowledgments

We wish to particularly thank Professor J. E. Bertie for providing the data file and the computer code on the dielectric dispersion of acetonitrile before publication. It is a pleasure to acknowledge the support of the National Science Foundation and the Office of Naval Research. One of us (Y. G.) would like to acknowledge the support of the James W. Glanville Postdoctoral Scholarship in Chemistry at Caltech and the

support in the early stages of this research by the Rueff-Wormser Fellowship.

References and Notes

[1] Bakhshiev, B. G., *Opt. Spectrosc.* **1964,** *16*, 446.

[2] Mazurenko, Y. T.; Bakshiev, B. G., *Opt. Spectrosc. (USSR)* **1970,** *28*, 490.

[3] Mazurenko, Y. T.; Udaltsov, V. S., *Opt. Spectrosc. (USSR)* **1978,** *44*, 417.

[4] Mazurenko, Y. T., *Opt. Spectrosc. (USSR)* **1980,** *48*, 388.

[5] Nee, T.-W.; Zwanzig, R., *J. Chem. Phys.* **1970**, *52*, 6353. van der Zwan, G.; Hynes, J. T., *J. Chem. Phys.* **1982**, *76*, 2993.

[6] Ware, W. R.; Lee, S. K.; Brant, G. J.; Chow, P. P. *J. Chem. Phys.* **1971**, *54*, 4729. Okamura, T.; Sumitani, M.; Yoshihara, K., *Chem. Phys. Lett.* **1983**, *94*, 339. Su, S.-G.; Simon, J. D., *J. Phys. Chem.* **1987**, *91*, 2693.

[7] Jarzęba, W.; Walker, G. C.; Johnson, A.E.; Kahlow, M. A.; Barbara, P. F., *J. Phys. Chem.* **1988**, *92*, 7039.

[8] Maroncelli, M.; Fleming, G. R., *J. Chem. Phys.* **1987**, *86*, 6221.

[9] Horng, M. L.; Gardecki, J. A.; Papazyan, A.; Maroncelli, M., *J. Phys. Chem.* **1995**, *99*, 17311.

[10] Gardecki, J.; Horng M. L.; Papazyan, A. Maroncelli, M., *J. Mol. Liq.* **1995,** *65-6*, 49.

[11] Maroncelli, M., *J. Phys. Chem.* **1997,** *106*, 1545.

[12] Kumar, P. V.; Maroncelli, M., *J. Chem. Phys.* **1995,** *103*, 3038.

[13] Jimenez, R.; Fleming, G. R.; Kumar, P. V.; Maroncelli, M., *Nature* **1994**, *369*, 471.

[14] Jarzeba, W.; Walker, G. C.; Johnson, A. E.; Barbara, P. F., *Chem. Phys.* **1991,** *152*, 57.

[15] Castner, E. W. Jr.; Maroncelli, M.; Fleming, G. R., *J. Chem. Phys.* **1987,** *86*, 1090.

[16] Maroncelli, M.; Castner, E. W. Jr.; Bagchi, B.; Fleming, G. R., *Faraday Discuss. Chem. Soc.* **1988**, *85*, 199.

[17] Castner, E. W. Jr.; Fleming, G. R.; Bagchi, B., *Chem. Phys. Lett.* **1988**, *143*, 270.

[18] Wolynes, P. G., *J. Chem. Phys.* **1987**, *86*, 5133. Rips, I.; Klafter, J.; Jortner, J., *J. Chem. Phys.* **1988**, *88*, 3246; *ibid.* **1988**, *89*, 4288. Nichols, III A. L. ; Calef, D. F., *J. Chem. Phys.* **1988**, *89*, 3783.

[19] Raineri, F. O.; Resat, H.; Perng, B.-C.; Hirata, F.; Friedman, H. L., *J. Chem. Phys.* **1994**, *100* , 1477. Zhou, Y.; Friedman, H. L.; Stell, G., *J. Chem. Phys.* **1989**, *91* , 4885. Fried, L. E.; Mukamel, S., *J. Chem. Phys.* **1990**, *93*, 932; Loring, R. F.; Mukamel, S., *J. Chem. Phys.* **1987**, *87*, 1272. Bagchi, B.; Chandra, A., *J. Chem. Phys.* **1989**, *90*, 7338.

[20] Maroncelli, M.; Fleming, G. R., *J. Chem. Phys.* **1988**, *89*, 875.

[21] Kahlow, M. A.; Jarzęba, W.; Kang, T. J.; Barbara, P. F., *J. Chem. Phys.* **1989**, *90*, 151.

[22] Bagchi, B.; Chandra, A., *Adv. Chem. Phys.* **1991**, *80*, 1; Bagchi, B., *Annu. Rev. Phys. Chem.* **1989**, *40*, 115.

[23] Roy, S.; Bagchi, B., *J. Chem. Phys.* **1993**, *99*, 9938.

[24] Nandi, N.; Roy, S.; Bagchi, B., *J. Chem. Phys.* **1995**, *102*, 1390.

[25] Biswas, R.; Nandi, N.; Bagchi, B., *J. Phys. Chem.* **1997**, *101*, 2968.

[26] Roy, S.; Komath, S.; Bagchi, B., *J. Chem. Phys.* **1993,** *99*, 3139.

[27] Gertner, B. J.; Whitnell, R. M.; Wilson K. R.; Hynes, J. T., *J. Am. Chem. Soc.* **1991**, *113*, 74.

[28] Ladanyi, B. M.; Stratt, R. M., *J. Phys. Chem.* **1995**, *99*, 2502; *ibid.* **1996**, *100*, 1266.

[29] Maroncelli, M.; Fleming, G. R., *J. Chem. Phys.* **1988**, *89*, 5044.

[30] Hsu, C.-P.; Song, X.; Marcus, R. A., *J. Phys. Chem. B* **1997**, *101*, 2546.

[31] Carter, E. A.; Hynes, J. T., *J. Chem. Phys.* **1991**, *94*, 5961.

[32] Rosenthal, S. J.; Jimenez, R.; Fleming, G. R.; Kumar, P. V.; Maroncelli, M., *J. Mole. Liq.* **1994**, *60*, 25.

[33] Fonseca, T.; Ladanyi, B. M., *J. Phys. Chem.* **1991**, *95*, 2116.

[34] Ando, K.; Kato, S., *J. Chem. Phys.* **1991**, *95*, 5966.

[35] Zhu, J.; Cukier, R. I., *J. Chem. Phys.* **1993**, *98*, 5679.

[36] Georgievskii, Y.; Hsu, C.-P.; Marcus, R. A., *J. Chem. Phys.* (submitted).

[37] Loring, R. F.; Yan, Y. J.; Mukamel S., *J. Chem. Phys.* **1987**, *87*, 5840.

[38] Loring, R. F.; Yan, Y. Y.; Mukamel S., *Chem. Phys. Lett.* **1987**, *135*, 23.

[39] Mukamel, S., *Principles of Nonlinear Optical Spectroscopy*; Oxford University Press: New York, 1995.

[40] For example, Mahan, G. D., *Many-particle Physics*, 2nd ed.; Plenum Press: New York, 1990.

[41] Fee, R. S.; Milsom J. A.; Maroncelli, M., *J. Phys. Chem.* **1991**, *95*, 5170.

[42] Fee, R. S.; Maroncelli, M., *Chem. Phys.* **1994**, *183*, 235.

[43] For example, Passino, S. A.; Nagasawa, Y.; Joo, T.; Fleming, G. R., *J. Phys. Chem.* **1997,** *101*, 725; Bardeen, C. J.; Shank C. V., *Chem. Phys. Lett.* **1994,** *226*, 310; Palese S.; Mukamel, S; Miller, R. J. D; Lotshaw W. T., *J. Phys. Chem.* **1996,** 100, 10380.

[44] Maroncelli, M. (private communication).

[45] Bagchi, B.; Oxtoby, D. W.; Fleming, G. R., *Chem. Phys.* **1984**, *86*, 257.

[46] Kubo, R., *J. Phys. Soc. Japan* **1962,** *17*, 1100.

[47] Kubo, R. in *Fluctuation, Relaxation and Resonance in Magnetic Systems*; D. ter Haar Ed. Edinburgh: Oliver & Boyd, 1962, p. 23. Kubo, R., *Adv. Chem. Phys.* **1969,** *15*, 101.

[48] We note incidentally that in the expansion leading to Eq. (5.17) the terms in t_1^2 and t_2^2 each canceled and there was no $t_1 t_2$ term.

[49] With Eq. (5.24) and Refs. [51, 52] below, the absorption spectrum is written as the Fourier transform of $\tilde{g}(\tau)$. If the high temperature approximation described in Eq. (5.27) and footnote [54] is used for the integrated correlation function $\zeta_f(\tau)$ (so that $\zeta_f(\tau) \approx \lambda_f k_B T \tau^2$), then the Fourier transform of $\tilde{g}(\tau)$ in Eq. (5.24) is

$$g(\omega) \sim \exp - \frac{(\Delta G^0_{\rm np} - \hbar\omega + \lambda_f)^2}{4\lambda_f k_B T}.$$

The above expression is of the same form as the activation factor in the rate expression of non-adiabatic electron transfer reactions (cf. Marcus, R. A.; Sutin N., *Biochim. Biophys. Acta* **1985,** *811*, 265) if the quantity λ_f replaces the reorganization energy λ in electron transfer reactions.

[50] In Eqs. (5.25) and (5.8), the integration limits for the time variables τ'' and u have been moved to positive and negative infinities, because the integration upper bound t for the old variables t_1 and t_2 is assumed to be much larger than the width of pump pulse profile τ_p. Thereby, with the majority of the excitation

process occurring at short times (τ_p), the integration limits for both t_1 and t_2 can be reasonable approximated as $-\infty$ to ∞, and so can the limits for τ'' and u.

[51] Lax, M., *J. Chem. Phys.* **1952**, *20*, 1752.

[52] In Ref. [51] the absorption and emission spectra are shown to be the Fourier transformation of their time-dependent characteristic functions (Eq. (8.20)). Expressions in Eqs. (5.23) and (5.24) are such characteristic functions (they correspond to Eqs (8.13) and (8.11) of Ref. [51], respectively.).

[53] The Fourier transformation of $\theta(\tau')\tilde{f}(\tau')$ is a complex-valued function whose real part is the Fourier transformation of $\tilde{f}(\tau')$ because

$$\tilde{f}(-\tau') = \tilde{f}^*(\tau').$$

where $*$ denotes complex conjugate. Such a time-reversal property arises from the similar property for the autocorrelation function $\langle X_f(t)X_f(0)\rangle$ (cf. eqs 5.23 and 5.13):

$$\langle X_f(t)X_f(0)\rangle^* = \langle X_f(0)X_f(t)\rangle = \langle X_f(-t)X_f(0)\rangle.$$

The first equality can be shown by taking the Hermitian conjugate (denoted as † below) of the operators inside the thermal average, with the time-evolution of $X_f(t)$ being replaced by $U(t)^\dagger X_f(0)U(t)$ where $U(t)$ is the time-evolution operator which, when operates on a wavefunction, propagates it forward for time t. The second equality makes use of the stationary property.

[54] This crude short-time approximation for $\zeta_s(t)$ can be seen by taking the $\beta \to 0$ (high temperature) limit of the real part of the expression in Eq. (5.35) (with $\coth \frac{\beta\hbar\omega}{2} \sim \frac{2}{\beta\hbar\omega}$), and then taking the leading term (which proves to be t^2) of the Taylor expansion in time t. In simplifying this result, the expression for λ_s in footnote [66] was used. The imaginary part of the correlation function $\langle X_s(t)X_s(0)\rangle$ is much smaller than its real part, at this high temperature limit.

[55] Ovchinnikov, A. A.; Ovchinnikova, M. Ya., *Sov. Phys. JETP* **1969**, *29*, 688.

[56] Abrikosov, A. A.; Gorkov, L. P.; Dzyaloshinski, I. E., *Methods of Quantum Field Theory in Statistical Physics*; Dover Publications, Inc.: New York, 1963.

[57] Caldeira, A. O.; Leggett, A. J., *Ann. Phys.* (N.Y.) **1983**, *149*, 374.

[58] Mukamel, S., *J. Phys. Chem.* **1985**, *89*, 1077.

[59] Georgievskii, Y.; Hsu, C.-P.; Marcus, R. A., *Linear Response Theory Approach for Solvation Dynamics and Nonlinear Spectroscopy*, in preparation.

[60] For example, D. Chandler, in *Liquids, freezing and glass transitions*, ed. Hansen,J. P.; Levesque D.; Zinn-Justin J., Elsevier Science Pub. Co.: North-Holland, 1991, p. 201.

[61] For example, Kubo, R.; Toda, M.; Hashitsume, N., *Statistical Physics*, Springer-Verlag: New York, 1983; Vol. II, Chapter 4.

[62] Onsager, L., *J. Am. Chem. Soc.* **1936**, *58*, 1486.

[63] Böttcher, C. J. F., *Theory of Electric Polarization*, Vol. 1; Elsevier: Amsterdam, 1983.

[64] van der Zwan, G.; Hynes, J. T., *J. Phys. Chem.* **1985**, *89*, 4181.

[65] Mazurenko, Y. T., *Opt. Spectrosc. (USSR)* **1974**, *36*, 283.

[66] In Eq. (5.37), it is seen that the second term vanishes as $t \to \infty$. If the expression for λ_s is similar to that for λ_f in Eq. (5.21), then the first term of Eq. (5.37) should be $-\lambda_s \hbar$. Namely,

$$\lambda_s \left(= -\frac{1}{\hbar} \lim_{t \to \infty} \mathrm{Im}\zeta_s'(t) \right) = \frac{1}{\pi} \int_0^\infty d\omega \frac{J(\omega)}{\omega}.$$

[67] Barthel, J.; Bachhuber, K.; Buchner, R.; Gill, J. B.; Kleebauer M., *Chem. Phys. Lett.* **1990**, *167*, 62.

[68] Barthel, J.; Kleebauer M.; Buchner, R., *J. Sol. Chem.* **1995,** *24* 1.

[69] Arnold, K. E.; Yarwood, J.; Price A. H., *Mol. Phys.* **1983,** *48*, 451.

[70] Ikawa S.; Ohba, T.; Tanaka, S.; Morimoto, S.; Fukushi, K.; Kimura M., *Int. J. Infrared Millimeter Waves*, **1985,** *6*, 287.

[71] Fujita, Y.; Ohba, T.; Ikawa S.-I., *Can. J. Chem.* **1991,** *69*, 1745.

[72] Ohba,T.; Ikawa, S., *Mol. Phys.* **1991,** *73*, 985.

[73] Firman, P.; Marchetti, M.; Xu, M.; Eyring, E. M.; Petrecci, S., *J. Phys. Chem.* **1991,** *95*, 7055.

[74] Goplen, T. G.; Cameron, D. G.; Jones, R. N., *Appl. Spec.* **1980,** *34*, 657.

[75] Bertie, J. E., *J. Phys. Chem. B* **1997,** *101*, 4111.

[76] The absorption coefficients reported in Ref. [70] are in good agreement with results from Arnold *et al.* [69] if the latter were scaled downwards by 7%. That scaled profile, as shown in Ref. [70], is in good agreement with the results later reported in Ref. [71, 72]. Since only a few numerical data are available for those results, the overall spectrum in the present work is obtained from the curve in Fig. 6 of Ref. [70] representing the scaled results of Arnold *et al.*.

[77] Press, W. H.; Flannery, B. P.; Teukolsky, S. A.; Vetterling, W. T., *Numerical Recipes*; Cambridge: Cambridge University Press, 1986.

[78] In the present calculation, the data available from Refs. [67, 70, 73, 75] have three 'blank' regions: from 3 to 10 cm^{-1}, 220 to 320 cm^{-1} and 430 to 700 cm^{-1}. We assume that for those regions $k(\tilde{\nu})$ can be approximated by smooth curves without any peaks. For the lowest frequency region, in order to avoid the oscillation artifact arising from the cubic spline fit, the spline fit and interpolation are performed at the logarithm scale of both k and $\tilde{\nu}$ for the data under 30 cm^{-1}.

[79] For example, McQuarrie, D. A., *Statistical Mechanics*; Harper & Row: New York, 1976; pp. 498-499.

[80] Bertie, J. E.; Lan, Z., *J. Chem. Phys.* **1995,** *103*, 10152. The numbers in the row denoted as "Eq.(3)+" of Table IV are used.

[81] At the lower frequency limit, there is a small but noticeable difference (≤ 0.1) in calculated n (eq.5.41) and those given by taking the real part of the square root of $\epsilon(\omega)$ given by the Cole-Cole equations in Ref. [67]. It may arise from the errors of extracting data from figures in literature [70, 73] and the subsequent use of spline fit to represent the real spectrum, or from the assumptions used to fill in the regions where the absolute absorption spectra are not available [78]. For the present work a linear combination of the refractive index predicted from the Cole-Cole equation (n_{Cole}) and the Kramers-Kronig integration (n_{KK}), $n = w\ n_{\mathrm{Cole}} + (1 - w)n_{\mathrm{KK}}$ is assumed, with a weighting factor w which varies linearly from 0 at $\tilde{\nu} = 3$ cm^{-1} to 1 at $\tilde{\nu} = 5$ cm^{-1}.

[82] Formally, the quantity $(\Delta G^{\mathrm{solv}} + \lambda_s)/\hbar$ is the difference in the position of the absorption spectra in nonpolar and polar solvents, if the solute were a simple two-state system. For molecules as complicated as C153, it can be obtained as follows: The absorption spectrum in a polar solvent can be estimated as [4, 41, 42]

$$g_{\mathrm{p}}(\omega) = \int_{-\infty}^{\infty} d\omega' g_{\mathrm{np}}(\omega - \omega') p_1(\omega')$$

where the absorption spectra in the polar solvent ($g_{\mathrm{p}}(\omega)$) and a nonpolar solvent ($g_{\mathrm{np}}(\omega)$) are related by a convolution over the inhomogeneous site distribution created by the polar environment. Horng *et al.* [9] have used a Gaussian functional form for $p_1(\omega')$ with its mean and variance adjusted to obtain the best agreement between the estimated and the experimental absorption spectrum in polar solvents, using the measured *nonpolar* absorption spectrum and the above equation. The desired quantity $(\Delta G^{\mathrm{solv}} + \lambda_s)/\hbar$ is then the averaged frequency change as described by the Gaussian probability $p_1(\omega')$, which is denoted by δ_0 in

Ref. [9]. The averaged spectral shift reported there is 1740 cm^{-1} for acetonitrile. However, since the absorption and emission spectra in nonpolar solvents that are used for the present calculation are inferred from figures in Ref. [9], the uncertainty from the inference is about 100 cm^{-1}. We have adjusted the δ_0 reported there to 1490 cm^{-1} in order to obtain the same zero-time estimation spectrum as that reported in Ref. [10], which does not depend on any dynamical quantities. (It only depends on this $p_1(\omega)$, the steady-state absorption and emission spectra in a nonpolar solvent (Eq. (5.2).)

[83] λ_s can be calculated using the expression discussed in footnote [66].

[84] Barthel, J.; Bachhuber, K.; Buchner, R.; Hetzenauer, H., *Chem. Phys. Lett.* **1990,** *165*, 369.

[85] Bertie, J. E.; Zhang, S. L.; Eysel, H. H.; Baluja, S.; Ahmed, M. K., *Appl. Spectrosc.* **1993,** *47*, 1100.

[86] Kindt, J. T.; Schmuttenmaer, C. A., *J. Phys. Chem.* **1996,** *100*, 10373.

[87] Kovalenko, S. A.; Ruthmann, J.; Ernsting, N. P., *Chem. Phys. Lett.* **1997,** *271*, 40.

[88] Raineri, F. O.; Perng, B.-C.; Friedman, H. L., *Electrochimica Acta* **1997,** *42*, 2749.

[89] For example, Weiner, A. M.; Desilvestri, S.; Ippen, E. P. *J. Opt. Soc. B* **1985,** *2*, 654; Bai, Y. S.; Fayer, M. D., *Chem. Phys.* **1988,** *128*, 135; Joo, T.; Albrecht, A. C., *Chem. Phys.* **1993,** *176*, 233; Meijers, H. C.; Wiersma, D. A., *J. Chem. Phys.* **1994,** *101*, 6927; Bardeen, C. J.; Shank, C. V., *Chem. Phys. Lett.* **1994,** *226*, 310.

[90] Nishiyama, K.; Okada, T., *J. Phys. Chem. A* **1997,** *101*, 5729.

Figure 5.1: Double-sided Feynman diagram for the process of excitation and fluorescence for a two-state system. In this diagram, the density matrix is represented by the two vertical lines. The line on the left represents the ket and the line on the right represents the bra, with time running vertically from bottom to top. An interaction with the radiation field is represented by an arrow. The direction of such an arrow determines the sign of the wave vector contribution to the polarization, which is not explicitly considered in the present study. t_1 and t_2 are any two times occurring during the absorption (pump) pulse. In the integration in eq (5.8), the excitation times t_1 and t_2 can be reversed. t_3 and t are the two times when fluorescence occurs.

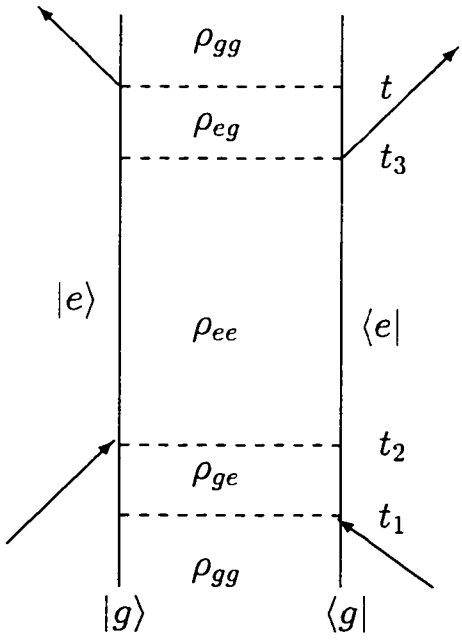

Figure 5.2: The calculated time-dependent emission spectra for coumarin 153 in acetonitrile at different delay times (solid lines) and the experimental data (dots inferred from the figures in Ref. [10]). The delay times are indicated in the units of picosecond. Baselines for different delay times are shifted vertically and are indicated at the left of the figure.

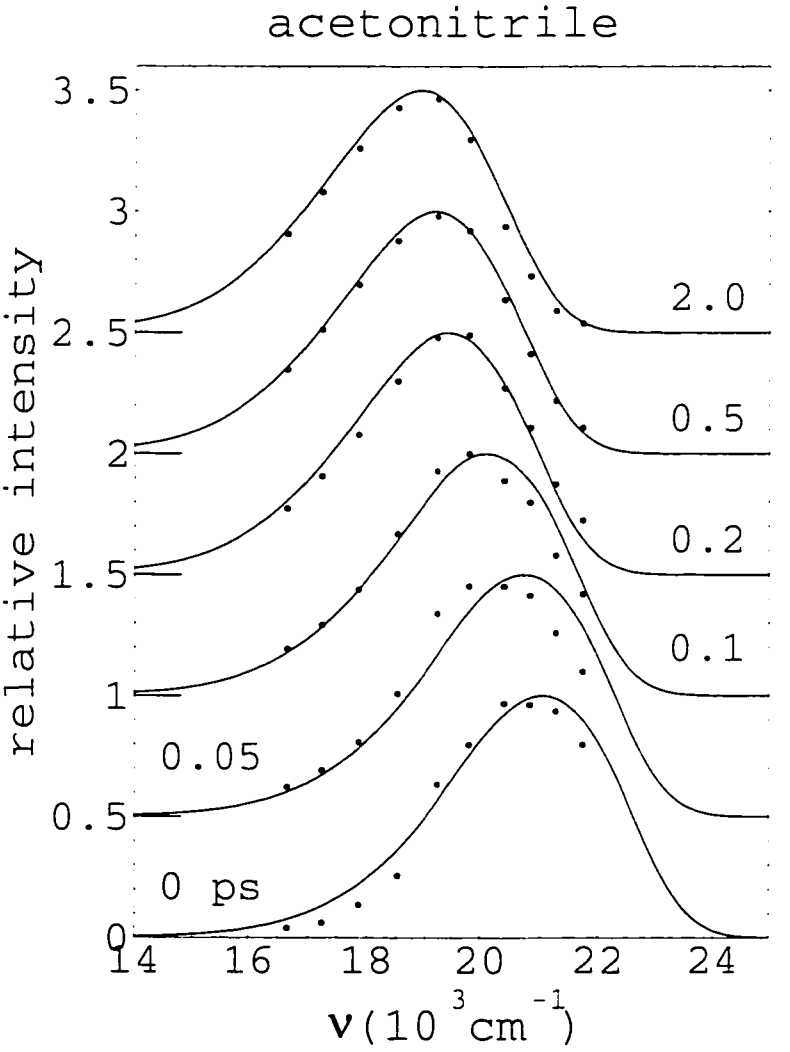

Figure 5.3: Top panel: the dynamic Stokes shift $S(t)$ for acetonitrile calculated using eq (5.33) (solid line) and the results fitted to experimental data [9] (dashed line). Bottom panel: calculated $S(t)$ using eq (5.34) (solid line) with $\epsilon_c = 2$ and the same experimental results (dashed line).

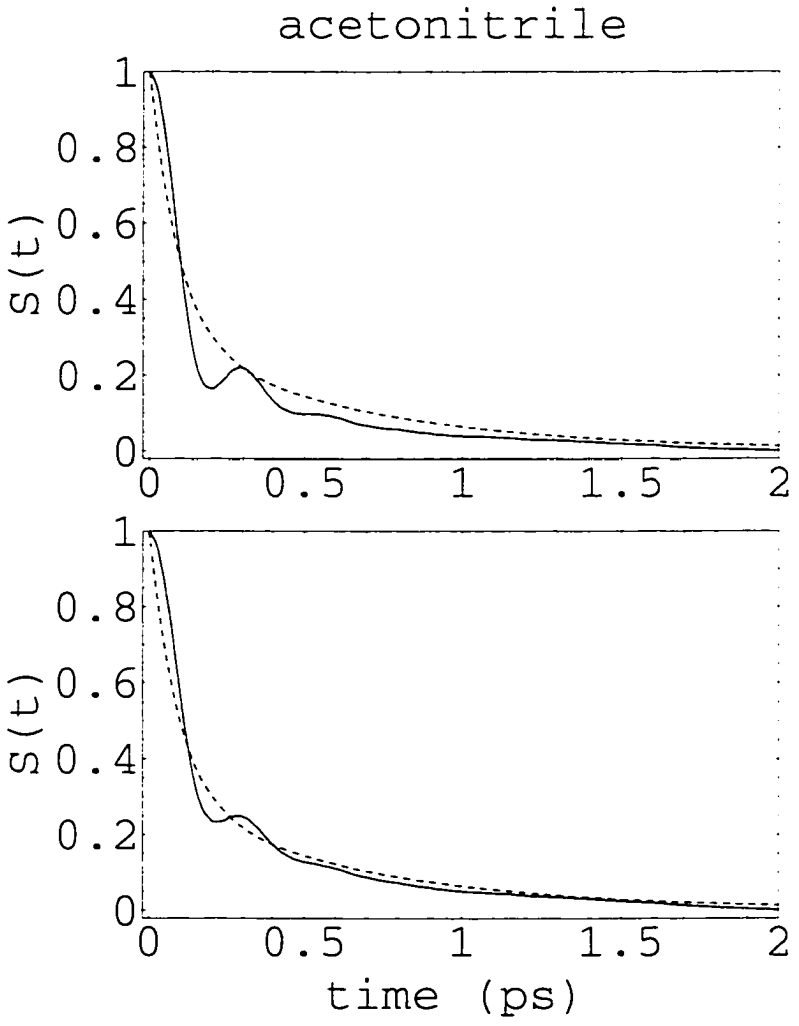

Figure 5.4: Top panel: the dynamic Stokes shift $S(t)$ for methanol calculated using Eq. (5.33) (solid line) and the results fitted to experimental data [9] (dashed line). Bottom panel: calculated $S(t)$ using Eq. (5.34) (solid line) with $\epsilon_c = 2$ and the same experimental results (dashed line).